Low-Energy, Low-Cost Production of Ethylene by Low-Temperature Oxidative Coupling of Methane

Final Technical Report

Federal Agency / Organization Element	DOE/EERE/ Advanced Manufacturing Office (AMO)
FOA Name and Number	Innovative Manufacturing Initiative DOE-FOA-0000560
Award Number	DE-EE0005769
Award Type	Cooperative Agreement
Project Period	10/01/2015 to 09/30/2017
Prime Recipient	Siluria Technologies 409 Illinois Street San Francisco, CA 94158
Prime Recipient Type	Private Company
Prime Recipient's DUNS Number	961825937
Project Title	Low-Energy, Low-Cost Production of Ethylene by Low-Temperature Oxidative Coupling of Methane
Principal Investigator(s)	Guido Radaelli VP Engineering guido@siluriatech.com

Acknowledgment: This material is based upon work supported by the Department of Energy's Office of Energy Efficiency and Renewable Energy (EERE) under the Advanced Manufacturing Office under Award Number DE-EE0005769.

Table of Contents

Executive Summary

Ethylene is the world's largest-volume and most energy intensive commodity chemical. Nearly 25 million tons are produced in the U.S. each year by steam cracking, an energy intensive process that burns 500 trillion BTUs/year of energy. Not only is the steam cracking process highly energy intensive, it also uses derivatives from limited natural resources such as oil (naphtha feedstock) or a natural gas liquid (ethane). Dependence on traditional steam crackers also bottlenecks the ethylene production capabilities to manufacturing sites located in vicinity of the ever-depleting oil resources.

Analysis of the downstream ethylene industry reveals that there is a significant mismatch between the scale of crackers (ca. 500 to 1500 KTA) that produce ethylene versus derivatives producers (ca. 50 to 150 KTA) that consume ethylene as a feedstock. The reason for this mismatch is crackers require a much higher minimum scale of ~500 KTA, below which is not economical to operate. As a result, a single cracker supplies multiple derivative units within a given region, which restricted the choice of location and scale.

Siluria Technologies is pioneering the commercial production of fuels and chemicals made from clean, abundant natural gas. Siluria's breakthrough Oxidative Coupling of Methane ("OCM") process technology is believed to be the first commercially viable process to directly convert methane to ethylene. This enables natural gas to potentially supplement petroleum as the worldwide basis for commodity chemicals. Furthermore, advances in exploration and production technologies have enabled access to shale reserves that were previously uneconomical to produce. As a result, proven natural gas supplies continue to grow. Hence, Siluria's OCM technology helps expand the manufacturing opportunities of ethylene across the nation and globe.

The simple design of Siluria's OCM reactor also enables scalability of ethylene process across a wide range. The current technology is capable to address mid-mega scale ethylene production capacities (150-1000 KTA). The project undertaken sought to further explore the feasibility of ethylene production at smaller scales (below 150 KTA), which would subsequently address the deep mismatch between the ethylene production and derivative industry.

While the design of the existing OCM technology distinguishes from an ethane cracker in being a direct catalytic reaction to produce ethylene instead of thermal cracking, it has some features in common with a cracker in terms of ethylene separation from the reactor effluent stream. Although the OCM reactor can be economically scaled-down, a traditional cryogenic separations section poses a notable roadblock in designing a small-scale ethylene unit.

In order to investigate and enable the OCM technology for small-scale design, the project was proposed and executed with well-defined milestones throughout its timeline. The project was implemented in the following steps by Siluria, in collaboration with a leading research institute

(RTI International), academia (University of California, Berkeley) and a specialist engineering firm (Norton Engineering):

- Evaluated current technology to identify process areas causing roadblocks to small-scale implementation.
- Researched alternative technologies for the most capex and energy intensive process area.
- Explored and developed materials that are best suitable for the technology implemented.
- Developed and optimized the process using experimental data and process modeling (more than 30 experiments with 150 measurements, evaluation of at least 5 different configurations, numerous simulations on Aspen Adsorption and HYSYS).
- Performed detailed techno-economic analysis to assess the benefits of the new process.

It was found that cryogenic separations for ethylene recovery from lighter OCM effluent components and heavy hydrocarbons posed a critical roadblock to small-scale implementation in the original design. An alternative and configuration was proposed and validated based on novel adsorption system (PSA) which provides multiple advantages, such as lower energy consumption and capital costs. The nature of the technology chosen allows for down-scalability and better energy utilization of the entire process. This remarkable accomplishment enables small scale distributed production of ethylene via OCM process that uses ubiquitous natural gas as its feedstock.

The scope of this project demonstrated an FEL-1 level technical and economic viability of the process. Thus, the efforts involved working with data from bench-scale experiments, reasonable assumptions on process simulations and techno-economics. Commercialization of the process would involve further steps such as refined materials development, process development and experimental validation, setting up an integrated pilot plant to test various scenarios at higher capacities, detailed simulations, potential adjustments and optimization to the final configuration to facilitate commercial deployment, and developing a comprehensive techno-economic model that proves suitability for commercial deployment. All these efforts would lead to a commercially viable process design of an OCM plant for distributed small-scale production of ethylene, which could redefine the value chain of the ethylene industry.

List of Acronyms

ACCE	Aspen Capital Cost Estimator
BET	Brunauer–Emmett–Teller Theory
dobdc	2,5-dioxido-1,4-benzenedicarboxylate
DOE	U.S. Department of Energy
FEL	Front End Loading
FTIR	Fourier transform infrared spectroscopy
GC	Gas Chromatograph
HP	High Pressure
IAST	Ideal Adsorbed Solution Theory
IRR	Internal Rate of Return
KTA	Kilo Tons per Annum
LT-OCM	Low Temperature Oxidative Coupling of Methane
MM	Million
MMBTU	Million British Thermal Units
MOF	Metal Organic Frameworks
MT	Metric Ton
NPV	Net Present Value
PSA	Pressure Swing Adsorption
RGA	Residual Gas Analyzer
RPPR	Research Performance Progress Report
RTI	RTI International - (formerly Research Triangle Institute)
SCCM	Standard Cubic Centimeters per Minute
TIC	Total Installed Cost
TPR	Temperature-programmed reduction
TSA	Temperature Swing Adsorption
XRD	X-ray diffraction

List of Figures

List of Tables

List of Appendices

Introduction

Ethylene, one of the highest volume production chemicals in the U.S. and globally, is an essential chemical building block that is used to manufacture countless products, from packaging to antifreeze to tires. Most ethylene is produced via a process called steam cracking, where the feedstock (mostly ethane, sometimes naphtha or propane) is heated to high temperatures over a catalyst. The naphtha feedstock typically comes from petroleum refineries, while ethane is becoming increasingly used as a feedstock in the U.S. due to the rise in domestic natural gas production from shale resources. However, steam cracking is energy intensive and occurs in large-scale facilities.

Low-temperature oxidative coupling of methane (LT-OCM) is an alternative ethylene production method that converts methane (natural gas) and optionally ethane to ethylene in a single-step, energy-producing conversion system using an innovative process including a novel reactor and inorganic catalyst Figure 1. While OCM has been studied for over 30 years due to its potential to reduce ethylene production cost, past efforts did not result in a viable catalyst with performance needed for commercialization. These catalysts, while at times achieving promising yield and selectivity, were hampered by very high operating temperatures, low activities, and short lifetimes on the order of hours to days.

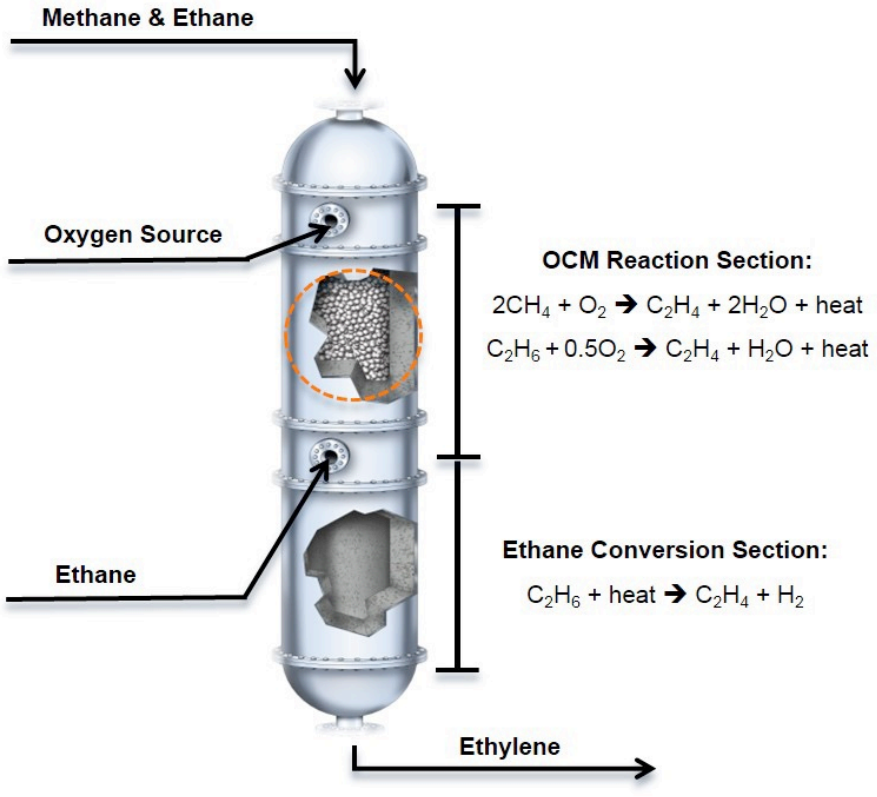

Figure 1: Schematic illustrating Siluria's new low-temperature oxidative coupling of methane (LT-OCM) catalyst and reactor for distributed production of ethylene

Recognizing this, Siluria applied a combination of new innovations in catalyst development and a thorough definition and understanding of the problem to develop unique catalysts that will enable commercialization of OCM. The OCM catalysts operate at significantly lower temperature (several hundreds of degrees lower) and practical operating pressures (5-10 atmospheres), have high activities and standard lifetimes of years under said conditions. In addition, the simple reactor design provides excellent scalability and flexibility to the process, especially when compared to today's mega-scale steam crackers, thus enabling small-volume "distributed scale" reactors for on-demand ethylene production for applications such as on-site conversion of ethylene to high-value polymer derivatives.

The project objective is to develop a new catalytic process for distributed small-scale production of ethylene by oxidative coupling of methane at low temperatures using the advanced OCM catalyst developed by Siluria Technologies. The current design shows excellent scalability for regional-world scale ethylene capacities. However, the specific operating and capital costs increase sharply for lower capacities. The project aims to overcome the hurdles for small-scale implementation of ethylene production through oxidative coupling of methane.

Benefits for Our Industry and Our Nation

This technology will reduce cost, energy consumption, and emissions across the U.S. chemical industry. This innovative technology has many potential benefits, including:

- Improved ethylene manufacturing energy efficiency.
- Reduced lifecycle emissions of carbon dioxide and other pollutant emissions compared to traditional ethylene production methods.
- Tapping ubiquitous natural gas reserves as feedstock for production of high value petrochemicals, lowering the dependence on crude oil.
- Enabling economically competitive, distributed, small-scale production of ethylene for on-site generation of high-value derivatives such as polymers.

Applications in Our Nation's Industry

Ethylene is an important chemical that is produced upstream by a small number of large-scale facilities, consumed downstream by many producers, and converted into a range of products. This project will offer distributed, small-scale ethylene production solution for the downstream consumers, due to its unique combination of utilizing cheap feedstock (natural gas) and simple overall process design.

Barriers to small-scale production

Following barriers limit small-scale production ability:

- Utilizing cryogenic separation systems that scale poorly at lower capacities.
- Certain unit operations in the current design require minimum capital expenditure and are cost efficient only at large scale.

Background

Siluria's catalytic process technology constitutes a novel system that feeds methane and optionally ethane into a fixed bed reactor and converts them to ethylene using Oxidative Coupling of Methane (OCM). The principal OCM reaction to produce ethylene from methane is given as:

$$2\ CH_4 + O_2 \rightarrow C_2H_4 + 2\ H_2O$$

This reaction is highly exothermic and catalytically occurs at temperatures above 450°C.

To improve the reaction yield, ethane can optionally be introduced downstream of the OCM catalyst bed in the ethane conversion section and thermally dehydrogenated via the following reaction:

$$C_2H_6 \rightarrow C_2H_4 + H_2$$

This reaction is endothermic, which best utilizes the exothermic reaction heat produced during methane conversion. Combining these two reactions in one vessel increases thermal efficiency while simplifying the process.

The OCM reactor produces a small, but non-negligible amount of CO and CO_2 co-products. To increase the carbon efficiency of the plant, a methanation reactor is used to convert the majority of the co-products back to methane via the following reaction:

$$CO + 3\ H_2 \rightarrow C_2H_4 + H_2O$$

$$CO_2 + 4\ H_2 \rightarrow C_2H_4 + 2\ H_2O$$

This process has been well-studied and is common in industrial use. The implementation of a methanation reactor in tandem with an OCM reactor to increase carbon efficiency is a novel approach.

Ethylene produced in the reactor is subsequently separated from the unreacted products/byproducts using a series of conventional unit operations. The resulting product is polymer grade ethylene as the principle product.

Description of the current OCM Process

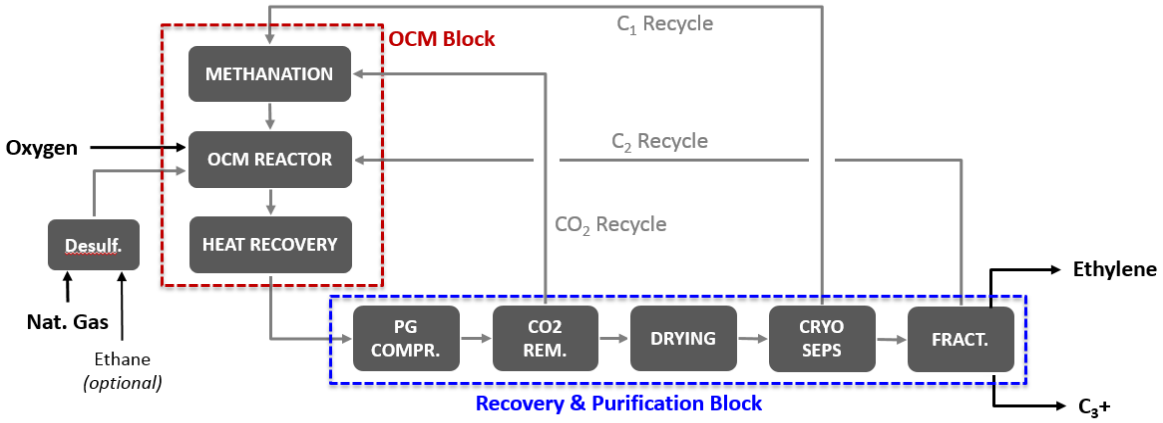

Figure 2: Block Flow Diagram of the current OCM Process

Figure 2 depicts a block flow diagram of the OCM process. Desulfurized natural gas feed from pipeline is fed into the OCM reactor, along with supplied oxygen and ethane feeds. The OCM reactor consists of two reaction sections as shown in Figure 1. The first reaction section ("OCM Reaction Section") consists of a fixed, adiabatic bed containing Siluria's OCM catalyst that converts methane and oxygen in an exothermic reaction to ethylene and other reaction co-products (mainly ethane, C_{3+}, CO_2, CO, H_2O, and H_2). The reaction heat generated is then utilized in a second reaction section ("Ethane Conversion Section") where ethane is injected to homogenously convert ethane to ethylene via non-oxidative dehydrogenation.

The reactor effluent consisting of unconverted CH_4, H_2, ethylene, ethane, CO_2, CO, H_2O, and C_{3+} components is quenched and cooled down while producing HP steam and reheating the C_1 recycle stream to OCM in gas/gas exchangers. After the compression of the process gas, CO_2 is removed from the process gas in a CO_2 Removal Unit consisting of a MEA Wash Unit and a Caustic Wash Unit.

The CO_2 free process gas is chilled and dried before being fed to the C1/C2 separation unit where the C2+ fraction is separated from the process gas and is sent to the Cyrogenic Separation Unit. The overhead (mainly methane and hydrogen) is sent to the Methanation Unit. In the Methanation Unit, H_2 and CO contained in the methane recycle stream react along with CO_2 removed from MEA wash, and are further converted to methane, thus increasing carbon efficiency of the overall process. The methane stream is recycled to the reactor for further utilization in the OCM reaction.

Converting ethane in the Ethane Conversion section of the OCM reactor via cracking and converting CO, CO_2 and H_2 in the Methanation Unit are integral reaction steps within the overall OCM process, aimed at enhancing the overall carbon efficiency of the process.

The process includes closed C2 and C3 refrigerant cycles to provide the appropriate level of refrigeration to the cryogenic sections.

While the reactor demonstrates excellent down-scalability, an analysis of unit operations and/or process steps in the separation section highlights certain areas that pose principle technical and economic roadblocks for small-scale implementation of ethylene production plants (100 KTA or below). For instance, cryogenic distillation of the effluent from the OCM reactor is a critical area where development of alternatives can have a significant impact on the ability to scale-down the technology.

Project Execution Plan

The focus of efforts in this project was to evaluate processes for the recovery and purification of ethylene product, and for the recycle of unconverted reactants. These alternative processes needed to be able to achieve the product specifications, separation performances and cost and energy targets.

Using the extensive in-house data on the LT-OCM catalysts, Siluria planned to perform a systematic process analysis based on process simulations, equipment sizing and capital cost evaluations, to fully identify and characterize the system bottlenecks that prevent scalability and manufacturability. Successively, alternative process schemes, and unit operations were to be researched and investigated to assess the techno-economic viability and performance in the LT-OCM catalyst system. The most promising alternative process configurations along with optimum catalyst selection would then be validated at the lab scale to confirm their technical feasibility and assess their performances in the specific operating conditions required for the LT-OCM catalyst system.

The goal of the project was to determine one or more technically and economically viable process concepts for small-scale ethylene production using LT-OCM, validated by process modeling, laboratory data, and techno-economic analysis. The information gained in the project would provide the basis for further work, including development and scale-up, necessary to commercialize distributed small-scale ethylene production.

Following milestones were set to achieve the project objectives:

- Target list of unit operations and/or process steps providing roadblocks to small-scale implementation
- Identification of alternative process concepts/technologies demonstrating potential to meet performance and cost targets
- Preliminary alternative process concepts/technologies, validated with preliminary experimental laboratory data suitable for application in small-scale OCM process.
- Refined alternative process concepts/technologies, validated with refined experimental laboratory data suitable for application in small-scale OCM process.
- One or more process concepts for small- scale OCM ethylene production.
- Techno-economic analysis of one or more process concept for small-scale ethylene production with total feed and energy consumption lower than 20 MMBTU per ton ethylene and cost advantaged to merchant ethylene produced by cracking.

Siluria utilized its expertise in R&D, process development and techno-econ analysis, and established new partnerships to effectively execute the project. Following are the capabilities of various agencies involved in this project.

Siluria Technologies (experise in OCM development):

- State-of-the-art high throughput screening platform for catalyst discovery and development.
- R&D and pilot facilities specifically developed for OCM and incorporating new separation technologies.
- Extensive process engineering and technology development experience.
- Techno-economic analysis & commercialization expertise.
- First of a kind (world's largest) OCM demonstration plant, co-located at an operating polymer plant in La Porte, Texas.

RTI International (Materials and process testing)

- Material development and testing capabilities - sorbent development for separation studies.
- Process development - strong competence in developing, designing and constructing separation systems for novel applications.

University of California, Berkeley (Novel Adsorbent Materials)

- World leading Metal Organic Framework (MOF) research capabilities.
- Invented multitude of MOF materials with excellent relevant properties.

Norton Engineering (Modeling of Adsorbent Systems)

- Decades of experience in conceptual design of commercial PSA systems.

Results and Discussion

In this project, Siluria, in collaboration with its partners did thorough analyses through experiments, literature surveys, modeling and techno-econ analysis to develop a technology that enables small-scale production of ethylene via OCM. Below is a summary of the work performed throughout the project, and a discussion of the results.

The project began by performing process analysis of Siluria's existing baseline design developed and optimized for large-scale ethylene production and determining specific unit operations and/or process steps impacting economies at small-scale. Scalability of each process area and unit operation was analyzed through evaluating technical and economic (specific capital and operating cost) factors at three capacity levels (scaled from the large-scale commercial and conceptual LT-OCM reference design case). A comparison of the three cases based on energy efficiency (measured as MMBtu of energy consumed per ton of ethylene produced) and capital cost per unit capacity (measured as $ per Metric Ton (MT) of annual ethylene capacity) was performed. Thus, unit operations that constitute the principal technical and economic roadblocks for small-scale implementation were identified and further explored.

The task was carried out in the following steps:

- Three cases of ethylene production with capacities of 135 KTA, 67 KTA and 27 KTA were chosen to identify the effects of scaling down Siluria's OCM technology.
- Complete process simulations (using commercial Aspen HYSYS software) for the three cases were performed assuming similar configuration, feed and product compositions and same design basis for each process equipment and unit operation.
- Equipment sizing was performed for the three different units – which correspond to the three different scales – based on commercial software including Aspen Exchanger Design and Rating software, first principles, proprietary tools for proprietary equipment and vendor driven inputs for critical equipment.
- Capital cost estimates were evaluated based on Aspen Capital Cost Estimator, Siluria's internal database and vendor quotes where necessary.
- The total investment cost, operating costs and Internal Rate of Return (IRR) were calculated and compared for the three units.
- Roadblocks were identified based on specific cost of production (operating and capital) and technical feasibility for each unit operation designed at the three different capacities when compared to the large-scale production units.
- An overall comparison of each unit's capital/operating costs and internal rate of return was performed.

Techno-Econ Analysis of the Existing OCM Process

The process economics for this analysis was performed using two factors:

- An overall project cost ($MM/KTA of ethylene product)
- An Internal rate of return of the unit

Overall Project Cost

Economies of scale are cost advantages that enterprises obtain due to size, output or scale of operation, with cost per unit generally reducing with increasing scale. Economies of scale in the engineering industry is typically governed by the 0.6 power rule for capital costs, which states that, if the capital cost for a given equipment is known, changing the size will change the capital cost by 0.6 power of the capacity ratio. Economies of scale work well and illustrate the cost advantages that industry obtains when scaling up the capacity of a unit while maintain a single train. The general trend indicates a consistent dip in the cost as the unit production capacity increases. This in turn implies that a lower capacity can result in a higher cost of production. The analysis shows that the specific unit cost of production and individual capital cost of certain equipment are even higher than expected from general trends expected based on economies of scale.

Figure 3 shows total specific project cost that was determined, expressed as project cost in $MM per KTA of ethylene produced annually. The figure shows an increase in project cost with reduction in capacity. The plot shows an inflection point at about 60 KTA. This signifies the rapid increase in the specific project cost below a capacity of 60 KTA. Hence, from a total investment cost perspective, any plant with a capacity lower than 60 KTA would be unlikely to result in a profitable investment.

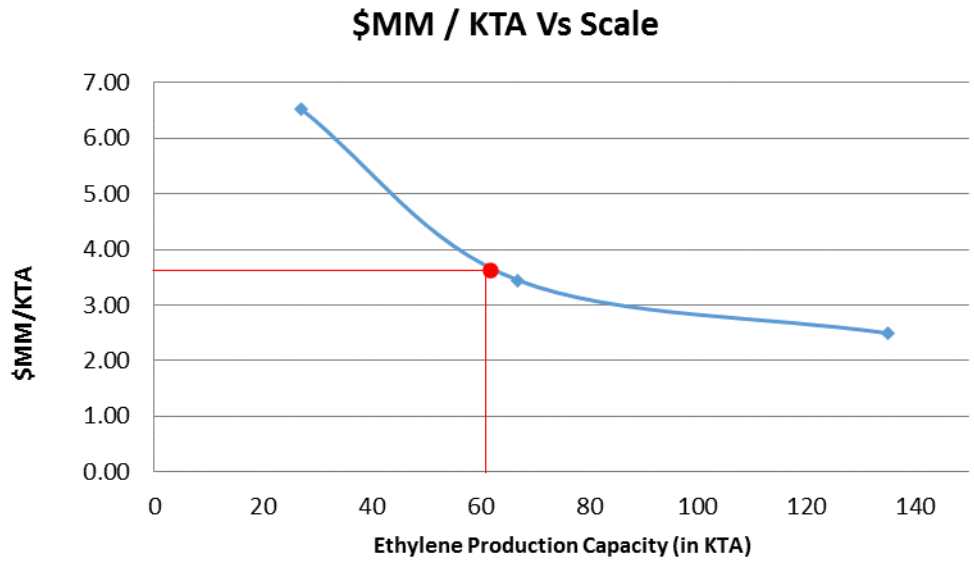

Figure 3: Capital intensity curve of the existing technology

The reason of the rapid increase in the project cost as you move to smaller scale can be derived from closely looking into the trends of capital cost of each section and equipment. This analysis was performed using Aspen Capital Cost Estimator for the entire process concept.

Internal Rate of Return

Internal Rate of Return (IRR) is a metric used in capital budgeting measuring the profitability of capital investments. Internal return rate is the discount rate that net present value (NPV) of all cash flows from a particular project equal to 0. IRR calculations can be deduced from the calculations of NPV. NPV is calculated as:

$$NPV = \sum_{t=1}^{T} \frac{C_t}{(1+r)^t} - C_o$$

Where,
C_t = net cash inflow during the period t.
C_o= total investment costs
r = discount rate, and
t = number of time periods

To calculate IRR, NPV is set equal to 0 and solved for discount rate r, which is the IRR.

The higher a project's IRR, the more desirable it is to undertake a project. Typically, in the energy industry for large enterprises, an IRR of 15 % is used as the hurdle rate for undertaking a new venture. IRR includes the effects of total project costs and the operating costs.

The unlevered pre-tax IRR was calculated for the 3 capacities (27 KTA, 67 KTA and 135 KTA). A plot describing the effect of reduction in capacity on IRR for two spreads (for a price ratio of oil/natural gas at 20) is shown in Figure 4.

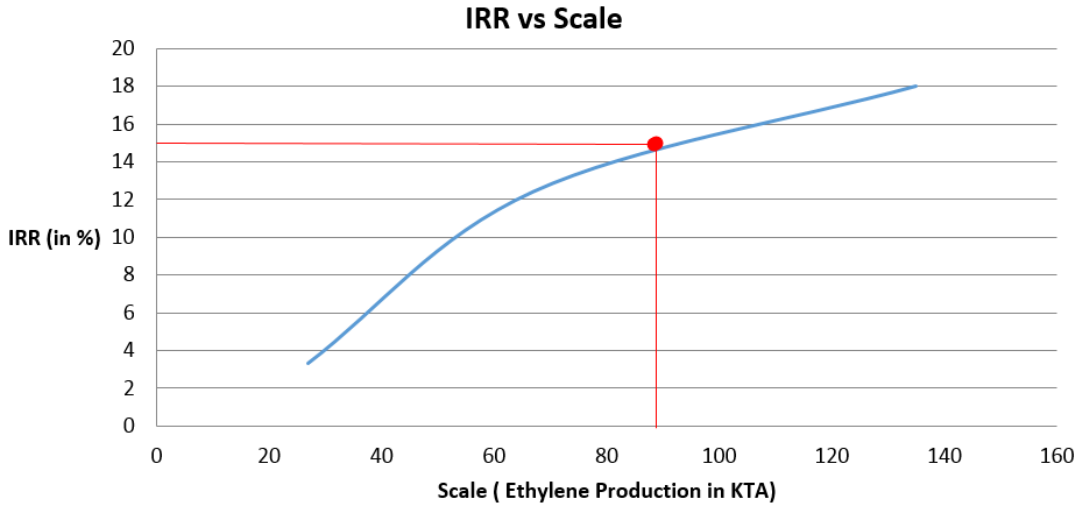

Figure 4: IRR curve of the current technology for small scale ethylene production

As seen from the figure, any investment for a production capacity that is lower than 80-85 KTA is considered unfavorable under the technical and economic assumptions utilized for all design cases.

Based on the above two charts, not only is implementing a project with a capacity below 60 KTA not likely to be cost effective, but also any unit smaller than 80 KTA is likely unfavorable from an economic point of view at the assumed conditions.

Analysis of individual process unit operations and a list of roadblocks:

In order to clearly identify the reasons for the poor process economics at low capacities, a detailed analysis was performed to examine each process unit technically and economically. It was observed that each unit operation was either "feasible" or "unfeasible" based on the following criteria:

1. Economic
2. Technical

Economic: A detailed breakdown of the TIC of each process area illustrates whether the selection of a certain type of equipment is economically viable or not. A good measure for economy of scale is the 0.6 power rule (as discussed previously). The 0.6 power rule is defined as:

$$C_B = C_A \left(\frac{S_B}{S_A} \right)^{0.6}$$

Where, C_B= the approximate cost ($) if equipment having size S_B

C_A= is the known cost ($) of equipment having corresponding size S_A (same units as S_B)

And (S_B/S_A) is the ratio known as the size factor, dimensionless.

If the exponent is lower than 0.6, decreasing the capacity of the unit will have a large impact on the specific cost. Conversely, if the exponent is higher than 0.6 reducing the unit capacity will not have a significant impact on the specific capital cost. For example, a unit that displays an exponent of 0.4 or lower is likely to present an economic roadblock when reducing its capacity since its cost will decrease significantly less than proportionally to capacity.

For each process area, two types of analysis were performed. First, the detailed analysis of total installation costs (breakdown of equipment cost + cost associated with overhead, piping, civil, instrumentation, etc.) was evaluated and second, the total installation cost for the area was calculated using the 0.6 power rule and compared with the value obtained from ACCE. Based on this analysis the list of process unit operations that are not economically scalable at lower capacities was determined. Reasons for poor economic scalability typically included:

- ***Scalability issues based on overall process unit cost:*** From observing the cost breakdown of each unit operation, it was found that when a unit operation in a process area is scaled down (reaction, fractionation, etc.), the equipment necessary for the operation itself might scale down accordingly but the piece count of the auxiliary equipment – such as instrumentation, control systems, associated piping, etc. – remain the same and their costs do not reduce in the same proportion. They require a minimum cost for investment. Hence, the specific project cost increases.

- ***High minimum capital cost:*** Equipment such as turbines, compressors, cold boxes, etc. require a certain minimum investment for their installation and operation irrespective of the production capacity of the unit. This is due to the sheer size and operational complexities of the equipment. The efficiency of such equipment typically is lower at smaller capacities (measured with parameters such as unit cost of the equipment/ power produced – in case of turbines). This trend can be derived by comparing the overall unit operation cost for small scale with the cost that would be obtained by using a 0.6 power rule to scale down.

Technical: In addition to performing the economic analysis, we examined the technical viability of scaling down a particular unit operation. In some cases, scaling down a process incurred additional technical challenges causing an economic impact or necessitating a change in design. For example, scaling down a distillation column result in towers having a small diameter and a very large height (Tangent-to-tangent length /Diameter of the column (L/D) > 30). Such high L/D ratios are not recommended due to high wind load and foundation concerns. To design such equipment, the material thickness of the column would need to be drastically increased to support this geometry, which in turn results in higher material cost and substantial increase in the over unit investment costs. Alternatively, for distillation columns that require a diameter lower than 600mm, a packed tower may be recommended due to poor separations resulting from insufficient vapor-liquid traffic and interaction in the column. However, in some cases, packed tower designs may generate operability concerns due to the fouling nature of the feed stream, thus forcing the designer to eventually adopt a larger than strictly required tray column. Such scenarios necessitate a change in the design when considering scale down to lower production capacities.

Unit Operations and Alternative Technologies

Figure 5 summarizes the findings of the techno-econ analysis on each unit operation. The impacts of capital cost and scalability of each unit operation has been depicted by:

a) color of the block - representing down-scalability of the unit operation
b) size of the block - representing capex contribution of the unit operation

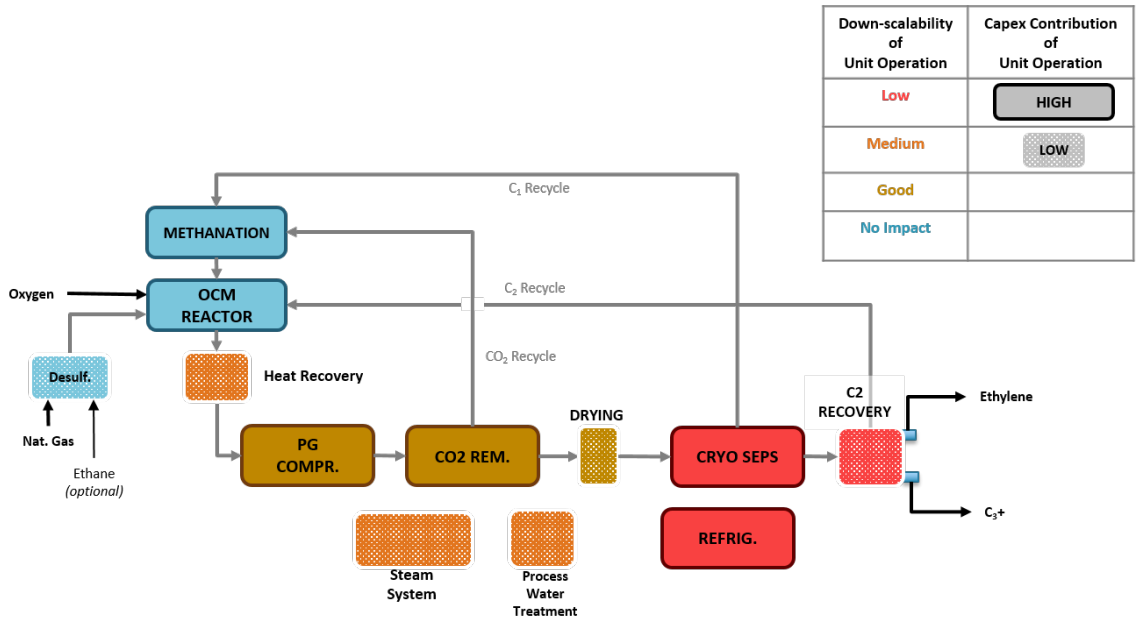

Figure 5: Techno-econ impact of individual unit operations on down-scalability and capex contribution

The overall process economics analysis illustrates the limitations in small scale implementation of the LT OCM process. While the OCM reactor has high capex contribution, it is easily down-scalable. Other sections, particularly ones requiring high pressure (process gas compression, CO_2 removal, cryogenic separations) and low temperature (cryogenic separations/refrigeration) have high capex contribution and low down-scalability.

Thus, the process areas that were found to require further investigation were:

- **Separations Section**: Due to unsuitable designs (high L/D ratios) and high costs of the distillation towers at small scale, separations section that includes C1/C2 separation (with the highest impact on capital intensity), C2/C3 Separation, C_2H_4/C_2H_6 separation and C3/C4 separation has limited implementation ability. There is a critical need for modifications or alternate technologies for performing the separations at small scale.

- **Refrigeration Section**: The current design incorporates energy intensive ethylene and propylene refrigeration systems for generating cryogenic conditions to recover the lighter hydrocarbons in the separations section. The refrigeration compressor sections utilize steam turbines to generate power for their operations. Although the steam is produced as a part of heat recovery within the process, the use of turbines at small scale results in high total investment costs for the plant.

- **CO_2 Removal Section:** The elaborate CO_2 removal technology that uses amine and caustic treatment followed by amine regeneration and spent caustic treatment does scale down well for the small-scale implementation. However, the total project costs and IRR could generally be improved, if a smaller/cheaper package unit at this scale could perform the same function.

After the identification of these critical process areas, different alternative technologies were explored for each process area such that the overall process for small-scale OCM would have the following features:

- It can recover ethylene at the polymer grade purity level.
- It addresses the high capital/operating cost and energy required for running the C1/C2+ bulk separation process (currently using a demethanizer).
- It can utilize the exothermic energy produced in the reaction to the greatest extent possible such that any energy requirements within the process can be fully satisfied.
- It results in an enhanced overall design with better economics for other areas, thus reducing total project costs.

Identified Alternative Technologies

Light Hydrocarbon Gas Separations in OCM design

Cryogenic separations typically require high gas compression and expensive refrigeration systems. Such systems do not scale down well for small-scale capacities due to high minimum capital costs and high operating costs of the associated equipment. Alternative gas separation technologies (non-cryogenic separations) such as Pressure Swing Adsorption/Temperature Swing Adsorption/ membrane systems have been studied and commercially deployed for some time, either as complete modular units for separations or as hybrid systems (specialized membranes that are followed by distillation units to de-bottleneck the distillation column). In this study, specific adsorbents and membranes that could help achieve the objectives of the study were explored.

Fixed Bed Adsorption Processes

The use of a solid adsorbent to remove component(s) from a gas stream in an adsorptive process is a well-established method for gas separation. It has been widely adopted for purification of hydrogen, nitrogen rejection units in natural gas upgrading, air separation, removal of water from gas streams and noble gas purification. In certain instances, such as air separation, adsorptive processes have been shown to offer a low capex and opex alternative to cryogenic separation especially on smaller scales.

In most processes, the adsorbents are usually in the form of small particles (beads and pellets) in a fixed bed. The adsorbent particles typically are porous materials, with pore volumes up to 50% of total particle volume. Adsorption is typically a surface phenomenon and occurs as a monolayer in the pores. These interactions can be either due to physisorption (van der Waals or electrostatic forces) or chemisorption (as a result of chemical reaction). The effectiveness of an adsorbent is characterized by equilibrium thermodynamics. This behavior is described by isotherms, an example of which is shown in Figure 6Figure 6. At a given temperature and partial pressure, the isotherm provides the amount of gas adsorbed by the adsorbent. The differences in equilibrium capacity of two or more gases on an adsorbent result in separation. Thus, the choice of adsorbents plays a major role in the development of adsorption processes. Typical adsorbents used in these processes include:

a) Zeolites/Molecular Sieves – These are hydrated aluminosilicate minerals made from tetrahedral of alumina and silica. They are heat and pressure stable solids which have an ability to adsorb polar compounds making them good candidates for separation of gases. With crystalline structures with well-defined pore sizes, they are able to act as molecular sieves as well.

b) Metal Organic Frameworks (MOFs) – MOFs are crystalline, high surface area materials with a metal ion and organic linkers. The choice of the metal and the linker has a significant effect on the structure and properties of the MOF. The large surface area and the flexibility in structures make them attractive candidates for use as adsorbents for OCM separation.
c) Polymeric Resins – Ion exchange resins are polymers that can exchange specific ions within the polymer with ions in a gas stream, thus resulting in adsorption. These polymeric adsorbents have the advantage of being robust, cheap and have a fixed pore structure in a three-dimensional matrix. Hence development of adsorptive routes using these materials for separation of OCM effluent offers the possibility of an attractive alternative to cryogenic separation.

Separation of gases using these adsorbents can be classified as either purification or bulk separation. These processes are regenerative, and are operated in a cyclic process. The bed is loaded with the feed gas containing the adsorbate. When the bed is saturated, i.e., all of the adsorption capacity is used, it is regenerated and the adsorbate is desorbed. Typically, two beds are used, and operate out of phase, with one on adsorption and the other bed on desorption. The driving force provided for the adsorption-desorption cycles distinguish the processes into two major categories:

(a) Pressure Swing Adsorption (PSA): In a PSA process, the driving force for the adsorption-desorption cycle is the difference in operating pressure between the two cycles. Since the nature of the isotherm is such that adsorption capacity increases with an increase in pressure, the adsorption step is carried out at higher pressures, and desorption is carried out at low pressures.

(b) Temperature Swing Adsorption (TSA): In a TSA, temperature differences drive the adsorption-desorption cycle. Adsorption capacity decreases with increase in temperature. Hence adsorption is carried out at low temperatures, and regeneration of the bed is performed at high temperatures by flowing an adsorbate-free hot purge gas over the bed.

Typically, in both PSA and TSA processes, the direction of flow in adsorption and desorption modes are opposite one another. The difference between a PSA and a TSA is shown in Figure 6. The choice of use of an adsorbent bed in PSA mode vs a TSA mode depends on the shape of the isotherm, the working capacity of the adsorbent, the mass transfer coefficient as well as available process options for regeneration.

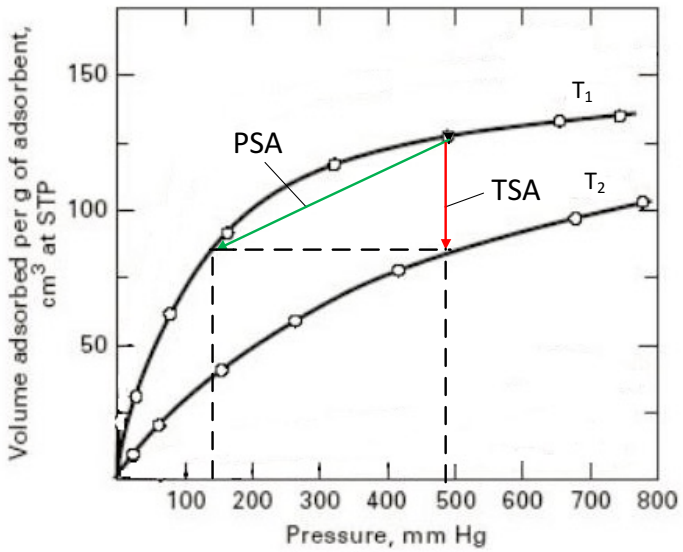

Figure 6: A sample adsorption isotherm showing driving forces for PSA (in green) and TSA (in red)

Membranes Based Separations

Membranes are another potential alternative approach to the cryogenic separation of gases. Since the first installation of a hydrogen separation in early 1980's, significant improvement in the quality of the membranes has been made, especially for air separation and CO_2 removal. Gases dissolve and diffuse in polymeric films under the influence of a pressure gradient resulting in establishment of a separation process based on differences in gaseous solubility and permeability across the membrane. The non-permeable molecules that remain in the feed stream side leave the membrane as retentate stream. Proper selection of the polymer membrane material is extremely important for ultimate performance of the gas separation.

Permeability and selectivity are the two main parameters that characterize the performance of the membrane material. They are connected to productivity and purity of the application. Glassy polymers are less permeable and more selective while rubbery polymers are more permeable and less selective.

Typical gas separation membrane module configurations with essential features is shown in Figure 7.

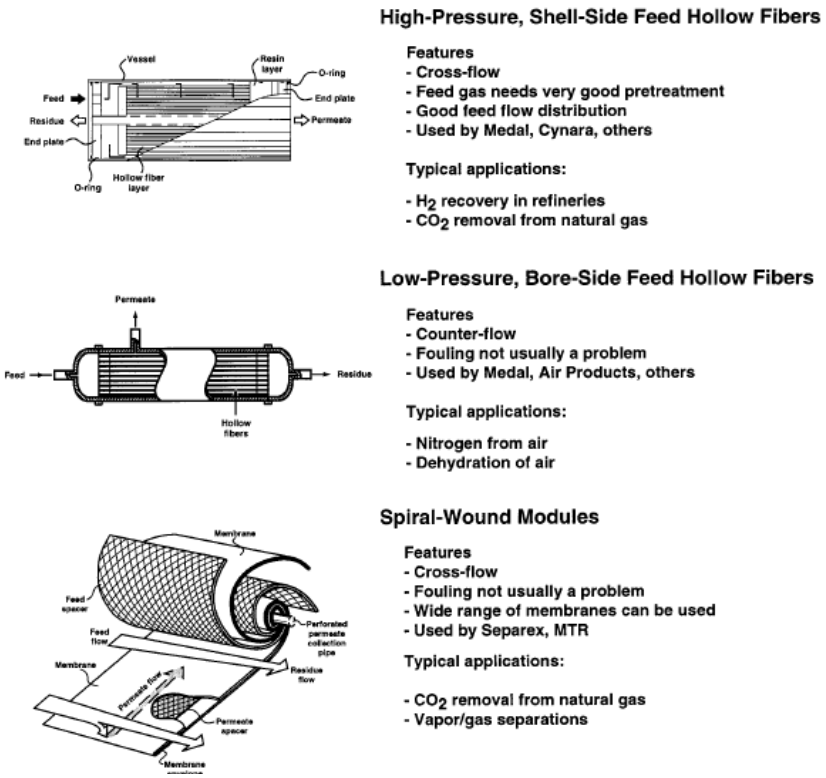

Figure 7: Principal gas separation membrane module configuration (Baker 2002)

Membranes can be made of different types of materials:

Polymeric membranes: These are largely used for their low initial costs and ability to be applied to various industries. Polymeric membranes are either rubbery or glassy depending on their glass transition temperatures. Glassy polymers result in less permeable but more selective membranes, while the rubbery polymers possess higher permeability and lower selectivity. Examples include polymers such as Polyether Sulfones (PES), which have more regular structures, higher bulk densities and elevated glass transition temperatures. These are considered dense films with good selectivity. Polysulfones (PSF) on the other hand have lower bulk densities and glass transition temperatures, being examples of rubbery polymers with high permeability. Polyvinylidene fluoride (PVDFs) are a class of highly non-reactive and pure thermoplastic having low glass transition temperature fluoropolymers exhibiting semi-crystallinity (containing both crystalline and amorphous phase). This unique tendency provides the polymer with high thermal stability, chemical resistance and flexibility making it a popular gas separation membrane polymer.

Inorganic Membranes: Zeolites and carbon molecular sieves are more selective than polymers for specific gas components, but have disadvantages such as difficulty to produce defect-free films, manufacturing costs, poor resistance to poisoning and stability.

Mixed Matrix Membranes: The combination of superior performance of inorganic materials with handling properties of the polymers is offered by Mixed Matrix Membranes (MMMs). In MMM, inorganic fillers are embedded within a polymer matrix provided a mixed matrix composite. Although MMMs have great

potential, crucial issues of homogenous dispersion and adhesion of the heterogeneous phases poses a challenge.

Membrane contactors: Membrane contactors are a new membrane-based concept where a hydrophobic microporous membrane operates as contact medium between a feed stream and an extracting phase. This approach takes advantage from the more efficient mass transfer achievable through the membrane pores with respect to conventional packing absorption towers.

MOF Membranes: Introduction of MOFs into polymeric membranes has been studied for the last 5-7 years. The research is geared towards utilizing the advantages of materials of both phases: high flux of polymer membranes and high selectivity of metallic complex. MOFs could be a part of the thin layer membranes or a part of MMMs. Commercially available MOFs can be incorporated into a polymer matrix for selective separation of olefins from paraffins.

Facilitated Transfer Membranes:

Highly selective membranes typically tend to have poor permeability, while highly permeable membranes have low selectivity. Such a limitation of membranes is usually circumvented by using facilitated transport (FT) membranes. In FT process, passive diffusion down a concentration gradient is aided by the presence of a carrier agent that selectively and reversibly binds with the targeted compound in a complexation reaction, thereby providing another route across the membrane in addition to a solution-diffusion mechanism. FT membranes are being widely used in research and lately in industry to improve the permselectivity of the membrane. These membranes can use a supported liquid film on the membrane with the metal ion carrier dispersed in the liquid film, an ion exchange membrane – ions dispersed in a hydrophylic polymer membrane, dry solid polymer electrolyte membranes or a polymer membrane doped with MOF nanocrystals. An example of ethylene/ethane separation using FT membrane with Ag^+ ion is shown in Figure 8.

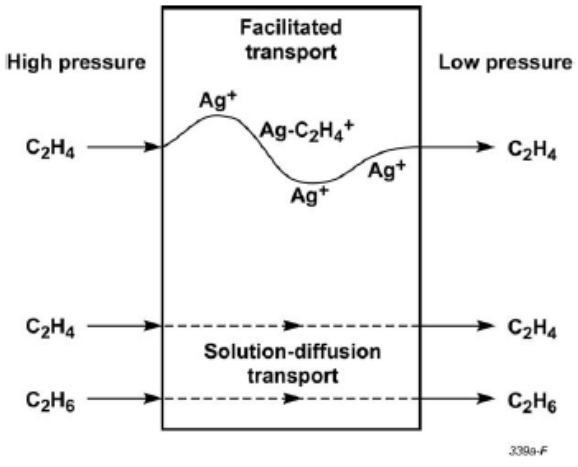

Figure 8: Facilitated transport of ethylene over ethane in a Ag+ dispersed membrane

Challenges with membranes

Aside from durability and stability of membranes, other drawbacks to membranes include film degradation, carrier poisoning, maintenance costs (associated with FT membranes). Some glassy polymers lose their gas selectivity and sometimes even productivity in presence of trace amounts of condensable hydrocarbons. Plasticization of the membrane layer by high acid gases (e.g. CO_2), partial pressure and temperature is also observed. Physical aging also occurs in polymers. This phenomenon is more significant and quick for thin films and it causes a generalized decrease of permeability and performance.

Engineering of the membrane systems faces different aspects ranging from membrane configuration to unit arrangement for optimal operational modes. In general, the durability and strength of the membrane to tolerate different feed compositions and conditions at commercial scale, will dictate their effective use.

CO_2 removal

There are many technologies available for CO_2 capture, such as from flue gases, natural gas, or from any process gas rich in CO_2. Various processes for post-combustion or pre-combustion capture can be used to reduce CO_2 emissions. The current OCM process utilizes an amine based absorption system for CO_2 removal, which is followed by use of a caustic scrubber to obtain high degree of separation. However, the main issues with an amine system is corrosion, solvent degradation, and above all, high energy requirement.

Gas Liquid Absorption: Several improved absorptions solvents have been explored in the past for CO_2 capture. These include solvents such as primary amines (e.g., MEA, DGA), secondary amines (e.g., DEA, DIPA), tertiary (e.g., MDEA, TEA), sterically hindered amines, chilled ammonia, potassium carbonate, and other compounds can be used to remove CO2 from process gases. Improved solvents, which can require less energy for regeneration of the solution, include the Benfield process and two stage diethanolamine process. Mixed or hybrid solvents such Sulfinol^{TM} (sulfolane, water, and amine), such as Sulfinol-M and Sulfinol-X can also be utilized. Physical absorption solvents used can include but are not limited to glycol dimethylethers (e.g., Selexol) and propylene carbonate.

Adsorption: Solid adsorbents, such as zeolites and activated carbon, can be used to separate CO_2 from gas mixtures. The temperature of the OCM process effluent will be the primary factor in determining whether to use a pre-combustion or post combustion capture material. If CO_2 is removed at high-temperature then the technology to utilize is magnesium oxide-based sorbent which can absorb at ~300°C and require regeneration at ~400°. At temperatures between 40° to 90°C post-combustion technologies can be used. These can be either sorbent- or solvent-based. Depending on how the stream is manipulated, it may have a low amount of water, in which case there could be an advantage in energy to utilizing a non-aqueous solvent for CO_2 removal. If a sorbent technology is preferred, a fluidized sorbent bed process utilizing molecular basket type sorbents can be used so long as the temperature of the stream is mild.

If the selectivity of the adsorbents is low, a hybrid system using an adsorbent based separation method can be used to separate bulk CO_2 followed by consuming the remaining CO_2 in a methanation reactor system, or by using a caustic scrubber to treat the remaining CO_2.

Membrane Systems: Many different types of membrane materials (e.g., polymeric, metallic, ceramic) can be used for CO_2 capture to preferentially separate CO_2 from a range of process streams. The main limitation of current membranes is the occurrence of severe plasticization of the membrane in the presence of high pressure CO_2. Due to excessive swelling of the polymer membrane upon exposure to CO_2, the performance (e.g., selectivity) can decrease significantly, thus reducing the purity of the CO_2 and consequently reducing the possibilities for reuse of the gas. However, recent research on new improved variety of membranes shows promising results. Novel work such as synthesizing zeolite-polymer composite membranes, polyvinyl amine membranes with amino acid salts for CO2 transport, use of spiral membranes that reduce gas leakage during separation are a few such examples. Polyionic liquid membranes can also be used for selective CO_2 separation. Poly RTILs can also be used to prevent the membrane from excessive swelling and deterioration of its performance at increased pressure and/or temperature.

Membrane and amine technologies can be combined to form a hybrid process to capture CO_2. Micro-porous hollow fiber membranes can be used for CO_2 separation using amine-based chemical absorption processes. Micro-porous membranes can be used in a gas-liquid unit where the amine solution is contacted with CO_2 containing gas. Using the membrane can lead to a reduction in the physical size and weight of the gas-liquid contacting unit.

The block flow diagram in Figure 9 captures all the different alternative technologies explored for the corresponding process areas highlighted. The alternative technologies in green represent the technologies that were studied to identify the ones for suitable further detailed study and experimentation.

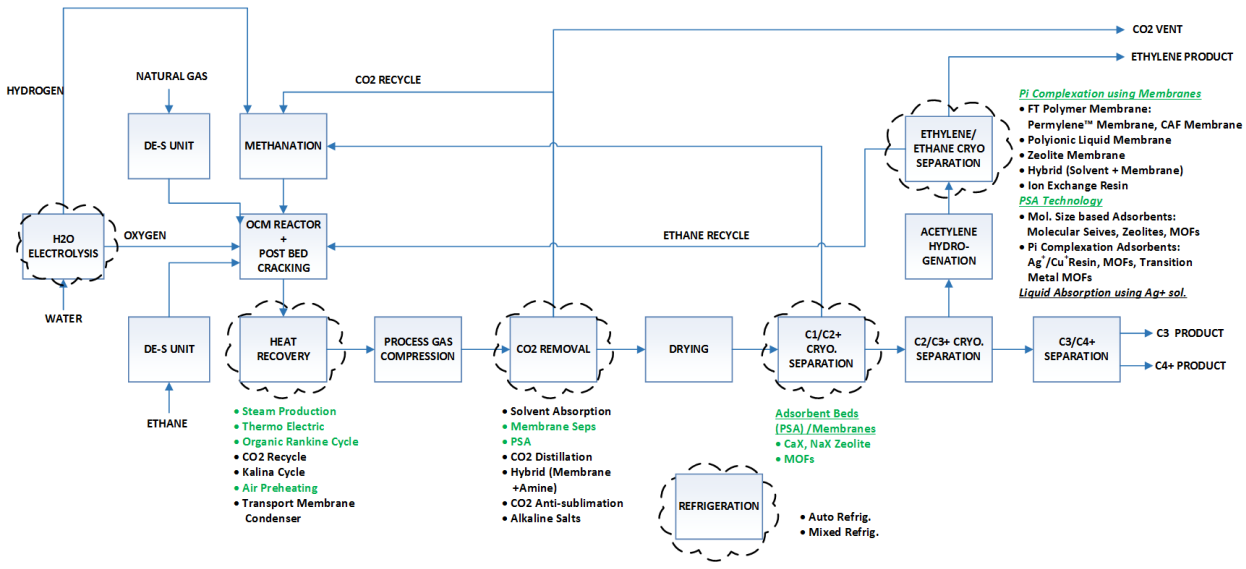

Figure 9: Alternative technologies explored for each process area

Selection Criteria for detailed study

The following criteria was used to select the technologies for detailed research and experimentation:

- Substantial evidence from literature for the effectiveness of the material/technology
- Applicability of the technology for the composition of the OCM process effluent and the operating conditions
- Applicability for use at small-scale capacities being studied
- Stage of commercialization or potential for commercialization (for the scales at which ethylene production is studied)
- Energy consumption for the technology – effect on operating costs
- Effect on capital costs
- Durability, lifetime and guarantees associated with the technology/material
- Modularization capabilities for different scales of production

Based on the above criteria, PSA/TSA based technology was found to be the most promising for further exploration.

Working mechanism of PSA/TSA technology

The separation of components in a gas stream is mainly the result of a difference in the affinity or equilibrium characteristics of an adsorbent. In order to assess the ability of a material to perform as an adsorbent for separations, several parameters are defined and evaluated. In addition to the process parameters, factors that affect the cost of the system such as adsorbent synthesis cost and scale up are also considered.

- Adsorption Capacity/Uptake Capacity/Loading (q_i)

The loading or adsorption capacity, expressed in mmol/g adsorbent, refers to the amount of gas adsorbed by the adsorbent at a particular temperature and pressure. This characterizes the equilibrium behavior of the adsorbent. When the adsorbent is exposed to a pure component gas feed, measurements of the amount adsorbed forms the basis of the adsorption isotherm. The adsorption capacity of an adsorbent exposed to a multi-component gas feed represents the effect of co-adsorption as well. Loading is an important adsorbent characteristic since it determines the size of an adsorbent bed. Higher loadings on the adsorbent result in smaller bed sizes. Typically, loadings of 3 mmol/g or more indicate high surface area and high adsorption capacities.

- Working Capacity (Δq_i) and Separation Factor (SF)/working selectivity

Once the temperatures and pressures at which adsorption/desorption will be carried out are determined, the working capacity, Δq_i, for any gas component i, can be calculated as the difference in loading at the adsorption and desorption conditions. The working capacity determines the actual adsorption capacity during a process cycle. In the case of a gas mixture consisting of, say, two components 1 and 2, the ratio of the working capacities, $\Delta q_1/\Delta q_2$, is called the separation factor or the working selectivity of the adsorbent. A separation factor of 1 indicates that no separation of the gas mixture is possible under the chosen working conditions. An example of the working capacities is shown in Figure 10 for air separation (O_2/N_2) on a LiX (Lithium exchanged Type X zeolite) adsorbent.

N_2 Working Capacity: $\Delta q\_N_2 = (q1\text{-}q2)N_2$
O_2 Working Capacity: $\Delta q\_O_2 = (q1\text{-}q2)O_2$
Separation factor = Working Selectivity = $[\Delta q]N_2/[\Delta q]O_2$

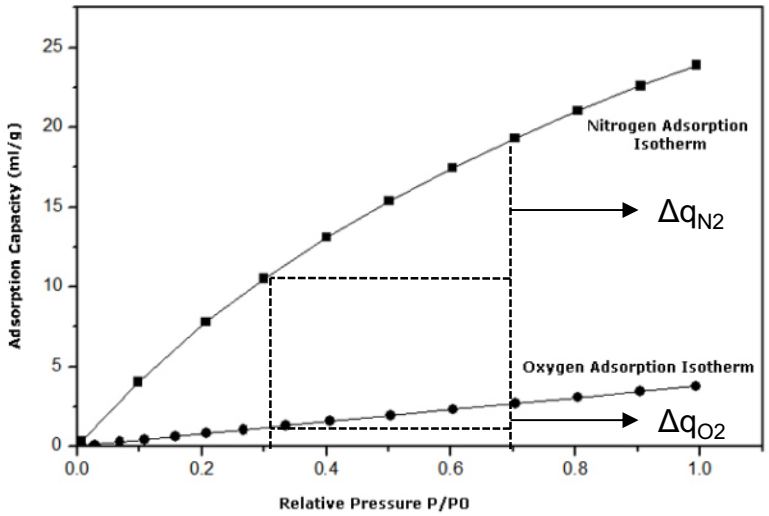

Figure 10: Example showing working capacities in a N_2/O_2 separation over LiX

- Breakthrough time (t_b)

Figure 11 represents a typical adsorption bed with feed as shown. The graphs on the left represent snapshots of concentration profiles of the adsorbate in the bed, while the graphs on the right represent the concentration of the adsorbate in the effluent. At time t_1 (>0) after the bed has been exposed to the feed gas containing the adsorbate, a mass transfer front is created. As the gases passes through the bed, the mass transfer front travels through the bed in the direction of flow leaving behind an equilibrium zone. In the equilibrium zone, the adsorbent is saturated at feed conditions, and no active mass transfer is taking place. The adsorption isotherms discussed earlier apply to this region of the bed. The mass transfer zone is the area of the bed in which adsorption is actively occurring. The mass transfer front moves at a rate slower than the linear gas velocity through the bed. As the mass transfer front moves through the bed, the concentration of the adsorbate in the product is zero/negligible. When the leading edge of the mass transfer front reaches the end of the bed, the adsorbate is detected in the product stream. The time at which this happens is called breakthrough time, t_b. At this stage, the bed can no longer be used for adsorption and must be regenerated. However, there is still a fraction of the bed that is unused though product purity cannot be maintained after $t=t_b$. At $t=t_e$, the exhaustion time, the concentration of the adsorbate in the effluent reaches the feed concentration.

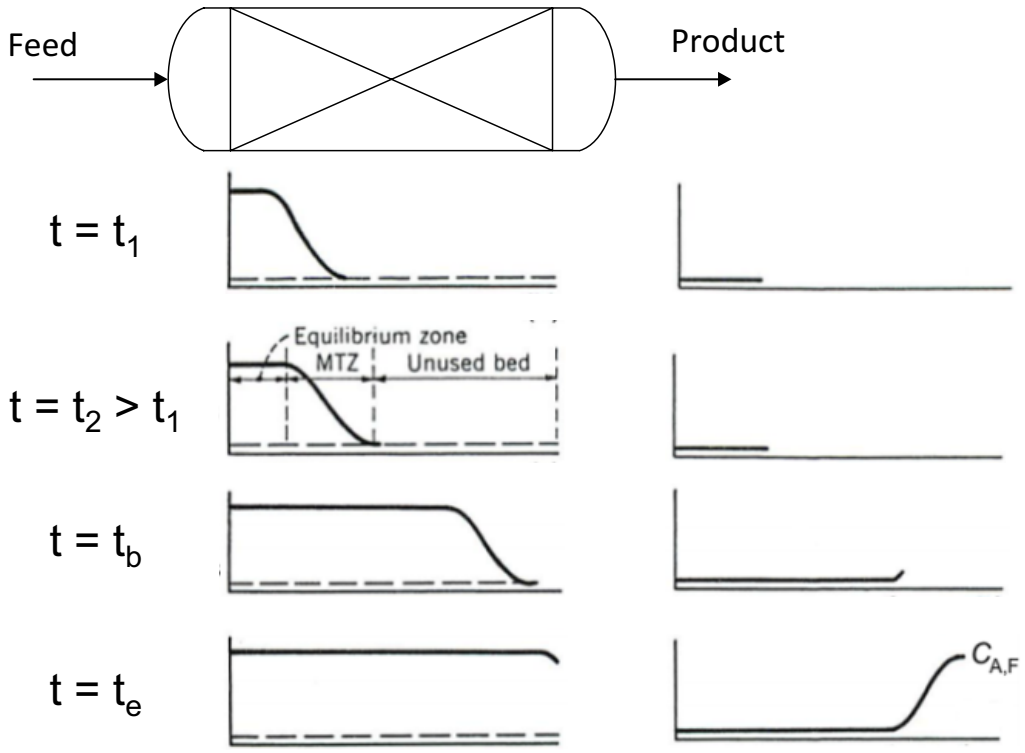

Figure 11: Dynamics of Adsorption - Concentration profile of adsorbate in the bed and in the effluent

Materials Screening & Performance Testing

Siluria partnered with RTI to perform synthesis of sorbents, material characterization and validation of sorbents (comparison of critical material parameters with the values reported in literature), development of adsorption isotherms (when not available from the literature) and finally breakthrough testing of the adsorbents at different pressures and temperatures. The breakthrough analyses were conducted using different feed mixtures.

Materials Screening

To enable OCM technology at small scale by replacing the cryogenic separation unit with adsorption based separation system, various adsorbent materials showing promise for selective ethylene adsorption were targeted and synthesized/purchased for testing. The following characteristics were identified as required criteria for the material:

- High capacity for ethylene at low partial pressure
- High IAST selectivity for ethylene
- Operation at moderate process conditions

- No adverse effect of most OCM effluent components

A comprehensive list of the materials which were considered is summarized in Table 1 and subsequently described in detail below. Figure 12 is a compilation of isotherms of few gas-adsorbent pairs.

Material	Reference
CaX Zeolite	(Hosseinpour et al. 2011)
Zorite (ETS-4)	(Pavel et al. 2002)
Cu_2(BTC)	(Martins et al. 2015)
Ag^+ exchanged Amberlyst 15 resin	(Yang and Kikkinides 1995)
ZIF-8	(Zhang et al. 2015)
Co_2(dobdc)	(Geier et al. 2013)
Fe_2(dobdc)	(E. D. Bloch et al. 2012)
Mg_2(dobdc)	(Geier et al. 2013)
UTSA-10	(He et al. 2014)
SB-MOF 2	(Plonka et al. 2016)

Table 1: Adsorbent materials considered for separation of OCM effluent

CaX zeolite is an ion exchanged version of Zeolite 13X, in which the pore size is narrowed due to substitution of calcium for sodium in the zeolite pore. Based on the isotherms it was determined to have less capacity for methane than ethane or ethylene. CaX was synthesized using a literature preparation starting with NaX zeolite. Ion exchange was performed in a calcium chloride solution over three exchange cycles and the resulting solid was filtered, washed, and dried. Isotherms for this material are available in Appendix 6.

Zorite (ETS-4) is a titanosilicate which has been reported for separation of methane from ethane. It is reported to be selective for methane up to 190°C with a selectivity (based on pure component isotherms) over C_2^+ of approximately 5 from 2.5-5 bar. It was synthesized using a mild solvo-thermal sol-gel method starting from titanium dioxide and sodium silicate. The as synthesized ETS-4 is considered Na-ETS-4 and is reported to be fairly unstable, but can be stabilized by exchange of strontium ions with sodium. In addition, dehydration at specific temperatures in the strontium exchanged ETS-4 narrows the channels formed by the eight –membered rings of the structure, and imparts C_1/C_{2+} selectivity, which can be lost due to excessive dehydration. Strontium exchange was accomplished by heating a slurry of Na-ETS-4 in three strontium chloride solutions with increased concentrations as described in the literature. Sr-ETS-4 has two-dimensional connectivity with continuous channels formed through the set of eight membered rings. Based

on the single-component isotherms, it is interpreted that methane can access the pores while C_{2+} is excluded, resulting in a fast breakthrough for C_1 over C_{2+}.

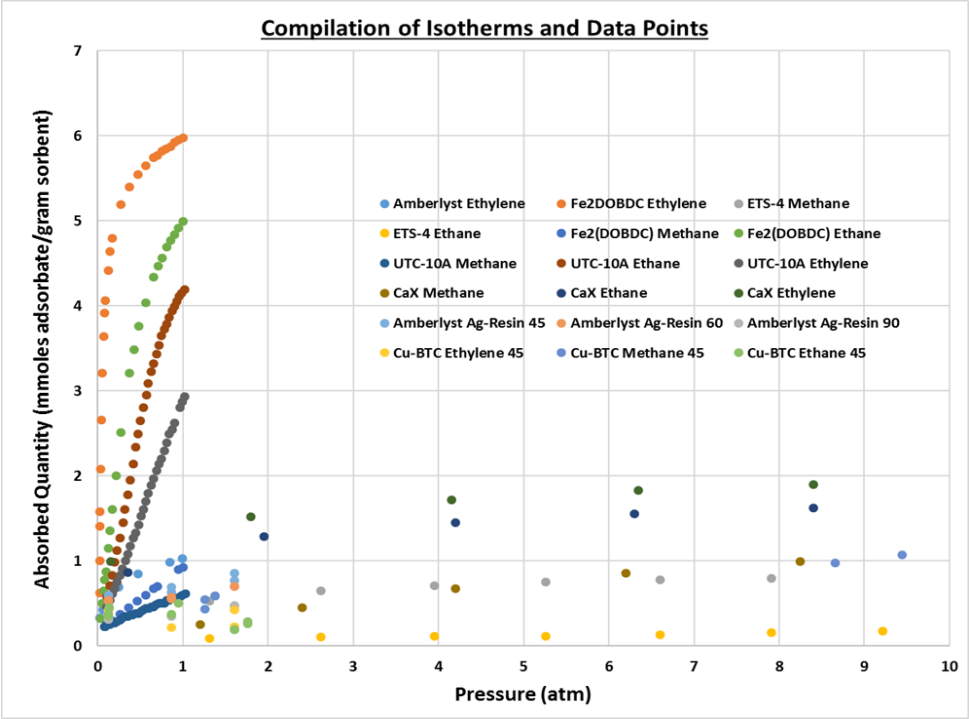

Figure 12: Isotherms for select sorbent materials

Fe_2(dobdc) is a MOF which has been reported to be selective for C_2^+ over methane. The pore size of the MOF is larger than the kinetic diameter of the C_1/C_{2+} components, so the separation is likely due to interaction of ethylene with one of the many iron metal sites which decorate the pore surface. The organic linker is available from reagent suppliers and is combined with iron salt in a solvothermal prep. Based on the isotherm measurement at ~45°C it can absorb as much as 18 wt% ethylene. While Fe_2(dobdc) shows a very promising ethylene capacity, the activation of Fe_2(dobdc) has been somewhat problematic in our hands. The batch-wise synthesis of the material seems to work well to get the structure as the characterization by FTIR and XRD of the synthesized material match reported information form the literature. However, BET surface area measurement indicated that the material did not have a high surface area as described in literature. Various measurements in the literature also disagree on the ethylene capacity of the material, and the discrepancies have been identified to be rooted in activation and removal of coordinated solvent molecules. The solvent molecules can be removed by solvent exchange, extraction, and evacuation techniques, and some success was achieved towards activation this past quarter. When the solvent molecules are removed the resulting MOF contains an unsaturated Fe(II) metal center, which can be rapidly oxidized. One particular extraction of solvent molecules from a 10-gram batch of Fe_2(dobdc) followed by exposure of the activated MOF to air during the drying process resulted in generation of a substantial exotherm and color change in the material consistent with formation of Fe(III).

Co_2(dobdc) is a MOF which is isoreticular to Fe_2(dobdc) but utilizing cobalt in the +2-oxidation state, which is more stable towards oxidation than iron, though still subject to slow oxidation over long periods of time. Co_2(DOBDC) has a slightly lower single component ethylene capacity, but still promising. This MOF was readily synthesized in 10-gram batches and tested in the fixed bed reactor. Isotherms for this material are available in Appendix 7.

Cu_2(BTC) is a MOF which is synthesized from terepthalic acid and copper nitrate. It is one of the earliest MOFs and is one of the few MOF materials offered commercially. It has been reported to have a high ethylene absorption capacity. It has been investigated heavily for methane storage at elevated pressures (35-65 bar) by the natural gas storage community due to the shape of micropores which readily accommodate CH_4 molecules at elevated pressure. It is thought to act as a π-sorbent towards ethylene.

ZIF-8 is a MOF structure composed of zinc metal centers which link imidazole ligands. It has a zeolitic cage structure, and is one of the most stable MOF materials with respect to temperature. It has been investigated for ethylene sorption. Under dry conditions, ZIF-8 has moderate ethylene capacity, however if a certain amount of water is present on the MOF (~40 wt%) then the ethylene capacity is enhanced. The OCM stream may contain water which could be used advantageously with the ZIF-8 MOF in a compressed product stream.

SB-MOF-2 is a calcium-based MOF. It has an appreciable ethylene single-component capacity. The linker required for SB-MOF-2 synthesis is more expensive compared to others.

Mg_2(dobdc) a MOF which is isoreticular to Fe_2(dobdc) but utilizing magnesium in the +2-oxidation state. This material has very high capacity for CO_2, and good capacity for ethylene. This material was purchased in bench-scale testing quantity.

Ag^+ exchanged Amberlyst 15 resin: Amberlyst 15, the substrate, is a functionalized, porous polystyrene cross-linked with 20% divinyl benzene. Exchange of H^+ by Ag^+ is performed on the substrate. The resulting material has much higher ethylene adsorption capacity than the base resin, whereas ethane capacity remains low.

UTSA-10 is a homologue of MOF-5, which is a prototypical MOF consisting of a cubic framework built from Zn4O clusters connected via benzenedicarboxylates. UTSA-10, is assembled from a readily available dicarboxylate, namely, 2-methylfumarate. Activated UTSA-10a shows a good potential for the separation of methane from C2 hydrocarbons at room temperature.

Experiment Equipment

The equipment used for testing of the absorbents was an automated fixed bed system equipped with an online RGA mass spectrometer for effluent gas analysis. A combination of pure component gases and certified standard gas mixtures were mixed using mass flow controllers to achieve the desired influent gas composition. The simulated OCM product gas stream was directed to the adsorbent bed during breakthrough tests using a series of selection valves. The adsorbent was maintained at desired temperature and pressure. After the adsorption step, a purge gas was directed to the adsorbent bed for

desorption. A slipstream directly after the adsorber was used for online gas analysis. Figure 13 is a simplified process flow diagram of the apparatus.

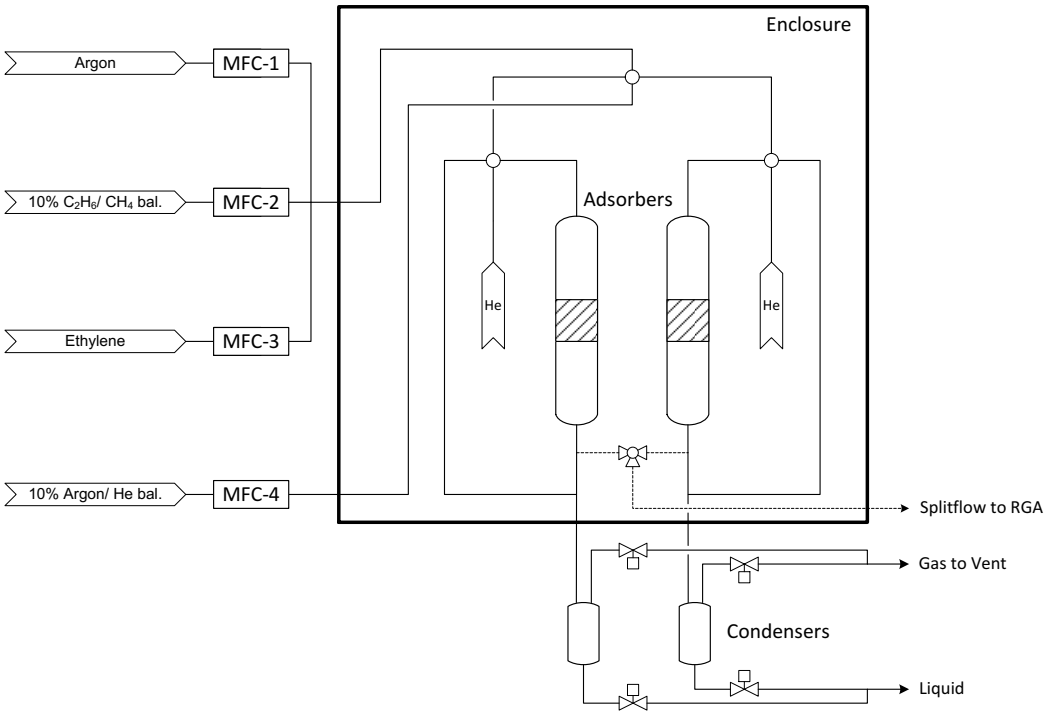

Figure 13: Simplified process flow diagram of automated fixed bed test system for evaluating absorbants

Preliminary breakthrough testing of CaX, Cu-BTC, Ag+/Amberlyst, Zn-SiF6, Sr/ETS-4, Co_2(dobdc), Mg_2(dobdc), and ZIF-8 was done in the automated fixed bed system. Table 2 is a summary of the qualitative performance of the materials.

	Material	Remarks
1.	CaX Zeolite	Showed highest selectivity for CO_2, followed by ethylene
2.	Zorite	Low separation was observed
3.	Cu_2 (BTC)	Some separation was observed but not as good as CaX
4.	Ag+ exchanged Amberlyst 15 resin	Reduction in Ag+ due to the presence of hydrogen
5.	Zn-SiF6	No noticeable separation was observed
6.	ZIF-8	No noticeable separation was observed
7.	Co_2(dobdc)	Showed highest selectivity for ethylene
8.	Mg_2(dobdc)	Showed highest selectivity for CO_2, followed by ethylene

Table 2: Performance summary of the materials studied

Comprehensive Adsorption & Desorption Performance Testing

The gas component breakthrough tests for the adsorbents were performed initially with three different feed gas mixtures as described in Table 3. First, Feed Mix 1 was used to evaluate the materials for separating ethane from methane. Next, ethylene was added in Feed Mix 2 to evaluate the separation efficiency of ethylene and ethane. Lastly, the effect of CO, CO_2 and hydrogen was evaluated on the separation of methane, ethane, and ethylene in Feed Mix 3. Argon was used as an internal standard for quantification. Breakthrough time in minutes and gas species capacity in mmol/g was determined for each material. Breakthrough is defined as the first sign of detection of a given species above the noise level of the mass spectrometer, typically about 100 ppm. Breakthrough time is defined as the time it takes for a given component to break through the adsorbent bed and show up on the analytics from the start of the adsorption step minus any delay time due to dead volume. The capacity is quantified by multiplying the gas species feed flow rate in mmol/min by the breakthrough time in minutes divided by the adsorbent mass in grams. This does not include any amount that may continue to adsorb between breakthrough and the end of the adsorption step after the bed reaches equilibrium with the feed.

	Feed Mix 1	Feed Mix 2	Feed Mix 3
Hydrogen			0.109
Argon	0.100	0.100	0.100
CO			0.018
CO2			0.043
Methane	0.818	0.750	0.608
Ethylene		0.075	0.061
Ethane	0.082	0.075	0.061

Table 3: Feed gas mixtures in mole fraction for material screening (representative of OCM Effluent)

Testing started with a series of space velocity screening tests at a fixed temperature and pressure to find a measurable breakthrough time for the first material. Once a reasonable breakthrough time was determined, the corresponding feed flow rate was used to measure the breakthrough time response for each component as a function of temperature and pressure. A desorption step was used after each adsorption test to ensure the sorbent is degassed prior to each adsorption step. Based on the equipment capabilities and gas composition requirements, an influent flow on the order of 300 sccm was determined to be optimal to run at the desired experiment conditions.

Through the material screening testing, it became evident that pressure had the greatest impact on adsorption capacity and that pressure swing adsorption would be more ideal configuration for a commercial process. Therfore, down selected sorbents were tested at more targeted temperatures (35 – 45°C) for the process and with moderate pressures (20 – 60 psig) during adsorption and low pressures (3 – 10 psig) during desorption.

CaX Zeolite

Feed Mix 1 and Feed Mix 2 breakthrough testing of CaX zeolite was performed with a total feed flow rate of 300 SCCM over 20.0 g of adsorbent. The experimental conditions for Feed Mix 1 is listed in Table 4Table 4. Selected breakthrough times and adsorption capacities determined with Feed Mix 1 are shown in Table 5. More detailed results are available in Appendix 1. The results show capacity generally decreased with increasing temperature for all gas components while pressure only had a significant positive effect on capacity from 10 to 155 psig. There was a significant increase in methane (0.19 – 1.02 mmol/g) and ethane (0.24 – 0.46 mmol/g) capacity from 10 psig to 155 psig at 60°C.

	Adsorption	Desorption

Factor	Low	Mid	High	
Pressure (psig)	10	155	300	const.
Temperature (°C)	60	180	300	300

Table 4: Experimental conditions for testing CaX zeolite with Feed Mix 1

Conditions		Breakthrough time (min)			Capacity (mmol/g)			
Temp. (°C)	Press. (psig)	Methane	Argon	Ethane	Methane	Argon	Ethane	Total
60	10	0.4	0.2	4.8	0.19	0.01	0.24	0.44
180	10	0.0	0.0	0.5	0.00	0.00	0.03	0.03
60	155	2.2	1.5	9.0	1.11	0.09	0.46	1.66
180	155	0.7	0.5	1.8	0.37	0.03	0.09	0.50
60	300	2.2	1.8	8.4	1.11	0.11	0.43	1.65
180	300	1.1	0.7	2.7	0.56	0.05	0.14	0.74

Table 5: Summary of breakthrough times and adsorption capacities for CaX zeolite with Feed Mix 1

Since very low capacities for methane and ethane were observed over CaX at 300°C, the temperature was reduced for testing with ethylene in Feed Mix 2. The temperature and pressure conditions for testing CaX zeolite with Feed Mix 2 is listed in Table 6. A summary of breakthrough times and adsorption capacities for CaX with Feed Mix 2 are listed in Table 7. More detailed results are available in Appendix 2.

With the addition of ethylene in the feed mixture, the general trends remained. Capacity generally decreased with increasing temperature for all gas components, whereas capacity generally increased with pressure. Significant separation of ethane and ethylene was observed with delta breakthrough times ranging from 16 to almost 20 minutes and ethylene capacity of 1.2 mmol per gram of sorbent.

	Adsorption			Desorption
Factor	Low	Mid	High	
Pressure (psig)	10	155	300	const
Temperature (°C)	60	120	180	250

Table 6: Experimental conditions for testing CaX zeolite with Feed Mix 2

Conditions		Breakthrough time (min)				Capacity (mmol/g)				
Temp. (°C)	Press. (psig)	Methane	Argon	Ethane	Ethylene	Methane	Argon	Ethane	Ethylene	Total
60	10	0.6	0.2	4.4	21.9	0.27	0.01	0.21	1.02	1.50
120	10	0.0	0.0	1.5	13.9	0.00	0.00	0.07	0.65	0.72
60	155	1.4	0.6	7.0	23.2	0.63	0.04	0.32	1.08	2.07
120	155	0.2	0.0	2.5	15.5	0.09	0.00	0.12	0.72	0.93
60	300	1.4	1.4	6.2	25.7	0.63	0.08	0.29	1.20	2.20
120	300	0.8	1.0	3.7	17.8	0.36	0.06	0.17	0.83	1.42

Table 7: Summary of breakthrough times and adsorption capacities for CaX zeolite with Feed Mix 2

The material was further tested with Feed Mix 3. Adsorption capacities are listed in Table 10. Representative breakthrough curves are shown in Figure 14. The addition of CO_2 in Feed Mix 3 reduced the capacity for ethylene from about 1.1 to 0.66 mmol/g due to competitive adsorption at 60 °C and 155 psig. CaX had very low capacity for CO and H_2 indicating that these gases have negligible impact on the adsorption of ethylene.

	Adsorption			Desorption
Factor	Low	Mid	High	
Pressure (psig)	---	155	---	const
Temperature (°C)	45	60	120	120

Table 8. Adsorption conditions for testing CaX with Feed Mix 3

Conditions		Breakthrough time (min)						
Temp. (°C)	Press. (psig)	Methane	Argon	Ethane	Hydrogen	Ethylene	CO	CO2
45	155	1.5	1.2	7.0	0.4	17.0	1.7	17.6
60	155	1.2	1.0	6.4	0.0	15.9	1.5	16.6
120	155	0.6	0.6	2.9	0.0	8.7	0.8	8.5

Table 9. Breakthrough times for CaX with Feed Mix 3

Conditions		Capacity (mmol/g)							
Temp. (°C)	Press. (psig)	Methane	Argon	Ethane	Hydrogen	Ethylene	CO	CO2	Total
45	155	0.64	0.08	0.29	0.03	0.71	0.02	0.51	1.76
60	155	0.48	0.07	0.26	0.00	0.66	0.02	0.49	1.49
120	155	0.24	0.04	0.12	0.00	0.36	0.01	0.25	0.77

Table 10. Capacity for CaX with Feed Mix 3

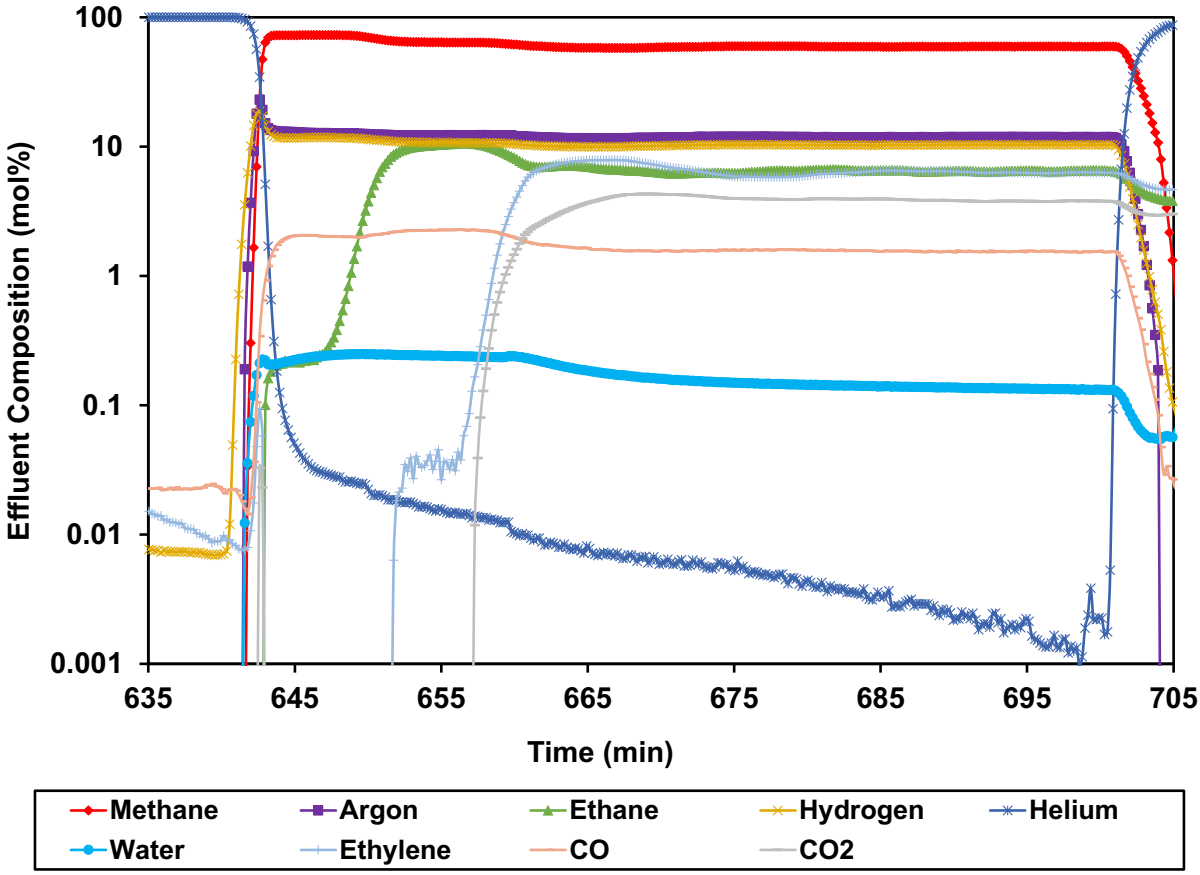

Figure 14. Breakthrough curves of Feed Mix 3 with CaX zeolite at 60°C, 155 psig

Cu-BTC

Feed Mix 1 and Feed Mix 2 breakthrough testing of Cu-BTC was performed with a total feed flow rate of 300 SCCM over 16.5g of adsorbent. The experiment conditions for Feed Mix 1 and Feed Mix 2 are listed in Table 11**Error! Reference source not found.**. Summary of breakthrough times and adsorption capacities determined with Feed Mix 1 are listed in Table 12. More detailed results are available in Appendix 3.

	Adsorption			Desorption
Factor	**Low**	**Mid**	**High**	
Pressure (psig)	10	155	300	const
Temperature (°C)	45	60	90	120

Table 11: Experiment conditions for testing Cu-BTC with Feed Mix 1 and Feed Mix 2

Conditions		Breakthrough time (min)			Capacity (mmol/g)			
Temp. (°C)	**Press. (psig)**	**Methane**	**Argon**	**Ethane**	**Methane**	**Argon**	**Ethane**	**Total**
45	10	1.0	0.8	7.4	0.59	0.06	0.45	1.10
60	10	0.8	0.6	6.4	0.48	0.04	0.39	0.91
45	155	1.7	1.5	8.1	1.07	0.12	0.50	1.69
60	155	1.7	1.5	7.5	1.07	0.12	0.46	1.65
45	300	1.5	1.5	4.6	0.95	0.12	0.29	1.35
60	300	1.4	1.4	3.7	0.83	0.10	0.23	1.16

Table 12: Summary of breakthrough times and adsorption capacities for Cu-BTC with Feed Mix 1

Breakthrough times and adsorption capacities determined with Feed Mix 2 are listed in Table 13. More detailed results are available in Appendix 4.

Conditions		Breakthrough time (min)				Capacity (mmol/g)				
Temp. (C°)	**Press. (psig)**	**Methane**	**Argon**	**Ethane**	**Ethylene**	**Methane**	**Argon**	**Ethane**	**Ethylene**	**Total**
45	10	1.0	0.6	6.6	7.4	0.54	0.04	0.37	0.41	1.37
60	10	0.8	0.6	5.8	6.6	0.44	0.04	0.33	0.37	1.18
45	155	1.7	1.5	6.6	7.5	0.98	0.12	0.37	0.42	1.89
60	155	1.7	1.5	6.4	7.2	0.98	0.12	0.36	0.40	1.86
45	300	1.5	1.5	3.5	3.9	0.87	0.12	0.20	0.22	1.40
60	300	1.4	1.5	3.3	3.9	0.76	0.12	0.19	0.22	1.28

Table 13: Summary of breakthrough times and adsorption capacities for Cu-BTC with Feed Mix 2

Conditions		Breakthrough time (min)			Capacity (mmol/g)			
Temp. (°C)	Press. (psig)	Methane	Argon	Ethane	Methane	Argon	Ethane	Total
45	10	1.0	0.8	7.4	0.59	0.06	0.45	1.10
60	10	0.8	0.6	6.4	0.48	0.04	0.39	0.91
45	155	1.7	1.5	8.1	1.07	0.12	0.50	1.69
60	155	1.7	1.5	7.5	1.07	0.12	0.46	1.65
45	300	1.5	1.5	4.6	0.95	0.12	0.29	1.35
60	300	1.4	1.4	3.7	0.83	0.10	0.23	1.16

Table 12: Summary of breakthrough times and adsorption capacities for Cu-BTC with Feed Mix 1

Capacities of each gas component generally decreased with increasing temperature. Methane capacity significantly increased with pressure, whereas ethane and ethylene capacities decreased with increased pressure, presumably because of reduced selectivity at high pressure. Cu-BTC demonstrated good separation of C1 and C2 hydrocarbons, however, ethane and ethylene separation was not as good as CaX zeolite.

Breakthrough tests of Feed Mix 3 were performed over 14.9 g of Cu-BTC with a total feed flow rate of 300 SCCM. The adsorption conditions used for testing is listed in **Error! Reference source not found.**. Breakthrough times are listed in Table 15. Adsorption capacities are listed in Table 16. Representative breakthrough curves are shown in Figure 15. The addition of CO_2 in Feed Mix 3 reduced the capacity for ethylene from about 0.4 to 0.2 mmol/g due to competitive adsorption at 60 °C and 155 psig.

	Adsorption			Desorption
Factor	Low	Mid	High	
Pressure (psig)	---	155	---	const
Temperature (°C)	45	60	120	120

Table 14. Adsorption conditions for testing Cu-BTC with Feed Mix 3

Conditions		Breakthrough time (min)						
Temp. (°C)	Press. (psig)	Methane	Argon	Ethane	Hydrogen	Ethylene	CO	CO2
45	155	1.2	1.2	2.9	0.4	5.2	2.9	2.3
60	155	1.2	1.2	2.3	0.4	4.1	3.7	2.5
120	155	0.8	0.8	1.7	0.2	3.9	4.8	1.2

Table 15. Breakthrough times for Cu-BTC with Feed Mix 3

Conditions		Capacity (mmol/g)							
Temp. (°C)	Press. (psig)	Methane	Argon	Ethane	Hydrogen	Ethylene	CO	CO2	Total
45	155	0.59	0.10	0.15	0.04	0.26	0.04	0.08	1.17
60	155	0.59	0.10	0.12	0.04	0.21	0.05	0.09	1.10
120	155	0.39	0.06	0.09	0.02	0.20	0.07	0.04	0.83

Table 16. Capacity for Cu-BTC with Feed Mix 3

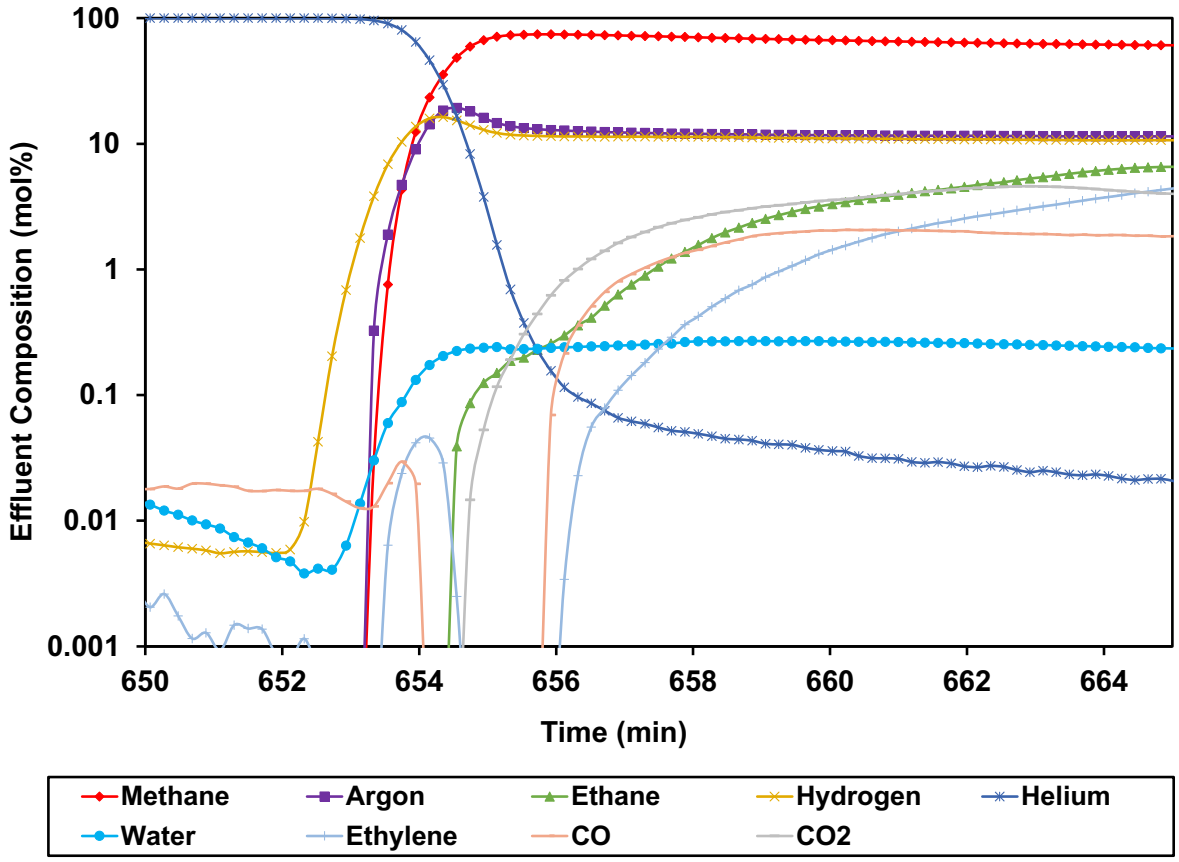

Figure 15. Breakthrough curves of Feed Mix 3 with Cu-BTC at 60°C, 155 psig

Ag+/Amberlyst

Breakthrough testing of Ag+/Amberlyst was performed starting with Feed Mix 2 since it was expected to perform as an olefin/paraffin separator. Testing was done with a total feed flow rate of 300 SCCM over 17.9g of adsorbent. The experiment conditions for Feed Mix 2 is listed in Table 17. Summary of breakthrough times and adsorption capacities determined with Feed Mix 2 are listed in Table 18. More detailed results are available in Appendix 5. Ag+/Amberlyst showed good ethylene capacity and performed as expected by separating ethylene from methane and ethane.

	Adsorption			Desorption
Factor	**Low**	**Mid**	**High**	
Pressure (psig)	10	155	300	const
Temperature (°C)	45	60	90	100

Table 17. Experiment conditions for testing Ag+/Amberlyst with Feed Mix 2

Conditions		Breakthrough time (min)				Capacity (mmol/g)				
Temp. (°C)	**Press. (psig)**	**Methane**	**Argon**	**Ethane**	**Ethylene**	**Methane**	**Argon**	**Ethane**	**Ethylene**	**Total**
45	10	0.0	0.0	0.0	11.6	0.00	0.00	0.00	0.60	0.60
60	10	0.0	0.0	0.0	10.3	0.00	0.00	0.00	0.53	0.53
45	155	0.0	0.0	0.4	12.2	0.00	0.00	0.02	0.63	0.65
60	155	0.0	0.0	0.4	11.0	0.00	0.00	0.02	0.57	0.59
45	300	0.0	0.0	0.4	14.9	0.00	0.00	0.02	0.77	0.79
60	300	0.0	0.0	0.4	13.5	0.00	0.00	0.02	0.70	0.72

Table 18: Summary of breakthrough times and adsorption capacities for Ag+/Amberlyst with Feed Mix 2

Breakthrough tests of Feed Mix 3 were performed over 15.4 g of Ag+/Amberlyst with a total feed flow rate of 300 SCCM. The adsorption conditions used for testing is listed in Table 19. Breakthrough times are listed in Table 20. Adsorption capacities are listed in Table 21. Representative breakthrough curves are shown in Figure 16. The addition of CO_2 in Feed Mix 3 reduced the capacity for ethylene from about 0.56 to 0.37 mmol/g due to competitive adsorption at 60 °C and 155 psig.

	Adsorption			Desorption
Factor	**Low**	**Mid**	**High**	
Pressure (psig)	---	155	---	const
Temperature (°C)	45	60	80	80

Table 19. Adsorption conditions for testing Ag+/Amberlyst with Feed Mix 3

Conditions		Breakthrough time (min)						
Temp. (°C)	Press. (psig)	Methane	Argon	Ethane	Hydrogen	Ethylene	CO	CO2
45	155	0.2	0.4	0.4	0.0	8.1	1.4	1.2
60	155	0.2	0.4	0.4	0.0	7.5	1.2	1.0
80	155	0.2	0.4	0.4	0.0	6.0	0.6	0.6

Table 20. Breakthrough time for Ag+/Amberlyst with Feed Mix 3.

Conditions		Capacity (mmol/g)							
Temp. (°C)	Press. (psig)	Methane	Argon	Ethane	Hydrogen	Ethylene	CO	CO2	Total
45	155	0.09	0.03	0.02	0.00	0.40	0.02	0.04	0.56
60	155	0.09	0.03	0.02	0.00	0.37	0.02	0.03	0.53
80	155	0.09	0.03	0.02	0.00	0.29	0.01	0.02	0.45

Table 21. Capacity for Ag+/Amberlyst with Feed Mix 3.

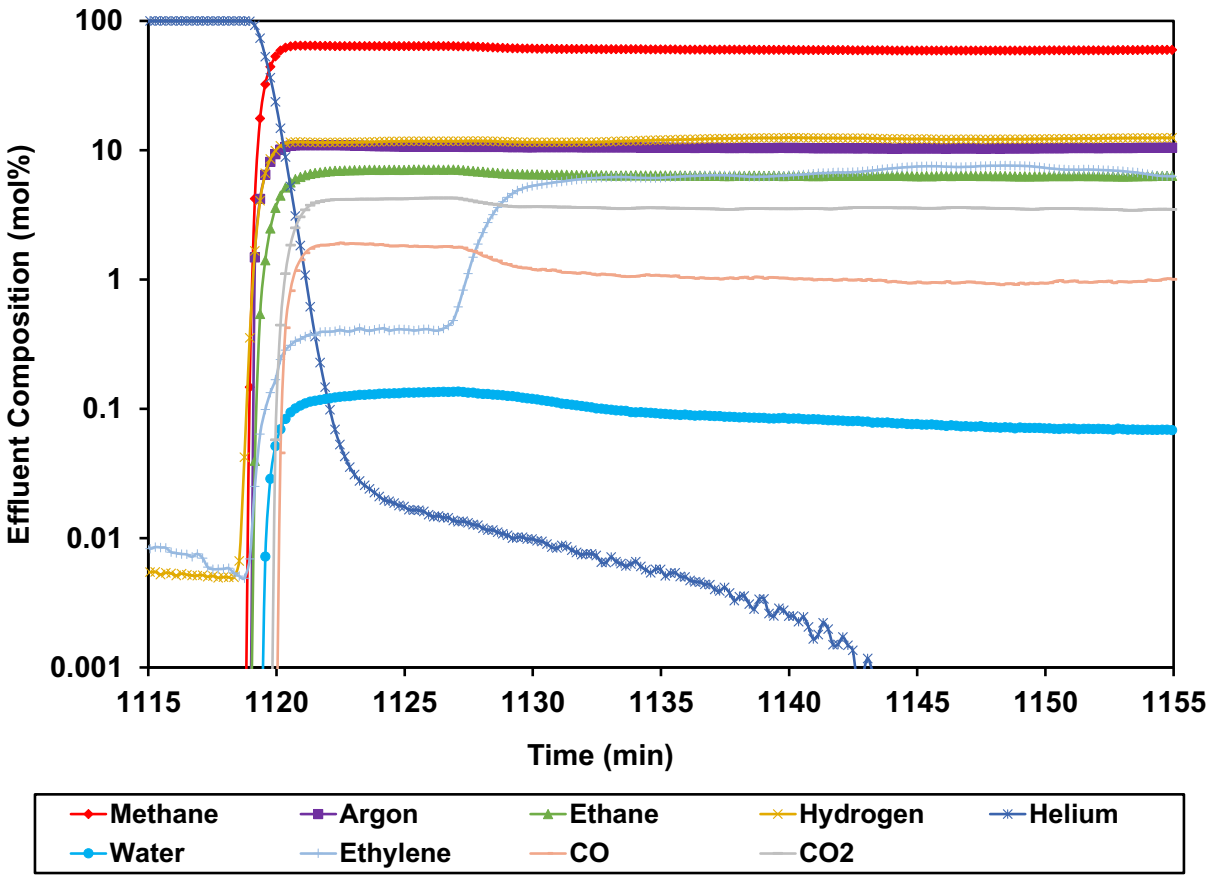

Figure 16. Breakthrough curves of Feed Mix 3 with Ag+/Amberlyst at 45°C, 155 psig

TPR testing done on Ag+/Amberlyst showed reduction with hydrogen at temperatures above 70°C. Since the OCM effluent has considerable amount of hydrogen, Ag+/Amberlyst was dropped from further consideration.

Zn-SiF6

Zn-SiF6 presented a challenge for testing in the automated fixed bed reactor system. Volatile material was driven off the adsorbent during the standard drying step at 120 °C and condensed downstream resulting in a blockage in the flow path. The Zn-SiF6 was removed from the reactor and dried in a vacuum oven at 120 °C for 1.5 hrs to drive off any remaining volatile material. After this adsorbent treatment process, the system experienced another blockage during the drying step. Another experiment was attempted at 45 °C without a drying step and the experiment could complete without a blockage, however, no measurable separation was observed.

Sr/ETS-4

Sr/ETS-4 was tested at 45 and 120°C at 10 psig, and at 45, 90, and 120°C at 155 psig and 300 psig. Each set of conditions were tested with Feed Mix 1 and no measurable separation was observed between methane and ethane. Each condition was also tested with Feed Mix 2. No separation was observed at low pressures, and very minimal separation was observed with ethylene at the highest pressures. Since this material had such low performance, Feed Mix 3 was not tested.

Co_2(dobdc)

Breakthrough tests of Feed Mix 2 and Feed Mix 3 were performed over 9.58 g of Co_2(dobdc) with a total feed flow rate at 300 SCCM. The experiment conditions used for testing with Feed Mix 2 and Feed Mix 3 are listed in Table 22 and Table 23. Breakthrough times and adsorption capacities are listed in Table 24, Table 25, and Table 26. A representative breakthrough curve for adsorption at 45 °C and 155 psig is shown in Figure 17.Figure 17.

	Adsorption			Desorption
Factor	**Low**	**Mid**	**High**	
Pressure (psig)	10	155	300	const
Temperature (°C)	45	---	120	120

Table 22. Adsorption conditions for testing Co_2(dobdc) with Feed Mix 2

	Adsorption			Desorption
Factor	**Low**	**Mid**	**High**	
Pressure (psig)	---	155	---	const
Temperature (°C)	45	---	120	120

Table 23. Adsorption conditions for testing Co_2(dobdc) with Feed Mix 3

Co_2(dobdc) showed the highest capacity for ethylene than any material tested reaching 3.2 mmol/g at 45°C and 155 psig with Feed Mix 2. However, it also has a high capacity for methane (2.3 mmol/g) and ethane (1.1 mmol/g) under the same conditions. On the other hand, this material would be favorable in a pressure swing adsorption process given the working capacity is 1.3 mmol/g for ethylene between 10 and 155 psig at 45°C with Feed Mix 2. The addition of CO, CO_2 and hydrogen in Feed Mix 3 reduced the ethylene capacity to 2.2 mmol/g at 45°C and 155 psig.

Conditions		Breakthrough time (min)				Capacity (mmol/g)				
Temp. (°C)	Press. (psig)	Methane	Argon	Ethane	Ethylene	Methane	Argon	Ethane	Ethylene	Total
45	10	0.4	0.2	3.3	19.3	0.38	0.03	0.32	1.88	2.59
45	10	0.6	0.2	3.5	20.9	0.56	0.03	0.34	2.03	2.95
45	10	0.4	0.2	3.5	21.3	0.38	0.03	0.34	2.06	2.80
120	10	0.0	0.0	0.4	2.9	0.00	0.00	0.04	0.28	0.32
120	10	0.0	0.0	0.6	2.9	0.00	0.00	0.06	0.28	0.34
45	155	2.3	2.1	11.4	32.9	2.25	0.28	1.11	3.19	6.82
120	155	1.4	1.2	4.3	12.4	1.31	0.15	0.41	1.20	3.08
45	300	4.3	4.3	7.7	19.5	4.13	0.55	0.75	1.89	7.32

Table 24. Breakthrough time and adsorption capacities for Co_2(dobdc) with Feed Mix 2

Conditions		Breakthrough time (min)						
Temp. (°C)	Press. (psig)	Methane	Argon	Ethane	Hydrogen	Ethylene	CO	CO2
45	155	2.3	2.3	11.0	1.0	28.2	18.8	11.4
45	155	2.5	2.3	11.4	1.0	26.9	20.3	11.8
120	155	1.4	1.4	5.0	0.4	9.3	8.5	4.6
120	155	1.4	1.2	4.3	0.4	8.7	7.9	4.3

Table 25. Breakthrough time for Co_2(dobdc) with Feed Mix 3

Conditions		Capacity (mmol/g)							
Temp. (°C)	Press. (psig)	Methane	Argon	Ethane	Hydrogen	Ethylene	CO	CO2	Total
45	155	1.82	0.30	0.87	0.14	2.23	0.44	0.63	5.80
45	155	1.98	0.30	0.90	0.14	2.12	0.47	0.66	5.91
120	155	1.06	0.18	0.40	0.05	0.73	0.20	0.26	2.62
120	155	1.06	0.15	0.34	0.05	0.69	0.18	0.24	2.48

Table 26. Capacity for Co_2(dobdc) with Feed Mix 3

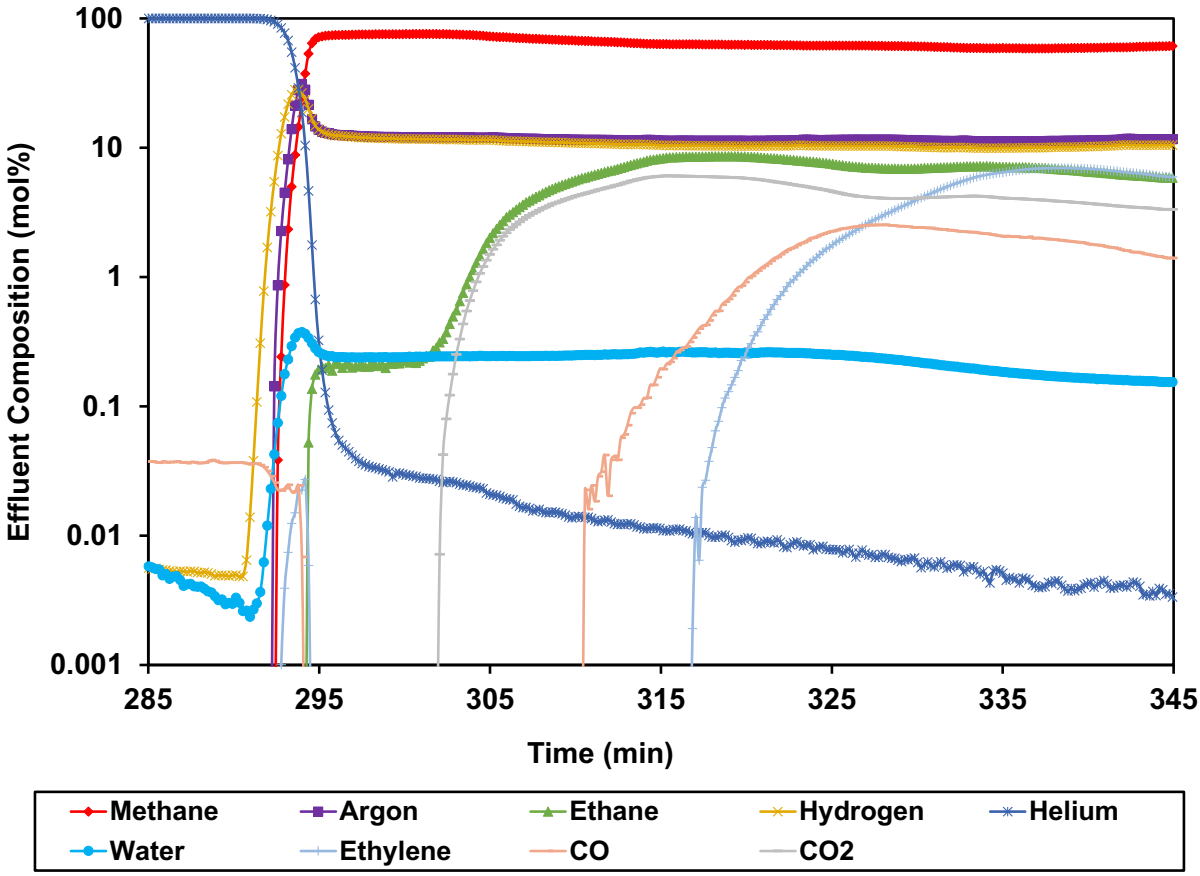

Figure 17. Breakthrough curves of Feed Mix 3 with Co2(dobdc) at 45°C, 155 psig

ZIF-8

ZIF-8 was tested with Feed Mix 2 at 25 °C and 10 psig without a drying step to retain the moisture level post synthesis. No measurable separation was observed between methane, ethane, or ethylene. Since no separation was observed, no further testing was performed.

Mg_2(dobdc)

Breakthrough testing was performed on Mg_2(dobdc) with Feed Mix 3 at 60 psig and 35°C. The bed mass for this test was 10.0 grams of Mg_2(dobdc). The total gas feed flow rate was 300 SCCM. After breakthrough, desorption testing with 90% ethane, and 10% argon at 3 psig was performed to determine product composition for experiments with Feed Mix 3. Table 27 and Table 28 show the breakthrough times and capacities based on the adsorption step until breakthrough. This material has a moderate capacity for ethylene at 0.82 g/mmol but also a relatively high capacity for CO2 at 0.73 mmol/g compared to other materials tested.

Conditions		Breakthrough time (min)					
Temp. (°C)	Press. (psig)	Methane	Ethane	H_2	Ethylene	CO	CO_2
35	60	2.2	2.4	1.3	10.8	3.5	13.7
35	60	1.1	---	0.9	10.6	3.0	13.4

Table 27. Breakthrough time for Mg-MOF with Feed Mix 3

Conditions		Capacity (mmol/g)					
Temp. (°C)	Press. (psig)	Methane	Ethane	H_2	Ethylene	CO	CO_2
35	60	1.63	0.18	0.18	0.82	0.08	0.73
35	60	0.81	---	0.12	0.80	0.07	0.71

Table 28. Component Capacities for Mg-MOF with Feed Mix 3

Effect of purge gas

Fixed-bed experiments were performed to evaluate the effect of different purge gases on the overall recovery of ethylene in the heavy product stream on materials that showed promising ethylene separation capability.

	Process Gas	Feed Mix 5
Hydrogen	0.109	0.109
Argon	0.003	0.100
Nitrogen	0.029	
Oxygen	0.000	
CO	0.018	0.018
CO2	0.043	0.043
Methane	0.711	0.526
Acetylene	0.001	
Ethylene	0.056	0.146
Ethane	0.023	0.058
Propene	0.005	
Propane	0.000	
n-Butane	0.000	
n-Pentane	0.000	
13-Butadiene	0.000	
H2O	0.002	
Helium		

Table 29. Feed gas mixtures for desorption testing in mole fraction

Experiments were performed with H_2, propane, CO_2, and ethane purge gases using feed mix 5 (composition in Table 29) on the down-selected materials. Feed Mix 5 was developed to achieve a similar ethane to ethylene ratio as in the process gas composition. The experiment conditions with the different purge gases on CaX are shown in Table 30.

Adsorption			Desorption		
Feed Mix	P (psig)	T (°C)	Gas	P (psig)	T (°C)
5	60	35	H_2	10	35
5	60	35	Propane	10	35
5	60	35	CO_2	10	35
5	60	35	Ethane	3	35

Table 30. Experiment conditions for various purge gases with CaX zeolite

The breakthrough times and sorbent capacities for each component were determined for each experiment and used in the process model to develop the mass transfer coefficients. Component capacities are defined as the amount of a given component desorbed from the bed in mmol/g. This amount is calculated by integrating the product composition measured from the start of desorption until ethylene reaches 10% of its initial composition in the product stream. Desorption with hydrogen took longer than the other gases because it does not adsorb as strongly to CaX zeolite and resulted in a diluted product stream with only 9%

ethylene. Propane and CO_2 each adsorb more strongly to CaX which drive the product components from the bed much faster. Propane and CO_2 desorption resulted in 43% and 44% ethylene in the product stream, respectively. Ethane purge at low pressure resulted in 27% in the desorption product. Desorption product compositions for each purge gas over CaX are listed in Table 31.

Experiment Cond.		Desorption Product Composition (mol%)					
Purge Gas	**P (psig)**	**Methane**	**Ethane**	**Hydrogen**	**Ethylene**	**Propane**	**CO2**
H_2	10	-	0.78	87.33	9.24	-	2.65
Propane	10	-	5.95	-	43.32	40.90	9.83
CO_2	10	7.32	5.19	-	44.42	-	43.07
Ethane	3	7.85	54.54	1.62	27.29	-	8.70

Table 31. Desorption product composition for CaX using various purge gases

The results from these experiments show that while propane and CO_2 can displace ethylene more effectively under these conditions since these gases adsorb too strongly to the sorbents which helps to drive off the product (ethylene) during desorption, they would reduce the bed capacity during the subsequent adsorption step. While ethane performs moderate desorption, it is not adsorbed as strongly on the bed as propane and CO_2 after the desorption step. Thus, it does not adversely affect the working capacity of the material and is considered to be a good choice for purge gas.

Berkeley MOF

Investigation of a new class of MOF materials was done in collaboration with University of California, Berkeley. The new Berkeley MOF materials showed considerably higher IAST selectivity for ethylene over most other components which could result in much better separation capability. Isotherms for this material are available in Appendix 8.

The novel adsorbent was tested with breakthrough experiments to measure its expected enhanced performance of separating ethylene from other gases in the OCM feed.

Breakthrough experiments were performed using a custom-built breakthrough apparatus, composed of primarily 1/8" copper tubing fitted with Swagelok fittings and valves to control the flow of the gas to either flow through the sample holder or bypass the sample holder and flow directly to a gas chromatograph (GC) used to monitor outflow composition. A premixed 1:1 ethane:ethylene cylinder, a CO_2 cylinder, and a CH_4 cylinder were attached to the breakthrough manifold via mass flow controller to control gas flow from the cylinders. A coil of tubing was placed after the mass flow controllers to ensure mixing of the gases. The sample was pelletized and broken into pieces using a 20-40 mesh sieve. Then, the sample was loaded into one vertical component of a U-shaped sample holder comprised of ¼" tubing and fitted with Swagelok VCR fittings with fritted (0.5 μm) gaskets to prevent the sample from escaping the bed. The U-shaped tubing was immersed in a water bath and connected to the breakthrough manifold. The sample was activated in

the sample holder by heating it with heating tape at 180 °C under flowing He. The sample was then cooled to 25 °C for the breakthrough experiments. A total flow rate of 3-4 mL/min was employed. The mixture was tested without flowing to the packed Berkeley MOF bed to ensure proper composition and separation using the GC monitoring the outflow. The GC effluent was then fed into a flow meter to monitor the volumetric flow rate of the gas through the column instantaneously. The flow rate of each individual component was then calculated using

$$F_i(t) = y_i(t) * F^{tot}(t)$$

where $F_i(t)$ is the flow rate of species *i* at time *t* in mL/min, y_i is the fraction of component *i* measured from the peak areas in the GC, and $F^{tot}(t)$ is the instantaneous total flow rate of gas at the time the sample was injected into the GC, in mL/min.

The mixture was then flowed through the packed bed and the outflow was recorded by GC every 2.0 min for each gas mixture. The outflow composition was analyzed by gas chromatography using a SRI Instruments 8610V GC equipped with a 6' HayeSep D column, which was kept at 90 °C. After all components for an experiment had broken through the packed bed, the flow was switched to He, or another purge gas, and heated to 180 ˚C using heating tape to fully desorb both adsorbed components from the column. The data were recorded and analyzed using PeakSimple software.

Single component breakthrough curves were generated with CH_4, CO_2, Ethane, and Ethylene (See Figure 18). Sharp breakthrough of all the gases was observed, thus demonstrating fast adsorption kinetics of the adsorbent.

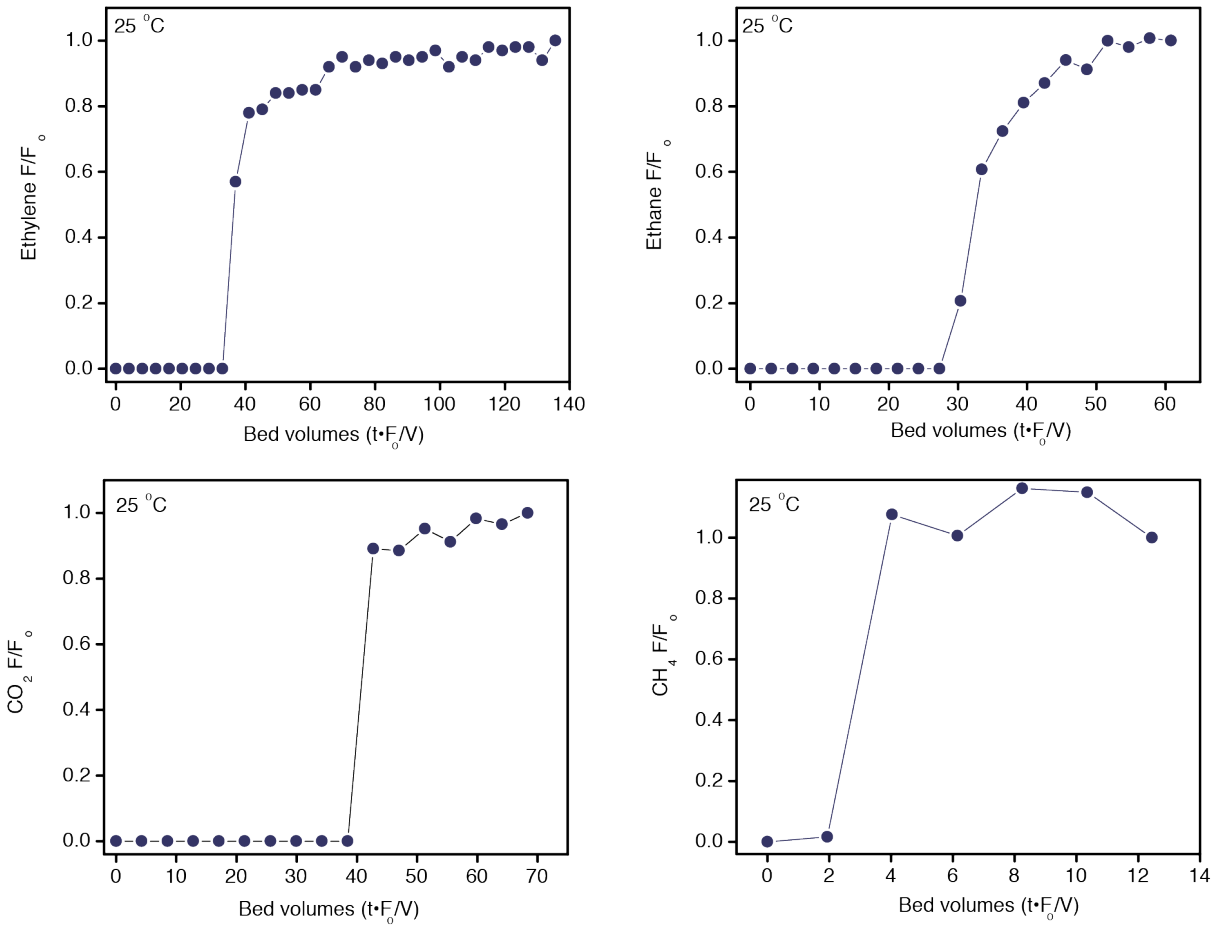

Figure 18: Breakthrough Curves of Single Component Gas in Berkeley MOF

Mixed gas breakthrough experiments were also performed. A 50:50 mixture of ethylene and ethane was flowed through the adsorbent bed to evaluate competitive adsorption (Figure 19). It was observed that high selectivity of the material for ethylene as compared to ethane results in much earlier breakthrough of ethane. This demonstrates preferential adsorption of ethylene, and thus high selectivity of the material for ethylene.

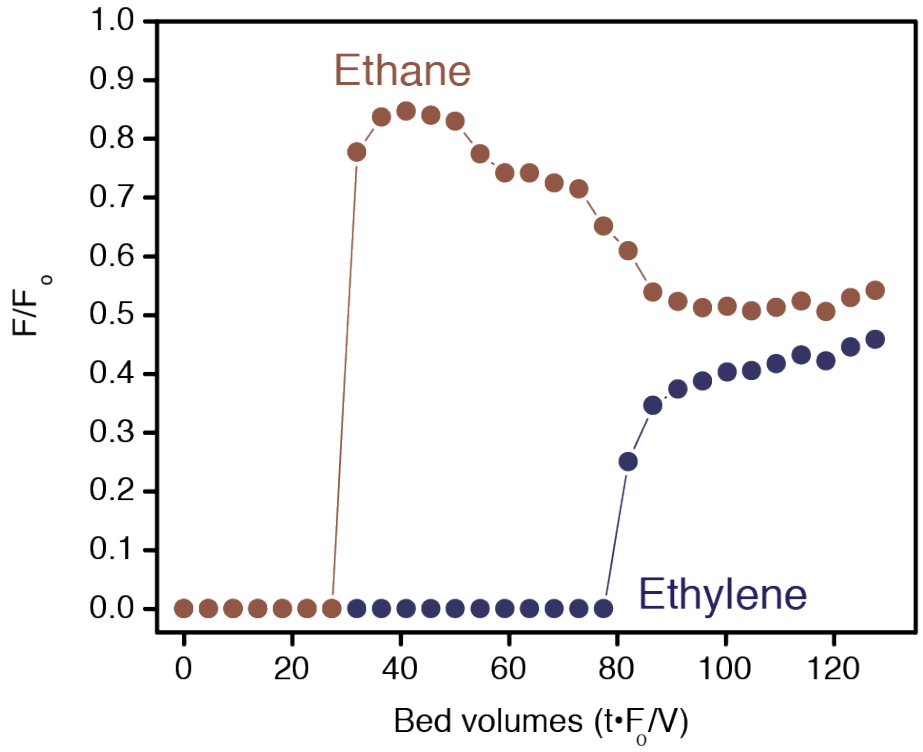

Figure 19: Binary Breakthrough Curve for Ethylene/Ethane Gas Mixture in Berkeley MOF at 25˚C

Single component breakthrough curves were generated with diluted CH_4, CO_2, Ethane, and Ethylene (Figure 20) also in order to simulate conditions similar to OCM effluent. Each gas was diluted with He to achieve relevant partial pressure, at total pressure of 6.2 bara.

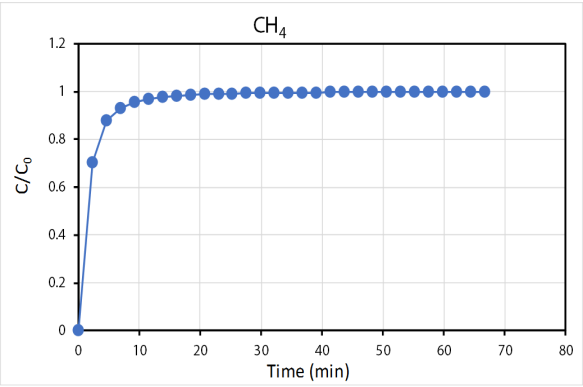

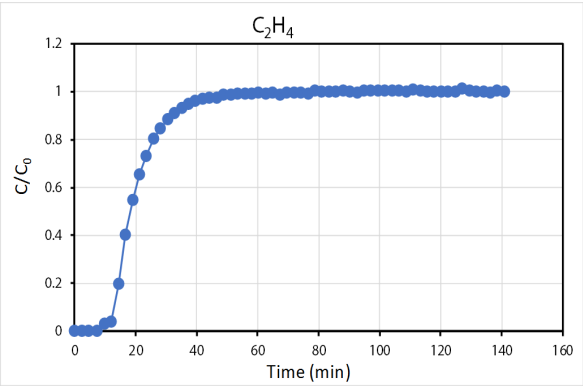

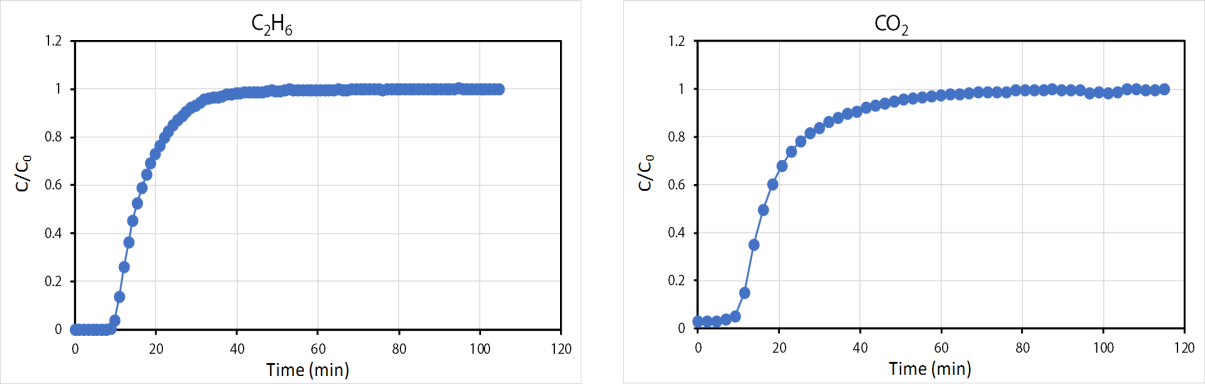

Figure 20: Breakthrough Curves of Single Component Gas on Berkeley MOF at 6.2 bara total pressure

High pressure mixed gas breakthrough experiments were also performed. A mixture of ethylene, ethane, methane and carbon dioxide was flowed through the adsorbent bed to evaluate competitive adsorption (Figure 21). It was observed that high selectivity of the material for ethylene results in its preferential adsorption and slowest breakthrough.

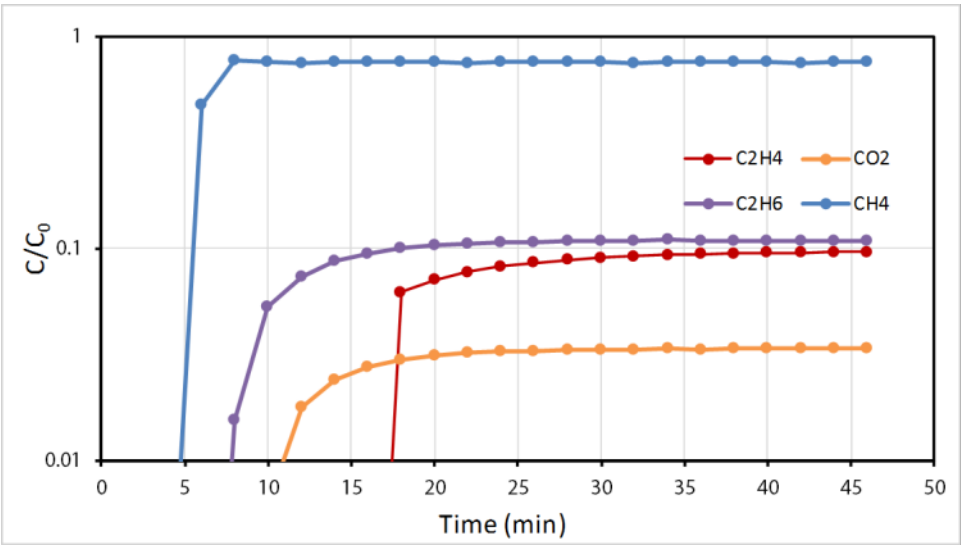

Figure 21: Breakthrough Curve of 4 Component Gas Mixture on Berkeley MOF at 6.2 bar total pressure

This material performed much better than CaX and Co_2(dobdc) because of its very low affinity for all the studied components other than ethylene.

Process Modeling

Modeling of an adsorbent bed system enables understanding of the adsorption profile across the bed (or in other words, the mass transfer zone), assessing the working capacity of the material, and making predictions of the performance of process cycles. The Aspen Adsorption simulation platform was used to model the experimental setup, and subsequently develop optimal configurations and cycles. Figure 22 is a representative layout of the Aspen Adsorption models simulated. Siluria partnered with Norton Engineering to develop the models.

Modeling Methodology

Process modeling was performed in following steps.

a) The model was setup with the same bed properties (such as the bed height, diameter, mass, particle radius) and process conditions (such as pressure, temperature, flow rate, gas composition) as the experimental setup. Experimentally obtained isotherms were used as the equilibrium model, while mass transfer coefficients for each component were kept as independent variables that were adjusted to match the breakthrough curve generated by the simulation model with the experimental breakthrough curves.

b) The mass transfer coefficients thus obtained (and hence the overall simulation model), were validated by comparing the results of the simulation model on a binary gas mixture with the experimental results.

c) Other components critical to the PSA system such as tank voids to simulate the vessel holding the adsorbent bed, purge and heavy product streams, valves for each of these streams, and interaction beds were added.

d) Cycle organizer was used to automate valve sequences, Cvs, and step timings so that the entire cycle, which includes all the steps can be run automatically. This also allows for the cycle to be run multiple times to reach steady state.

e) The validated simulation model was then used to predict the performance of the material with OCM gas effluent mixture. Parameters such as valve Cvs and step timings were varied to arrive at an optimum configuration to maximize product recovery and minimize losses.

Model Configuration

The following configuration was used for the simulation model:

Material Balance Assumption: Plug flow without dispersion effects (convection only)

Momentum Balance Assumption: Gas velocity and pressure drop was represented by Ergun equation:

$$\frac{\partial P}{\partial z} = -\left(\frac{1.5 \times 10^{-3}(1-\varepsilon_i)^2}{\left(2r_p\psi\right)^2 {\varepsilon_i}^3}\mu v_g + 1.75 \times 10^{-5}\mathrm{M}\rho_g \frac{(1-\varepsilon_i)}{2r_p\psi{\varepsilon_i}^3}{v_g}^2\right)$$

where,

P = pressure
z = position in the column
ε_i = bed (interparticle) voidage
r_p = particle radius
μ = gas mixture viscosity
ψ = particle shape factor
v_g = superficial gas velocity
M = moledular weight of the gas mixture
ρ_g = gas density

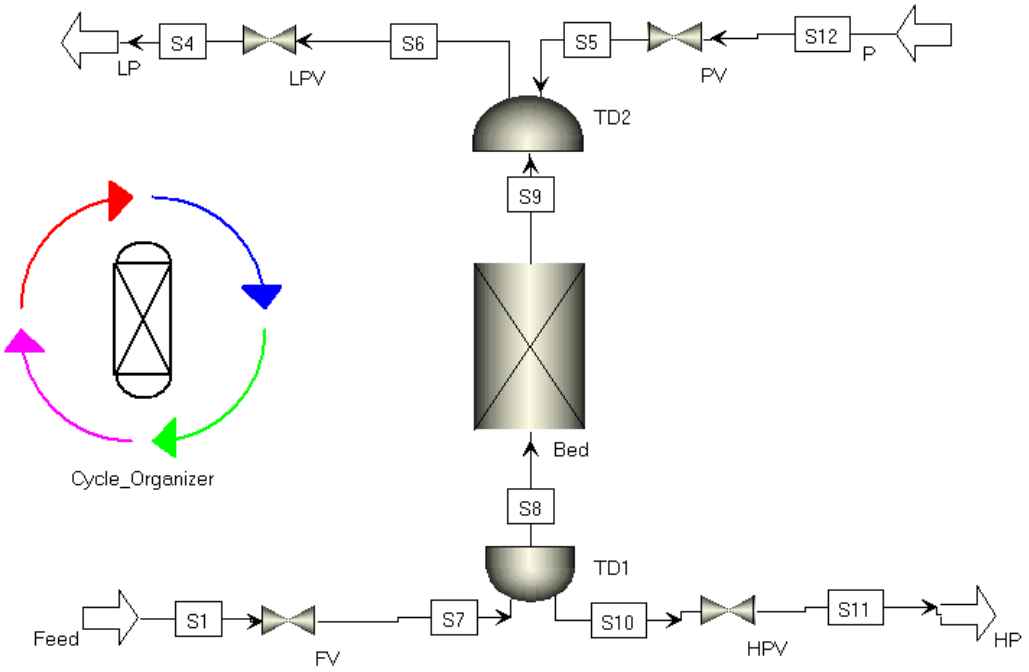

Figure 22: Representative layout of the Aspen Adsorption model

Kinetic Model Assumption: Separate mass transfer resistances were lumped as a single overall factor, according to:

$$\frac{\partial w_i}{\partial t} = MTC_{si}\left(w_i^* - w_i\right)$$

where,

w_i = loading of component i due to adsorption

w_i^* = equilibrium loading of component i due to adsorption
MTC_{si} = mass transfer coefficient of component i
t = time

and,

$$MTC_i = \frac{k_{0pi}}{P} \exp\left(\frac{-E_{acti}}{RT}\right)$$

where,

k_{0pi} = Pre-exponential factor
P = Pressure
E_{acti} = Activation Energy
R = Gas Constant
T = Temperature

Isotherm Model: Two forms of isotherm models, Dual-site Langmuir-Freundlich model, and pressure and temperature dependent Langmuir-Freundlich, as fitted to the experimentally obtained equilibrium loading data, were used in the simulation.

$$w_i = \frac{IP_1 IP_2 P_i^{IP_3}}{1 + IP_1 IP_2 P_i^{IP_3}} + \frac{IP_4 IP_5 P_i^{IP_6}}{1 + IP_4 IP_5 P_i^{IP_6}}$$

$$w_i = \frac{IP_1 IP_2 P_i^{IP_3} e^{IP_4/T_s}}{1 + IP_2 P_i^{IP_3} e^{IP_4/T_s}}$$

Energy Balance: The simulation was setup to be isothermal.

Numerical Method: First order upward differencing scheme was used as the numerical discretization method to solve the partial differential equations. The bed was divided in 20 nodes.

Reaction: It was assumed that no reactions take place on the bed.

Simulation Results and Discussion

Single component breakthrough experiments were emulated on the simulation model, with mass transfer coefficients varied to closely match the shape of the breakthrough curve. Figure 23 demonstrates the fitting of two such breakthrough curves, of ethane and ethylene on Co_2(dobdc).

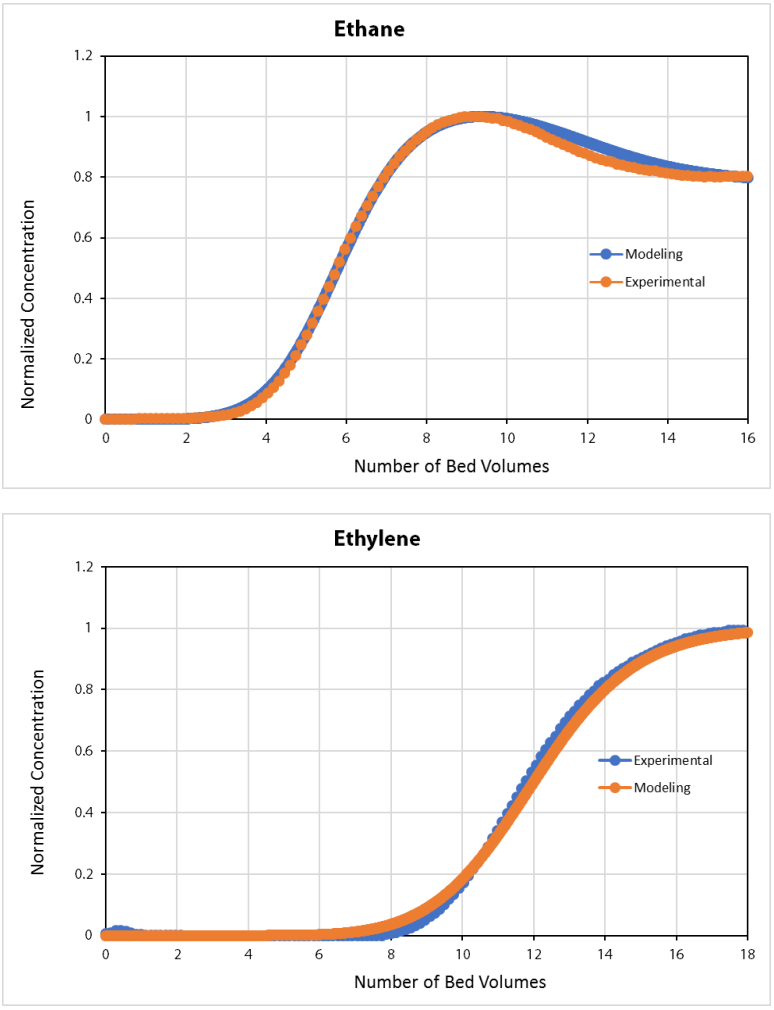

Figure 23: Comparison of breakthrough curves generated by experiment and simulation model on Co_2(dobdc)

The models were subsequently validated by doing binary mixture and multi-component simulations and comparing it with the experimental results. Figure 24 demonstrates validation of ethane-ethylene 50:50 mixture breakthrough on Berkeley MOF. The point of breakthrough is representative of the loading capacity of the adsorbent, whereas the shape of the breakthrough curve is representative of the mass transfer kinetics.

It was observed that the model demonstrated a very similar breakthrough point, and shape of the component breakthrough curves. It should be noted that the point of breakthrough in the simulation was consistently found to be slightly shifted to the right (thus indicating higher capacity), when compared with experimental results. This is a result of heat effects on the capacity of the adsorbent. Although the experimental conditions were attempted to be close to isothermal, the dissipation of heat of adsorption is

not as rapid. Thus, we observe higher adsorption capacity on the simulated material than the adsorbent in the experimental setup.

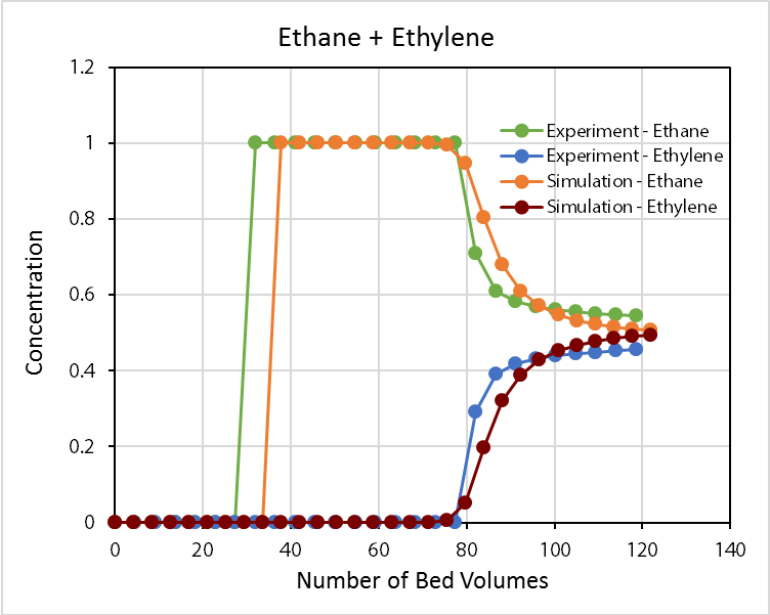

Figure 24: Breakthrough test of 50:50 ethylene & ethane mixture on Berkeley MOF

Multi-Bed Cycles

PSA models were made more sophisticated by incorporating multiple bed design. To integrate a dynamic PSA unit in a steady state process system, it is imperative to have more than one adsorbent bed so that the OCM effluent always has at least one bed available for the adsorption step. The PSA models were developed as 2-bed and 3-bed systems and evaluated for their relative performance.

2-Bed Model

A 4-step cycle that can be performed on 2 beds (as 6 steps) was considered. The cycle layout is provided in Figure 25. A 50-node bed was simulated in Aspen Adsorption.

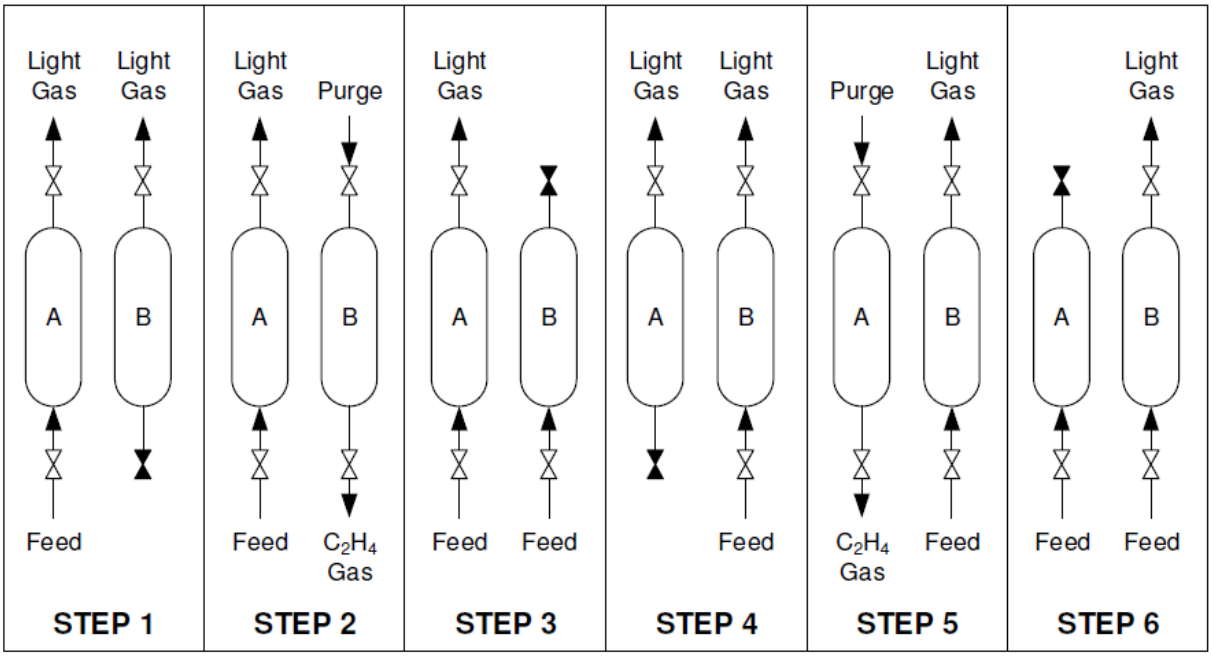

Figure 25: Cycle layout of a 2-bed adsorption system with 6 steps

The 4 steps are:

- Adsorption
- Depressurization
- Desorption
- Repressurization

In first case, which was considered the base case, the purge gas ethane is at 20 °C higher temperature than feed gas (OCM effluent). The purge gas flow rate is kept at 40% of the feed gas. A constraint was applied to this cycle that the time for Depressurization + Desorption + Repressurization must equal the time for Adsorption so that feed can always be processed from the OCM reactor without interruptions.

The pressure profiles in the bed are demonstrated in Figure 26. The ΔP across the bed was 0.8 bar or less throughout the cycle.

Figure 27 is a plot of normalized concentration of ethylene in gas phase at each node, and at different positions in the cycle. This is an indicator of the mass transfer zone in the bed at various stages in the cycle. This cycle demonstrated very little breakthrough of ethylene and thus recovery of about 99.9%.

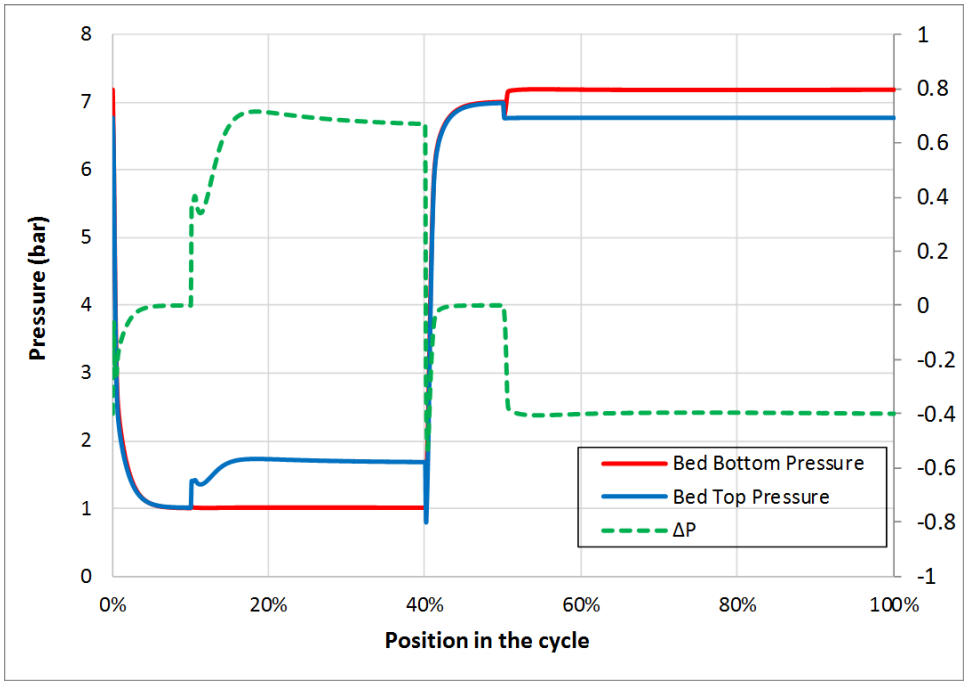

Figure 26: Pressure profile of top and bottom of the bed (Case 1)

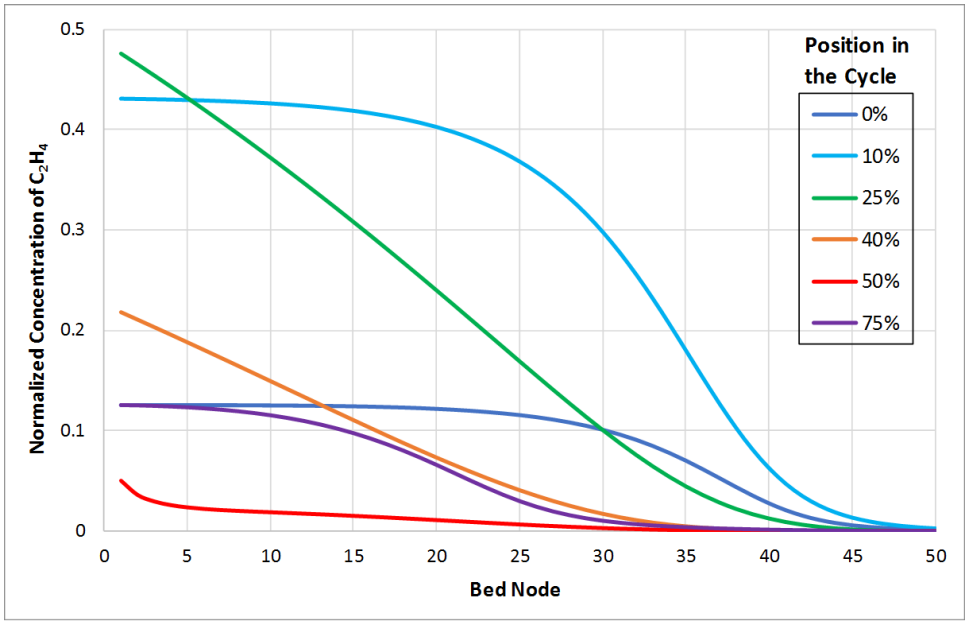

Figure 27: Ethylene concentration profile of ethylene in gas phase across all nodes in the bed (Case 1)

In case 2, purge gas flow was reduced to 30% of the feed flow rate, while keeping everything else the same. Lower purge resulted in less effective desorption than the base case. This in turn resulted in more breakthrough of ethylene during the adsorption step (for the same step time), and the recovery reduced to about 98.5% (See Figure 29). The pressure profile in this case is very similar to the base case (See Figure 28).

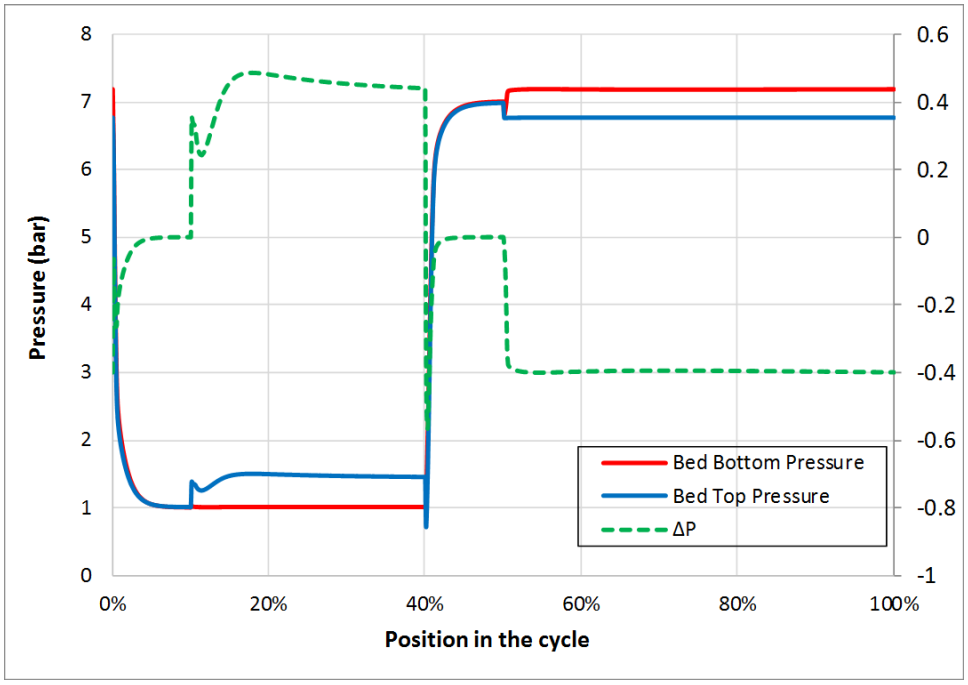

Figure 28: Pressure profile of top and bottom of the bed (Case 2)

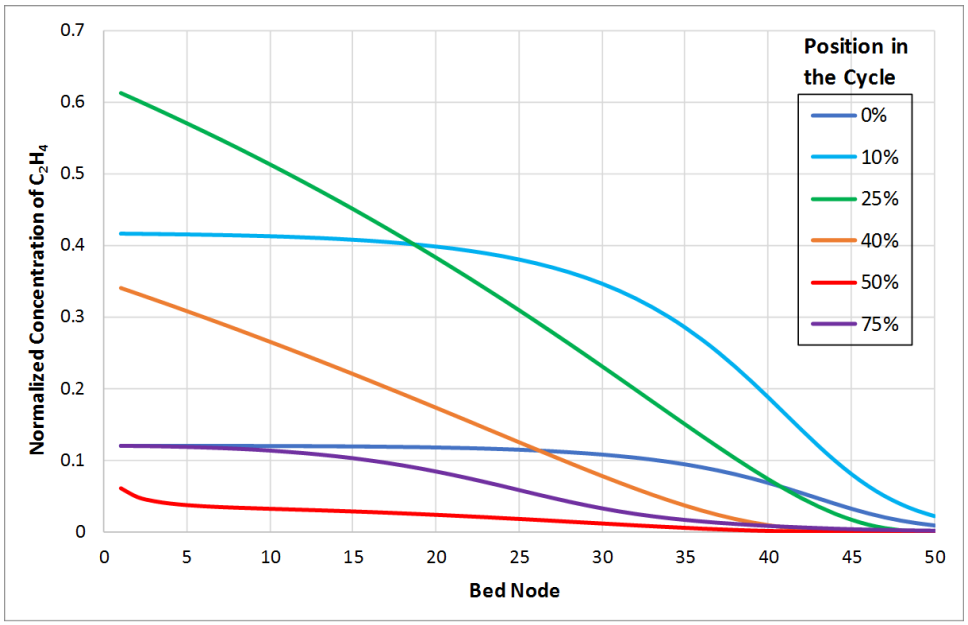

Figure 29: Ethylene concentration profile of ethylene in gas phase across all nodes in the bed (Case 2)

In case 3, the ethane purge temperature was kept the same as the feed temperature, and its flow rate was 30% of the feed flow rate. These changes impacted the performance of the PSA, resulting in reduced recovery of 84%.

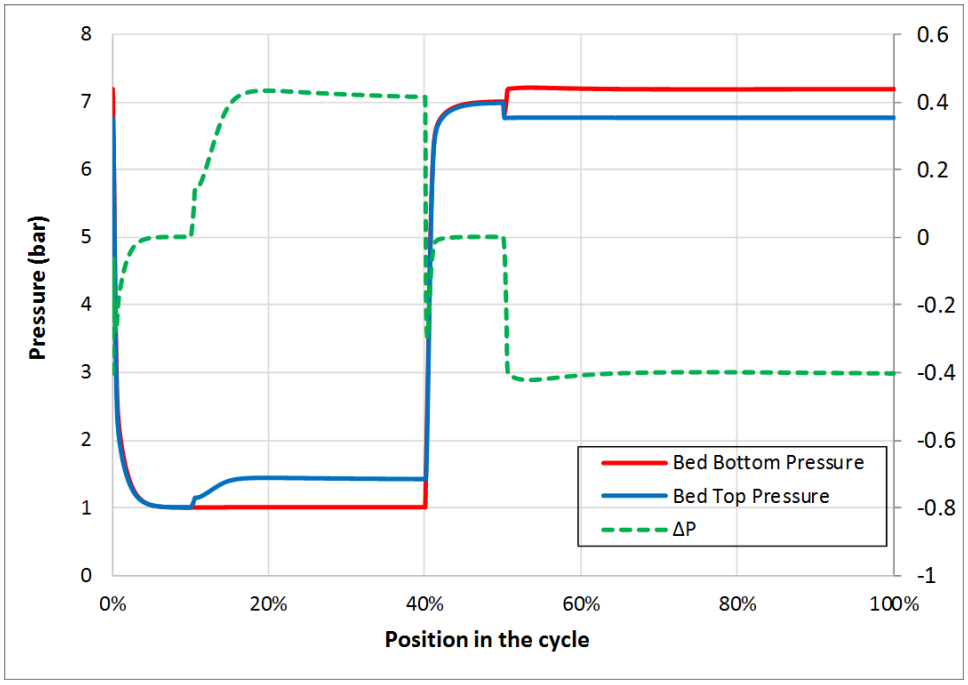

Figure 30: Pressure profile of top and bottom of the bed (Case 3)

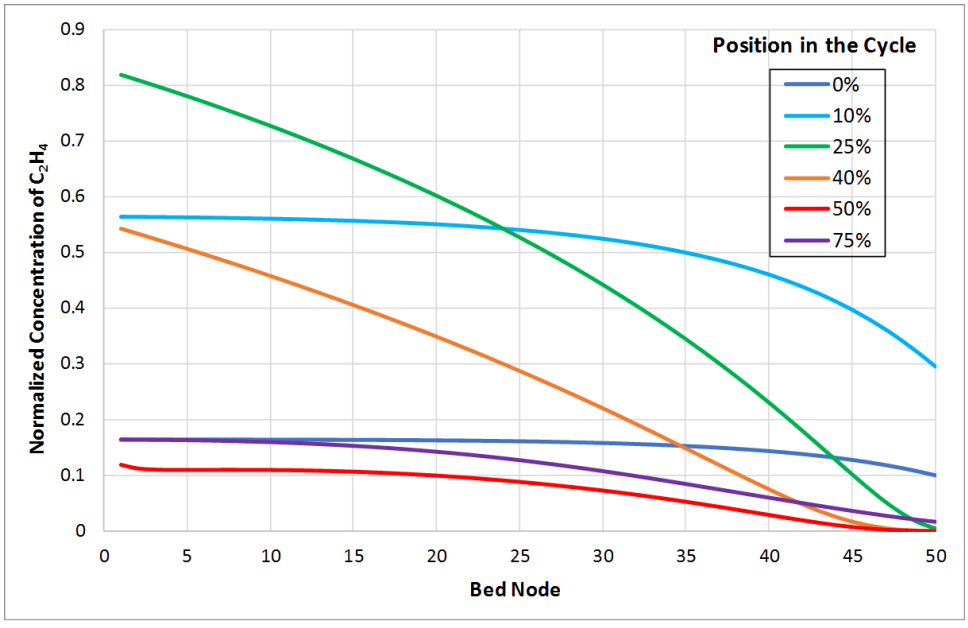

Figure 31: Ethylene concentration profile of ethylene in gas phase across all nodes in the bed (Case 3)

In case 4, the ethane purge temperature was again kept the same as the feed, but its flow was increased to 45% of the feed flow. Also, the bed size was increased by 20%. This resulted in improved desorption, leading to lesser loss of ethylene. The ethylene recovery in this case was observed to be about 96%.

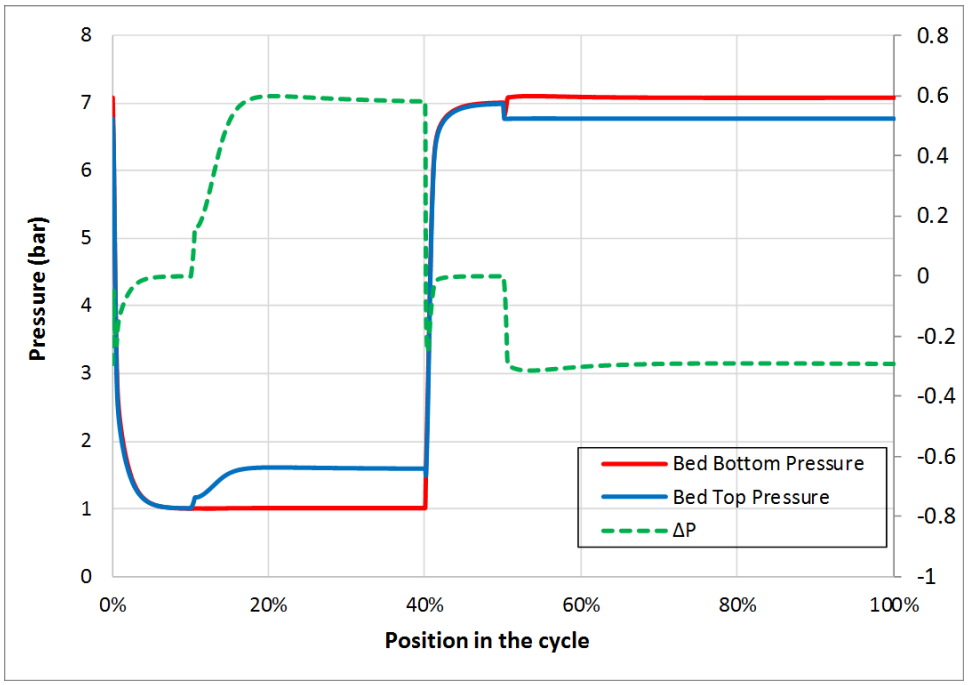

Figure 32: Pressure profile of top and bottom of the bed (Case 4)

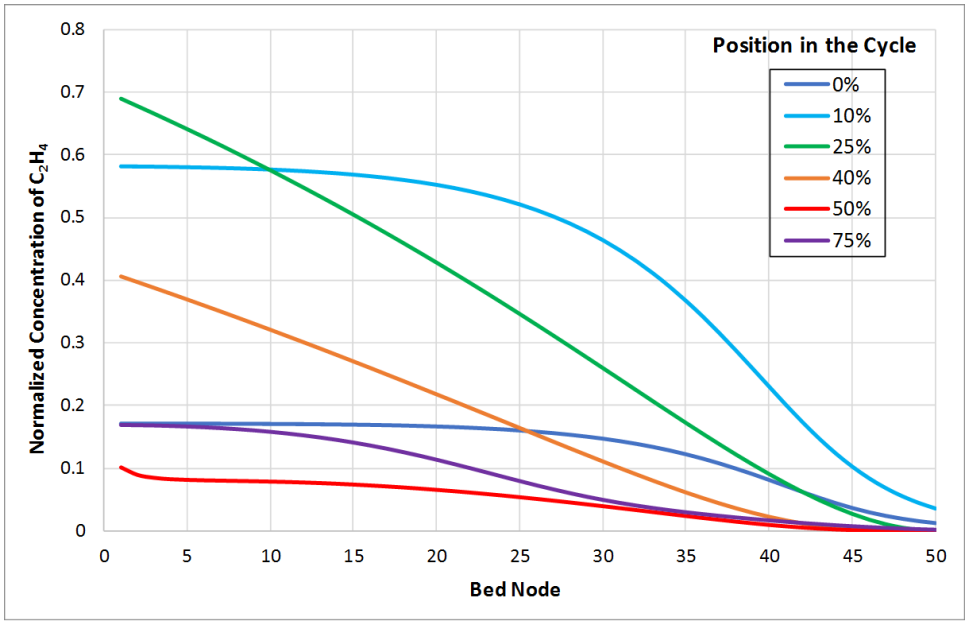

Figure 33: Ethylene concentration profile of ethylene in gas phase across all nodes in the bed (Case 4)

3-Bed Model

A disadvantage of 2-bed system is that there are large pulsations of gas flow affecting both, downstream equipment (during depressurization step), and upstream equipment (during repressurization). These effects can be eliminated in a 3-bed system by implementing pressure equalization steps. Thus, a 3-bed model was investigated to assess its performance in comparison with the 2-bed model. A 3-bed, 9-step cycle that represents a potential improvement over the 2-bed cycle as described above is provided in Figure 34.

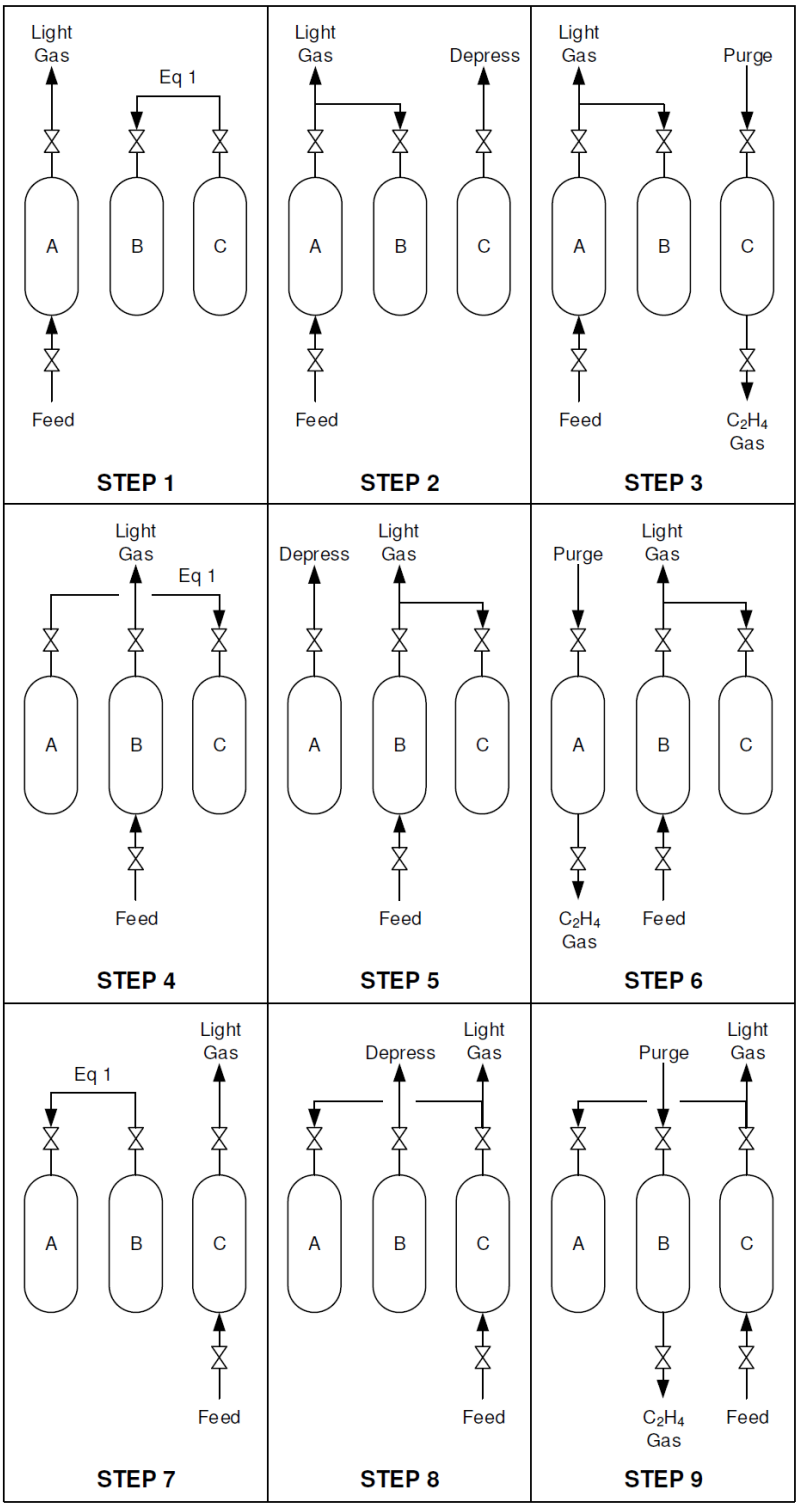

Figure 34: Cycle layout of a 3-bed adsorption system with 9 steps

Interaction beds were used in Aspen Adsorption to simulate the equalization steps. A constraint was applied to this cycle that the time for Step 1 MUST align with Steps 4 and 7, the time for Step 2 MUST align with Steps 5 and 8, and the time for Step 3 MUST align with Steps 6 and 9.

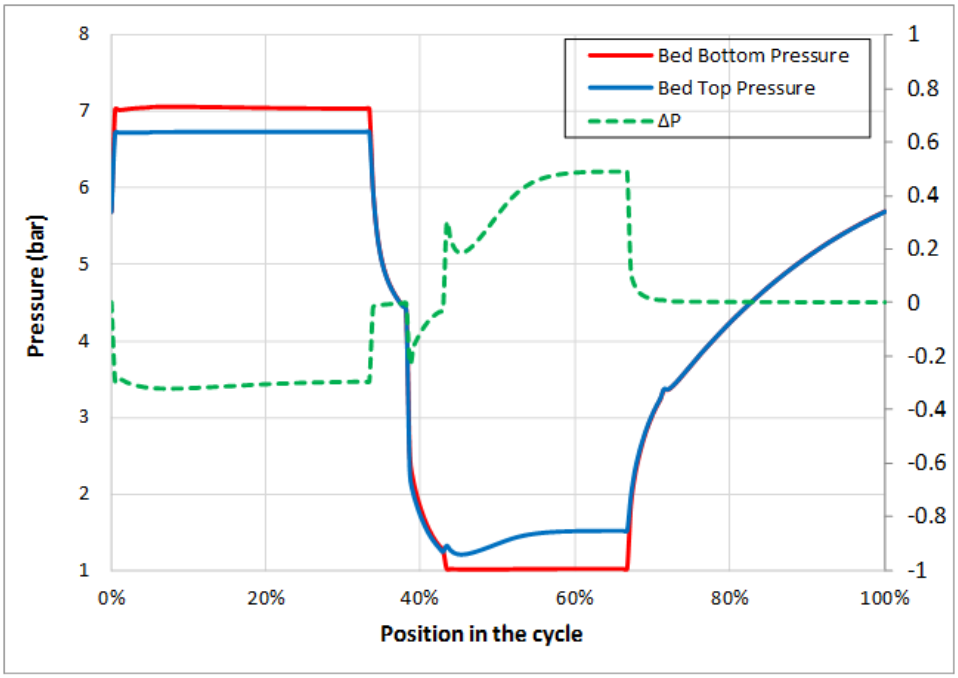

Figure 35: Pressure profile of top and bottom of the bed

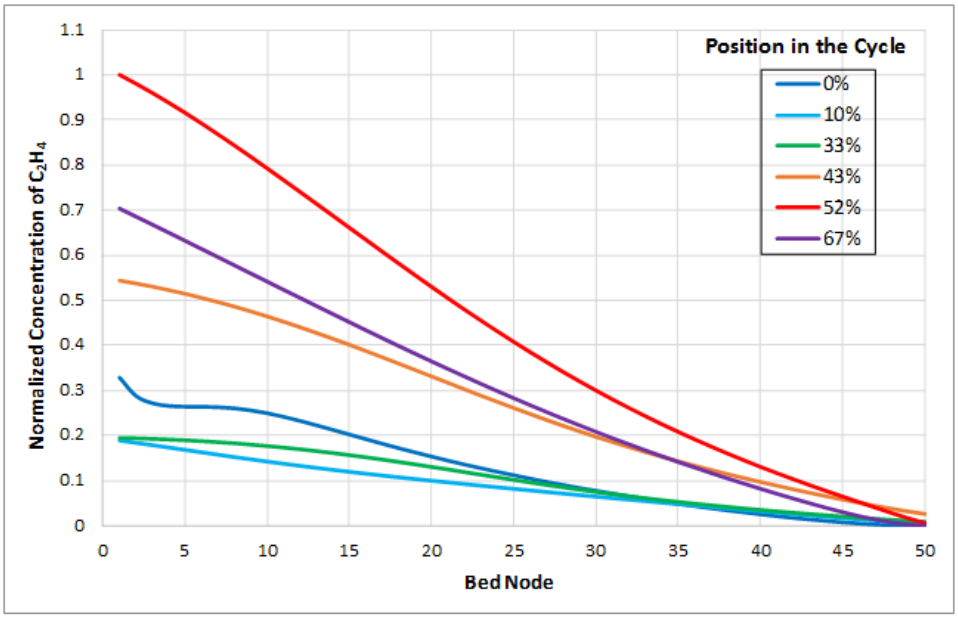

Figure 36: Ethylene concentration profile of ethylene in gas phase across all nodes in the bed

It was observed that the ethylene recovery achieved in this system was about 95% and that the equalization gas was not helping recovery as the product species is in the adsorbed phase. This behavior is unlike other PSA separations such as H_2 PSA or O_2 VSA where equalizations typically improve recovery by moving the product gas in the vapor phase into other beds. Therefore, performing the depressurization and repressurization steps as fast as possible (within the limits of fluidization and upstream/downstream equipment) with no pressure equalization steps appears to be the best approach.

Process Configurations

Various process configurations were evaluated for effective ethylene separation and integration with the overall OCM process. It included process concepts with one or more adsorbent beds in series, with one or more materials in an adsorbent bed. A final process scheme is proposed (Figure 37) after optimizing the model by doing sensitivity analysis over several parameters:

- Feed Flow rate
- Feed Temperature
- Feed Pressure
- Desorption Time
- Desorption Temperature
- Desorption Pressure
- Ethylene Recovery

The sensitivity analysis was performed to optimize the following:

- Working Capacity of the Adsorbent
- Mass Transfer Profile in the Bed
- Concentration of Ethylene in the Heavies Product Stream
- Concentration of Ethylene in the Lights Product Stream
- Adsorption Step Length

Below is a description of the final process concept that demonstrated significant technical and economic gains (discussed later in Benefits Assessment section) to the existing OCM process.

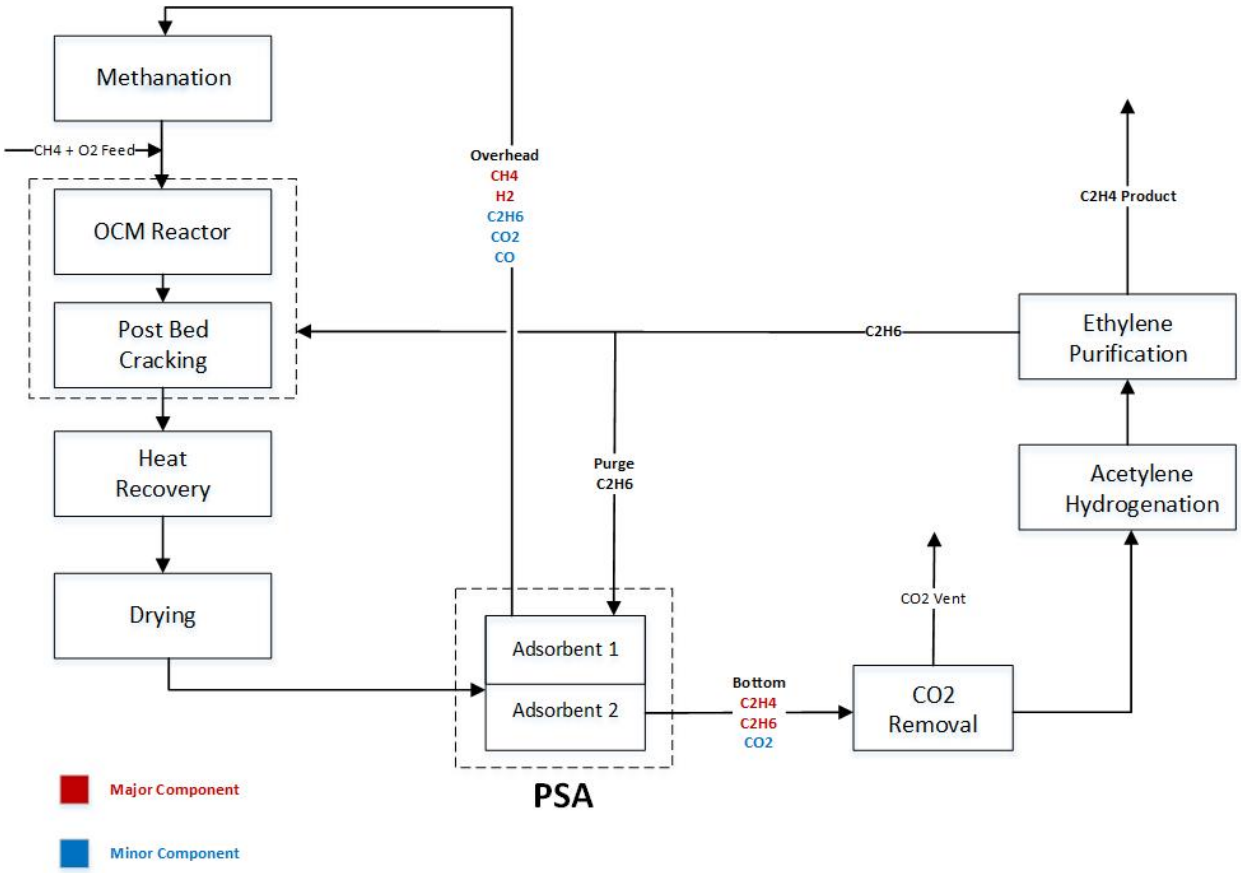

Figure 37: Final process configuration using two-layered bed approach and ethane purge

Natural Gas and oxygen are fed to the OCM reactor. The effluent from the reactor contains majority of unreacted methane, followed by hydrogen, ethylene, CO_2, ethane, CO, propylene and other minor components. The exothermic heat from the OCM reactor is utilized for steam generation for use within the process or for export. The heat is also utilized for any internal stream heat exchange. The effluent is then sent into a quench tower to remove heavies and water and further dried to remove any leftover process water in molecular sieves.

The scheme so far largely represents the current OCM design. The configuration from hereon reflects specific separations from the PSA bed. This configuration is based on detailed evaluation of the breakthrough and desorption experiments performed by RTI/UC, Berkeley followed by modeling for OCM specific compositions and conditions. The cycles were optimized to give high ethylene purity and recovery in the heavies product stream. The model was then integrated with the overall OCM unit simulation and further tweaking of the models was done to get a final configuration for optimized capex and opex.

The effluent from drying is sent into a two-layered bed PSA system of adsorbent 1 (such as Berkeley-MOF) and adsorbent 2 (such as CaX or Mg_2(dobdc)). Berkeley MOF has shown strong adsorption for ethylene, whereas CaX and Mg_2(dobdc) have shown strong adsorption for ethylene and CO_2 both when compared to ethane and other lighter components. Thus, the relative thickness of the two adsorbent layers is chosen to get a desired split of CO_2 such that a portion of it goes in the Lights stream and the other portion goes in

the heavies stream. Lighter components such as methane and hydrogen can easily breakthrough the bed during the adsorption step. Thus methane, hydrogen and CO are removed in this step. This stream is directly sent into the methanation section before the OCM reaction.

The lights product stream, containing methane, hydrogen, ethane, CO, and CO_2 is sent into methanation reactor. In the methanation reaction, hydrogen from the system is utilized to convert CO and CO_2 back into methane, thus improving the overall carbon efficiency.

The regeneration of the bed is performed using ethane. Ethane binds on the adsorbent sites and releases ethylene. The portion of CO_2 captured by the CaX/Mg_2(dobdc) layer is released as well.

The heavies product stream from regeneration is sent to a CO_2 removal unit from where CO_2 is vented off.

The product stream now containing ethylene and ethane is sent into a C2 splitter, which does the final purification of ethylene to produce polymer grade ethylene product. The C2 splitter in the original design was technically not viable due to its extremely small flow rate at capacities lower than 60KTA ethylene production (L/D > 30, due to small flow rates). In the current design, however, the unit is also more compatible due to higher flow rate and better proportions of ethylene and ethane thus improving the overall economics.

The advantage in the new process is seen in utilizing smaller process units for separations instead of huge compression systems, refrigeration systems, CO_2 removal and demethanizer column that process entire effluent streams.

The abovementioned process satisfies most of the feature requirements set in the project.

Benefits Assessment

The objective of the project was to investigate the feasibility of using OCM at smaller-scales, given the excellent down-scalability of the OCM reactor as compared to typical existing commercial ethylene steam cracking technology. A detailed analysis encompassing process simulations, equipment sizing and project economics was conducted at three different scales of ethylene capacity earlier in the project. It was found that not only did the project show poor economics (increase in total project cost) at capacities below 60 KTA, but also any plant smaller than 80 KTA is likely unfavorable based on the projected Internal Rate of Returns (IRR), at commodity prices assumed at the time. The analysis had also revealed that the major roadblock to the scalability was the inability of the separations section to effectively scale down at lower capacities.

The newly proposed and refined configuration (shown in Figure 37) addresses the scalability issue by incorporating a novel PSA system as part of the separations and recovery section. This eliminated the use of a cryogenic Demethanizer. The C2 splitter is kept in the process as a backstop to ensure polymer grade ethylene product specification is met (ca. 99.95 wt% minimum). Overall, substantial savings were realized in the following sections:

- C1/C2+ separation
- CO_2 removal
- Process gas compression

The overall project cost ($MM/KTA of ethylene) and internal rate of return are two metrics that can evaluate the benefits of the new configuration. A comparison of the trend of overall total project cost reveals that the overall project cost with the new design is lower at all the capacities previously considered (Figure 38). It also shows that the overall project cost curve does not increase as sharply as before with the reduction in capacities. Hence, the unit can still be reasonably costed at capacities below 60 KTA.

The IRR curve similarly reveals that project returns are improved compared to the previous design at all the three capacities (27, 67, and 135 KTA) and provide favorable returns at capacities below 80 KTA (Figure 39).

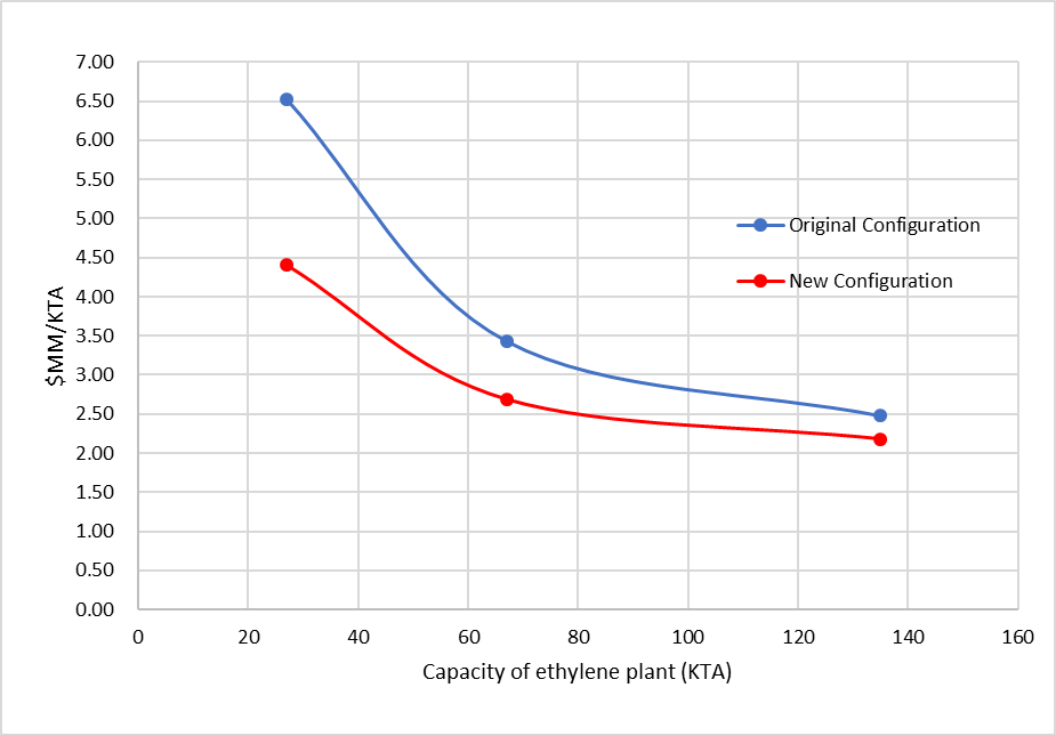

Figure 38: Comparison of trends for total project costs between the original and the new configuration

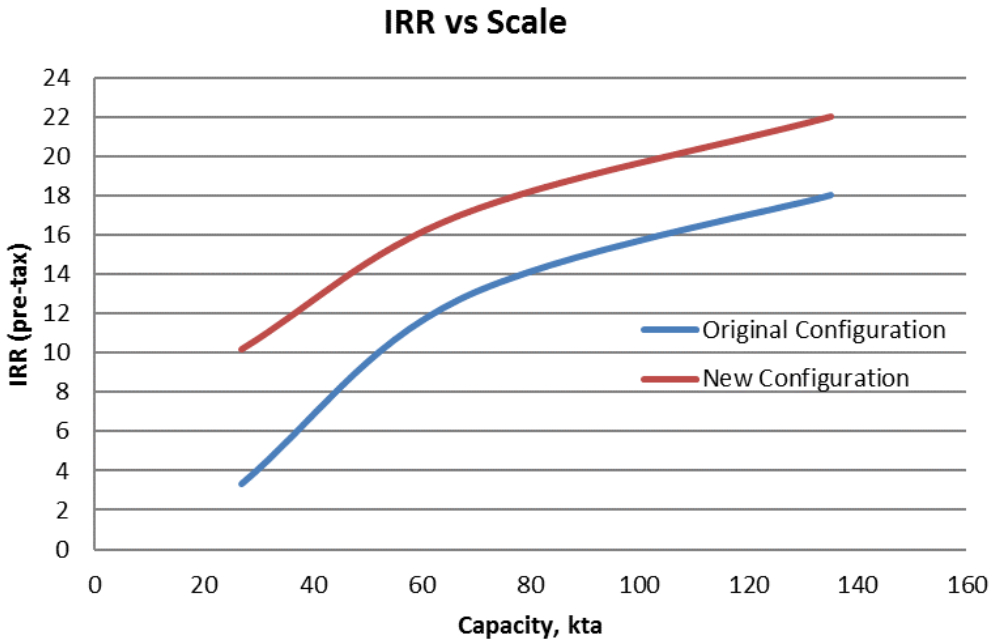

Figure 39: Comparison of trends for IRR between the original and the new configuration

Energy Savings

As discussed earlier, the refined configuration with PSA based C1/C2 separation results in significant reduction in energy consumption (over 15%) of the overall unit besides reducing the capital cost. This is achieved by (a) eliminating ethylene refrigeration system; (b) an embedded partial CO_2 separation in the adsorption bed that reduces circulation rate and energy consumption of the CO_2 removal unit; and (c) providing a smaller process gas stream for compression downstream of PSA.

Small scale OCM unit with the new configuration has demonstrated energy intensity of less than 20 MMBTU/ton of ethylene.

Table 32 shows a comparison for energy intensities between a commercial cracker (Worrel et al. 2000) and a small scale OCM unit with the new configuration.

Process Area	**Estimated SEC (GJ/tonne)**	**Process Area**	**Estimated SEC (GJ/tonne)**
Cracker *Heat of Reaction* *Dilution Steam* *Heating + Losses*	**11.0** *5.4* *1.4* *1.2*	**OCM Process** *Heat of Reaction* *Heating*	**7.0** -* (Exothermic Reaction produces heat that is used to produce steam and run the compressor turbines) *7.0*
Compression	**5.2**	**Compression** (two compressors for a) C1 and lighter compounds stream b) C2+ stream)	**2.6**
Separation *Chiller* *Condenser* *Separator* *Steam* *Acetylene Removal* *Heavies Separation*	**7.3** 5.0 *3.8* *1.2* 2.3 *0.7* *1.6*	**Separation** *Chiller* *Refrigeration* *Steam* *CO_2 Removal*	**8.7** *2.6* *6.1*
		Misc.	**0.8**
Total	**23.5 GJ/ton, or 22.3 MMBTU/ton**		**19.1 GJ/ton, or 18.1 MMBTU/ton**

Table 32: Comparison of energy intensities (per tonne of ethylene) between a typical cracker and proposed small-scale OCM unit

* Conservative estimate is provided that does not include contributions from the exothermic energy released from the OCM reaction.

In summary, the new design is more cost and energy favorable to implement at lower capacities.

This achievement will enable a new market paradigm of distributed, small-to-medium scale production of ethylene that can be located throughout the United States, given the ubiquitous availability of natural gas delivered on a network of over 305,000 miles of pipelines. This enables OCM Plants to be built either closer to natural gas resources or processing facilities and paired with derivative units, such as polymer plants, of a similar scale; or closer to end users like existing derivative plants, thereby significantly reducing their costs. This sharply contrasts to current ethylene production in the United States which is inherently driven towards centralized production, as these world scale plants require supporting infrastructure such as utilities, feedstock fractionation and transportation, storage, and pipeline infrastructure. Much of this critical infrastructure has been built up along the Gulf Coast over the past century and more continues to be built there today, which is why substantially all crackers are concentrated in the U.S. Gulf Coast ("USGC") region (Figure 40).

Figure 40: Location of Ethylene Crackers in the United States. Each red circle represents one cracker plant. The vast majority are located in the Gulf Coast.

Commercialization

In this project, we developed a novel process to replace the cryogenic separation of light hydrocarbon gas streams with a much simpler, down-scalable, and less expensive solution to enable small scale distributed production (<<100 KTA) of ethylene via OCM process that uses abundant natural gas as its feedstock.

The scope of this project included bench-scale experiments, modeling and engineering design to demonstrate FEL-1 level technical and economic viability of the process. In order to commercialize the technology and prepare it for deployment, further refined materials development, process development and scale-up (pilot and demonstration scale) will be necessary. Many of the promising materials identified in this project are from the Metal Organic Framework class, which currently have limited commercial deployment when compared with traditional zeolite adsorbents. Thus, further research will be required to mature these materials and make them ready for commercial use.

Traditionally, PSA/TSA systems separate gas streams that comprise of simple streams of few gas components. OCM effluent, however, comprises a multiple of gas components with challenging requirements including recycling certain components back to the reactor and others downstream for further processing. While in this project the development of materials and process has successfully met these requirements, the investigation was done using a simulated feed comprising of major species of the OCM effluent. Setting up a pilot plant with this technology that is fully integrated with an OCM reactor will verify the current observations and assist in investigating the behavior of minor species in the stream.

Finally, more detailed simulations will be needed to make a final commercial design of the PSA/TSA cycles and process configuration. Adsorbent based separation systems have a multitude of operation parameters that affect the recovery and purity of the product. This requires reconfiguration of the downstream units, and ultimately understanding the impact on the economics of the overall unit

Accomplishments

In this project, we have developed a novel process that can perform separation of complex hydrocarbon streams, which is currently only possible using energy intensive cryogenic distillation methods that require high minimum capital cost, and have poor down-scalability. By taking a holistic approach on materials development, process development, and process modeling, we developed an alternative commercially viable separations technology that accomplishes the same level of performance, with lower energy, cost, and improved scalability.

During the study, we performed a comprehensive evaluation including detailed laboratory testing of over 10 adsorptive type materials (see Table 1). These studies led to the identification of a novel MOF adsorbent that exhibited nearly ideal behavior (Figure 41) for recovery of ethylene from the OCM effluent (e.g. extremely high selectivity to separate each primary component in the OCM effluent).

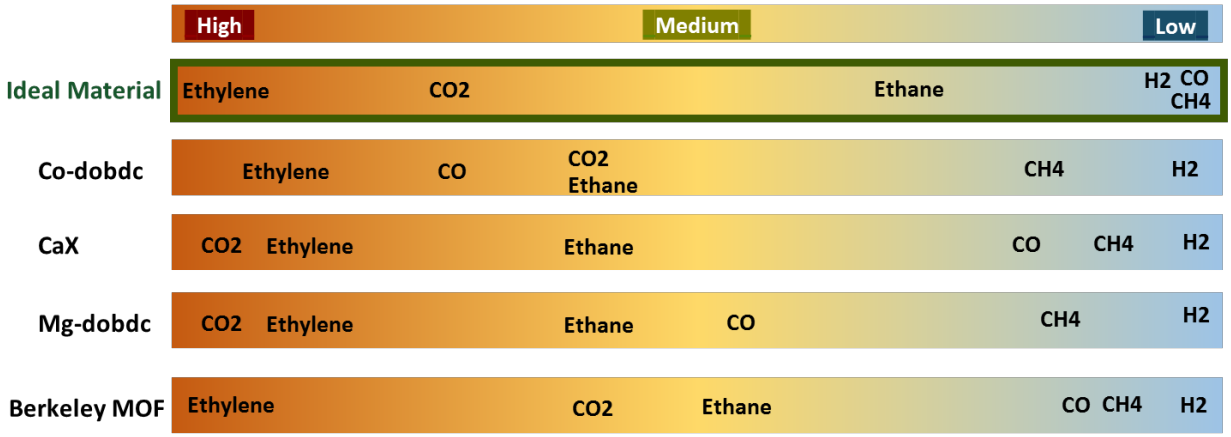

Figure 41: Qualitative adsorption strength of various OCM effluent gas components on different materials

The process developed in this project also enables recovery of ethylene from the OCM reaction effluent at the required purity level (e.g. polymer grade), reduces the energy intensity and capital and operating costs of the separations, and results in an enhanced overall design with substantially improved economics. While this process has been optimized for ethylene recovery, it can potentially be extending in the future to other gas separation applications involving other complex streams.

Conclusions

Siluria, in collaboration with its partners successfully met the objectives of the project.

The project involved detailed analyses through experiments, literature surveys, modeling and techno-econ analysis to develop a novel technology that enables small-scale production of ethylene via OCM. As a part of this project, a novel material was developed that displayed remarkable ethylene separation capabilities which was integrating into a novel adsorption based separation process capable of the complex multi-component OCM effluent stream. The final configuration has demonstrated a potential significant energy savings (>15%) and improved down-scalability (below 60 KTA) of the OCM process than the existing design using conventional cryogenic separations. This remarkable accomplishment enables small scale distributed production of ethylene via OCM process that uses ubiquitous natural gas as its feedstock.

References

Baker, R.W. 2002. “Future Directions of Membrane Gas Separation Technology.” *Industrial and Engineering Chemistry Research* 41 (6): 1393–1411. doi:10.1021/ie0108088.

Bloch, E. D., W. L. Queen, R. Krishna, J. M. Zadrozny, C. M. Brown, and J. R. Long. 2012. “Hydrocarbon Separations in a Metal-Organic Framework with Open Iron(II) Coordination Sites.” *Science* 335 (6076): 1606–10. doi:10.1126/science.1217544.

Bloch, Eric D., Matthew R. Hudson, Jarad A. Mason, Sachin Chavan, Valentina Crocellà, Joshua D. Howe, Kyuho Lee, et al. 2014. “Reversible CO Binding Enables Tunable CO/H2 and CO/N2 Separations in Metal-Organic Frameworks with Exposed Divalent Metal Cations.” *Journal of the American Chemical Society* 136 (30): 10752–61. doi:10.1021/ja505318p.

Geier, Stephen J., Jarad a. Mason, Eric D. Bloch, Wendy L. Queen, Matthew R. Hudson, Craig M. Brown, and Jeffrey R. Long. 2013. “Selective Adsorption of Ethylene over Ethane and Propylene over Propane in the Metal–organic Frameworks M2(dobdc) (M = Mg, Mn, Fe, Co, Ni, Zn).” *Chemical Science* 4 (5): 2054–61. doi:10.1039/c3sc00032j.

He, Yabing, Chengling Song, Yajing Ling, Chuande Wu, Rajamani Krishna, and Banglin Chen. 2014. “A New MOF-5 Homologue for Selective Separation of Methane from C2 Hydrocarbons at Room Temperature.” *APL Materials* 2 (12): 1–7. doi:10.1063/1.4897351.

Hosseinpour, S., S. Fatemi, Y. Mortazavi, M. Gholamhoseini, and M. Takht Ravanchi. 2011. “Performance of Cax Zeolite for Separation of C2H6, C2H4, and CH4 by Adsorption Process; Capacity, Selectivity, and Dynamic Adsorption Measurements.” *Separation Science and Technology* 46 (2): 349–55. doi:10.1080/01496395.2010.508478.

Martins, Vanessa F.D., Ana M. Ribeiro, Alexandre Ferreira, U. Hwang Lee, Young Kyu Hwang, Jong San Chang, José M. Loureiro, and Alírio E. Rodrigues. 2015. “Ethane/ethylene Separation on a Copper Benzene-1,3,5-Tricarboxylate MOF.” *Separation and Purification Technology* 149. Elsevier B.V.: 445–56. doi:10.1016/j.seppur.2015.06.012.

Mason, Jarad A., Mike Veenstra, and Jeffrey R. Long. 2014. “Evaluating Metal–organic Frameworks for Natural Gas Storage.” *Chem. Sci.* 5 (1): 32–51. doi:10.1039/C3SC52633J.

Pavel, C. C., D. Vuono, L. Catanzaro, P. De Luca, N. Bilba, A. Nastro, and J. B. Nagy. 2002. “Synthesis and Characterization of the Microporous Titanosilicates ETS-4 and ETS-10.” *Microporous and Mesoporous Materials* 56 (2): 227–39. doi:10.1016/S1387-1811(02)00489-4.

Plonka, Anna M., Xianyin Chen, Hao Wang, Rajamani Krishna, Xinglong Dong, Debasis Banerjee, William R. Woerner, Yu Han, Jing Li, and John B. Parise. 2016. “Light Hydrocarbon Adsorption Mechanisms in Two Calcium-Based Microporous Metal Organic Frameworks.” *Chemistry of Materials* 28 (6): 1636–46. doi:10.1021/acs.chemmater.5b03792.

Queen, Wendy L., Matthew R. Hudson, Eric D. Bloch, Jarad A. Mason, Miguel I. Gonzalez, Jason S. Lee, David Gygi, et al. 2014. “Comprehensive Study of Carbon Dioxide Adsorption in the Metal–organic Frameworks M 2 (Dobdc) (M = Mg, Mn, Fe, Co, Ni, Cu, Zn).” *Chem. Sci.* 5 (12): 4569–81. doi:10.1039/C4SC02064B.

Worrel, Ernst, Dian Phylipsen, Dan Einstein, and Nathan Martin. 2000. “Energy Use and Energy Intensity

of the U.S. Chemical Industry." *Lawrence Berkeley National Laboratory* LBNL-44314 (April): 34. doi:10.2172/773773.

Yang, R T, and E S Kikkinides. 1995. "New Sorbents for Olefin Paraffin Separations by Adsorption Via Pi-Complexation." *AIChE Journal* 41 (3): 509–17. doi:10.1002/aic.690410309.

Zhang, Xiao Xin, Peng Xiao, Chang Hua Zhan, Bei Liu, Rui Qin Zhong, Lan Ying Yang, Chang Yu Sun, et al. 2015. "Separation of Methane/Ethylene Gas Mixtures Using Wet ZIF-8." *Industrial and Engineering Chemistry Research* 54 (32): 7890–98. doi:10.1021/acs.iecr.5b00941.

Appendices

Appendix 1: Breakthrough times and adsorption capacities for CaX zeolite with Feed Mix 1

Conditions		Breakthrough time (min)			Capacity (mmol/g)			
Temp. (°C)	Press. (psig)	Methane	Argon	Ethane	Methane	Argon	Ethane	Total
60	10	0.4	0.2	4.8	0.19	0.01	0.24	0.44
60	10	0.4	0.2	4.8	0.19	0.01	0.24	0.44
180	10	0.0	0.0	0.5	0.00	0.00	0.03	0.03
180	10	0.0	0.0	0.5	0.00	0.00	0.03	0.03
300	10	0.0	0.0	0.2	0.00	0.00	0.01	0.01
300	10	0.0	0.0	0.2	0.00	0.00	0.01	0.01
60	155	2.0	1.5	9.0	1.02	0.09	0.46	1.57
60	155	2.2	1.5	9.0	1.11	0.09	0.46	1.66
180	155	0.7	0.5	1.8	0.37	0.03	0.09	0.50
180	155	0.7	0.5	1.8	0.37	0.03	0.09	0.50
180	155	0.7	0.5	1.8	0.37	0.03	0.09	0.50
180	155	0.5	0.5	1.6	0.28	0.03	0.08	0.40
180	155	0.5	0.5	1.6	0.28	0.03	0.08	0.40
300	155	0.2	0.2	0.7	0.09	0.01	0.04	0.14
300	155	0.4	0.4	0.7	0.19	0.02	0.04	0.25
60	300	2.2	1.8	8.4	1.11	0.11	0.43	1.65
60	300	2.2	1.8	8.4	1.11	0.11	0.43	1.65
60	300	2.0	1.6	8.1	1.02	0.10	0.41	1.53
180	300	1.1	0.7	2.7	0.56	0.05	0.14	0.74
180	300	1.1	0.9	2.7	0.56	0.06	0.14	0.75
180	300	1.1	0.9	2.6	0.56	0.06	0.13	0.74
300	300	0.4	0.4	1.1	0.19	0.02	0.06	0.26
300	300	0.2	0.4	0.9	0.09	0.02	0.05	0.16
300	300	0.4	0.4	1.1	0.19	0.02	0.06	0.26

Appendix 2: Breakthrough times and adsorption capacities for CaX zeolite with Feed Mix 2

Conditions		Breakthrough time (min)				Capacity (mmol/g)				
Temp. (°C)	Press. (psig)	Methane	Argon	Ethane	Ethylene	Methane	Argon	Ethane	Ethylene	Total
60	10	0.2	0.0	4.3	21.5	0.09	0.00	0.20	1.00	1.28
60	10	0.6	0.2	4.4	21.9	0.27	0.01	0.21	1.02	1.50
120	10	0.0	0.0	1.4	13.9	0.00	0.00	0.06	0.65	0.71
120	10	0.0	0.0	1.5	13.9	0.00	0.00	0.07	0.65	0.72
180	10	0.0	0.0	0.6	7.0	0.00	0.00	0.03	0.32	0.35
180	10	0.0	0.0	0.6	7.0	0.00	0.00	0.03	0.32	0.35
60	155	1.4	0.6	7.0	23.2	0.63	0.04	0.32	1.08	2.07
60	155	1.5	0.8	7.2	23.2	0.72	0.05	0.33	1.08	2.18
120	155	0.2	0.0	2.5	15.5	0.09	0.00	0.12	0.72	0.93
120	155	0.2	0.0	2.7	15.5	0.09	0.00	0.13	0.72	0.93
180	155	0.0	0.0	1.2	9.1	0.00	0.00	0.05	0.42	0.48
180	155	0.0	0.0	1.4	9.3	0.00	0.00	0.06	0.43	0.49
60	300	1.4	1.4	6.2	25.7	0.63	0.08	0.29	1.20	2.20
60	300	1.5	1.4	6.0	25.5	0.72	0.08	0.28	1.19	2.27
120	300	1.0	1.0	3.7	17.8	0.45	0.06	0.17	0.83	1.51
120	300	0.8	1.0	3.7	17.8	0.36	0.06	0.17	0.83	1.42
180	300	0.4	0.4	2.3	11.6	0.18	0.02	0.11	0.54	0.85
180	300	0.4	0.4	2.3	11.6	0.18	0.02	0.11	0.54	0.85

Appendix 3: Breakthrough times and adsorption capacities for Cu-BTC with Feed Mix 1

Conditions		Breakthrough time (min)			Capacity (mmol/g)			
Temp. (°C)	Press. (psig)	Methane	Argon	Ethane	Methane	Argon	Ethane	Total
45	10	1.0	0.8	7.4	0.59	0.06	0.45	1.10
45	10	1.0	0.8	7.4	0.59	0.06	0.45	1.10
60	10	0.8	0.6	6.4	0.48	0.04	0.39	0.91
60	10	1.0	0.8	6.4	0.59	0.06	0.39	1.04
90	10	0.6	0.4	4.1	0.36	0.03	0.25	0.64
90	10	0.8	0.6	4.3	0.48	0.04	0.26	0.78
45	155	1.7	1.5	8.1	1.07	0.12	0.50	1.69
60	155	1.7	1.5	7.5	1.07	0.12	0.46	1.65
90	155	1.4	1.2	5.8	0.83	0.09	0.36	1.28
45	300	1.5	1.5	4.6	0.95	0.12	0.29	1.35
45	300	1.4	1.4	4.3	0.83	0.10	0.26	1.20
60	300	1.4	1.4	3.7	0.83	0.10	0.23	1.16
60	300	1.5	1.5	3.7	0.95	0.12	0.23	1.29
90	300	1.2	1.2	3.1	0.71	0.09	0.19	0.99
90	300	1.4	1.4	3.1	0.83	0.10	0.19	1.12

Appendix 4: Breakthrough times and adsorption capacities for Cu-BTC with Feed Mix 2

Conditions		Breakthrough time (min)				Capacity (mmol/g)				
Temp. (C°)	Press. (psig)	Methane	Argon	Ethane	Ethylene	Methane	Argon	Ethane	Ethylene	Total
45	10	1.0	0.6	6.6	7.4	0.54	0.04	0.37	0.41	1.37
45	10	0.8	0.6	6.4	7.4	0.44	0.04	0.36	0.41	1.25
60	10	0.8	0.6	5.8	6.6	0.44	0.04	0.33	0.37	1.18
90	10	0.6	0.4	4.1	4.4	0.33	0.03	0.23	0.25	0.83
45	155	1.7	1.5	6.6	7.5	0.98	0.12	0.37	0.42	1.89
60	155	1.7	1.5	6.4	7.2	0.98	0.12	0.36	0.40	1.86
90	155	1.5	1.4	5.4	6.0	0.87	0.10	0.30	0.34	1.62
45	300	1.5	1.5	3.5	4.1	0.87	0.12	0.20	0.23	1.41
45	300	1.5	1.5	3.5	3.9	0.87	0.12	0.20	0.22	1.40
60	300	1.4	1.5	3.3	3.9	0.76	0.12	0.19	0.22	1.28
60	300	1.4	1.4	3.3	3.7	0.76	0.10	0.19	0.21	1.26
90	300	1.4	1.4	2.9	3.3	0.76	0.10	0.16	0.19	1.21
90	300	1.4	1.4	2.9	3.3	0.76	0.10	0.16	0.19	1.21

Appendix 5: Breakthrough times and adsorption capacities for Ag+/Amberlyst with Feed Mix 2

Conditions		Breakthrough time (min)				Capacity (mmol/g)				
Temp. (°C)	Press. (psig)	Methane	Argon	Ethane	Ethylene	Methane	Argon	Ethane	Ethylene	Total
45	10	0.0	0.0	0.2	11.4	0.00	0.00	0.01	0.59	0.60
45	10	0.0	0.0	0.0	11.6	0.00	0.00	0.00	0.60	0.60
60	10	0.0	0.0	0.0	10.3	0.00	0.00	0.00	0.53	0.53
60	10	0.0	0.0	0.0	10.4	0.00	0.00	0.00	0.54	0.54
90	10	0.0	0.0	0.0	6.6	0.00	0.00	0.00	0.34	0.34
90	10	0.0	0.0	0.0	6.6	0.00	0.00	0.00	0.34	0.34
45	10	0.0	0.0	0.0	10.3	0.00	0.00	0.00	0.53	0.53
45	10	0.0	0.0	0.0	10.3	0.00	0.00	0.00	0.53	0.53
60	10	0.0	0.0	0.0	9.5	0.00	0.00	0.00	0.49	0.49
60	10	0.0	0.0	0.0	9.3	0.00	0.00	0.00	0.48	0.48
90	10	0.0	0.0	0.0	6.0	0.00	0.00	0.00	0.31	0.31
90	10	0.0	0.0	0.0	6.0	0.00	0.00	0.00	0.31	0.31
45	155	0.0	0.0	0.4	13.3	0.00	0.00	0.02	0.69	0.71
45	155	0.0	0.0	0.4	12.2	0.00	0.00	0.02	0.63	0.65
60	155	0.0	0.0	0.4	11.0	0.00	0.00	0.02	0.57	0.59
60	155	0.0	0.0	0.4	11.0	0.00	0.00	0.02	0.57	0.59
60	155	0.0	0.0	0.4	10.8	0.00	0.00	0.02	0.56	0.58
60	155	0.0	0.0	0.4	10.8	0.00	0.00	0.02	0.56	0.58
60	155	0.0	0.0	0.4	10.6	0.00	0.00	0.02	0.55	0.57
90	155	0.0	0.0	0.4	6.8	0.00	0.00	0.02	0.35	0.37
90	155	0.0	0.0	0.4	7.0	0.00	0.00	0.02	0.36	0.38
45	300	0.0	0.2	0.4	16.4	0.00	0.01	0.02	0.85	0.89
45	300	0.0	0.0	0.4	14.9	0.00	0.00	0.02	0.77	0.79
60	300	0.0	0.0	0.4	13.5	0.00	0.00	0.02	0.70	0.72
60	300	0.0	0.0	0.4	13.5	0.00	0.00	0.02	0.70	0.72
90	300	0.0	0.0	0.4	9.1	0.00	0.00	0.02	0.47	0.49
90	300	0.0	0.0	0.4	9.3	0.00	0.00	0.02	0.48	0.50

Appendix 6: Adsorption isotherms of CaX at three temperatures: (a) 308 K, (b) 298 K, (c) 288 K (Hosseinpour et al. 2011)

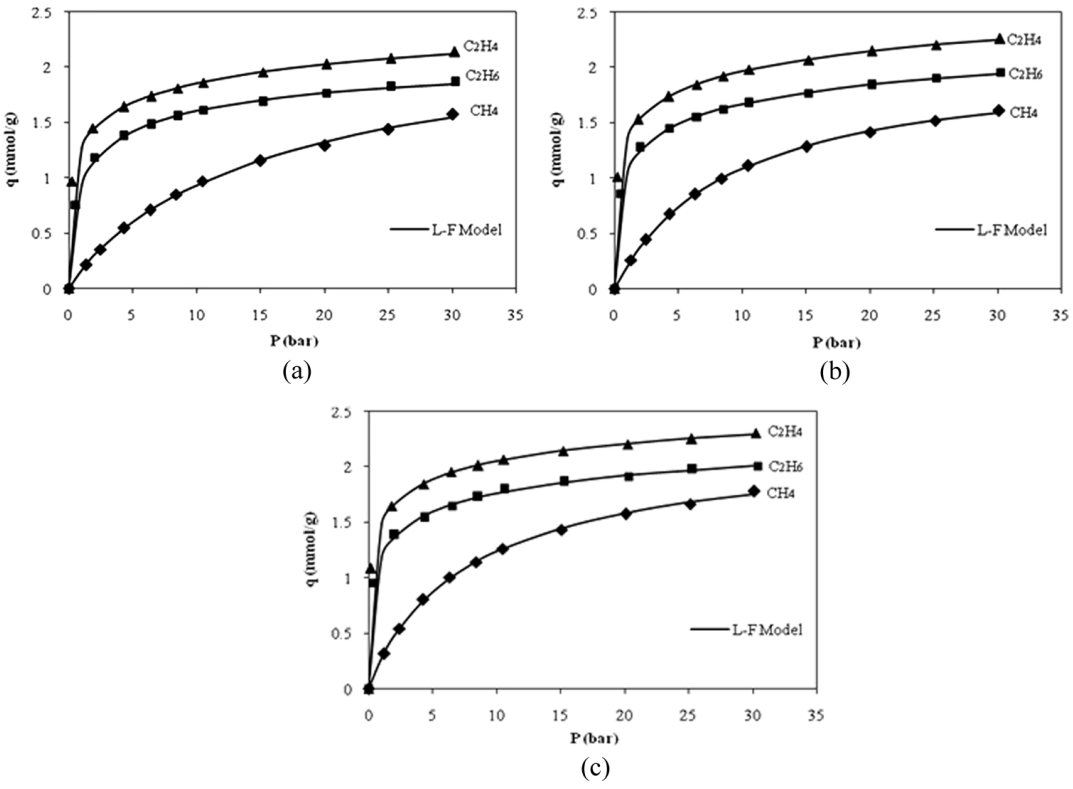

Appendix 7: Isotherms of different gases on Co_2(dobdc)

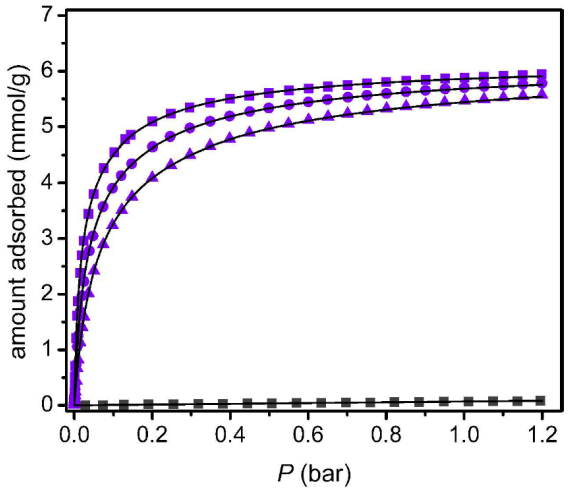

CO isotherms (purple) at 25 °C (squares) 35 °C (circles), and 45°C (triangles)

(Eric D. Bloch et al. 2014)

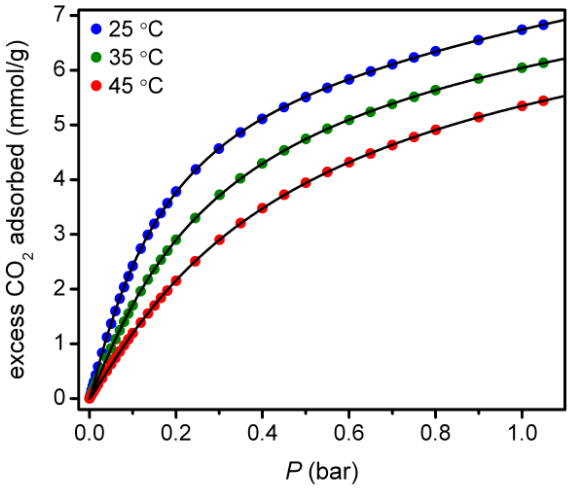

CO_2 isotherms at 25, 35, and 45 ºC

(Queen et al. 2014)

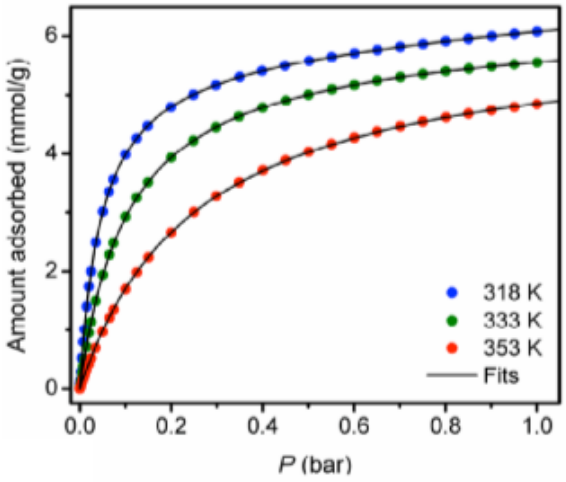

Ethane isotherms at 318K, 333K, and 353K

(Geier et al. 2013)

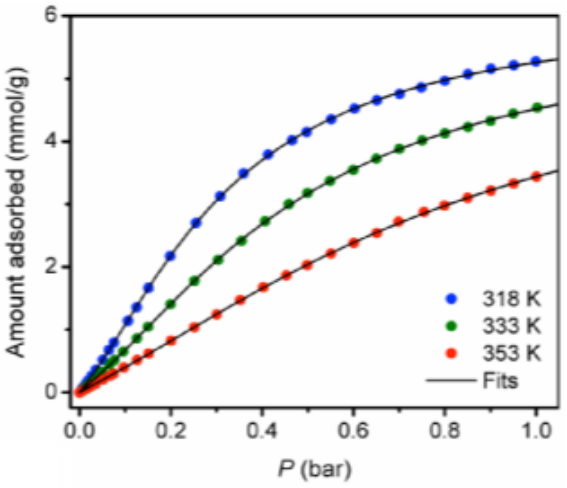

Ethylene isotherms at 318K, 333K, and 353K

(Geier et al. 2013)

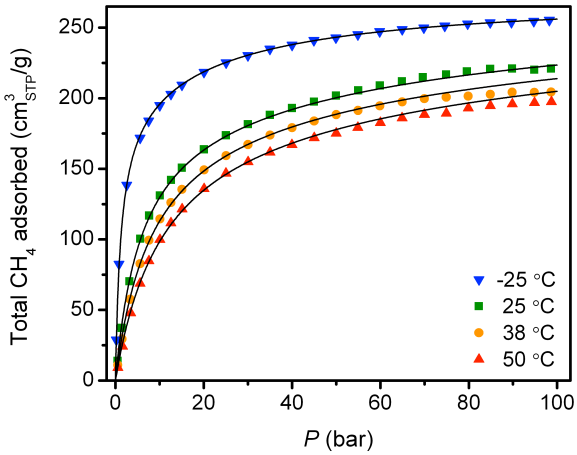

CH4 adsorption isotherms at −25, 25, 38, 50 °C

(Mason, Veenstra, and Long 2014)

Appendix 8: Isotherms of different gases on Berkeley MOF